DESIGN AND CONTROL OF POWERED LOWER LIMB PROSTHESES

by

MOLEI WU

XIANGRONG SHEN, COMMITTEE CHAIR

S. NIMA MAHMOODI
KEITH A. WILLIAMS
HWAN-SIK YOON
TIM A. HASKEW

A DISSERTATION

Submitted in partial fulfillment of the requirements
for the degree of Doctor of Philosophy
in the Department of Mechanical Engineering
in the Graduate School of
The University of Alabama

TUSCALOOSA, ALABAMA

2016

ABSTRACT

In the development of powered lower-limb prostheses, providing sufficient power and torque to support amputees' locomotion is a major challenge, considering prostheses' weight and size limits. Furthermore, regulating the power delivery during locomotion is equally important that gives amputees safe and natural movements. This dissertation aims to address these challenges by investigating new approaches in the actuation and control of powered lower-limb prostheses, with the overarching objective to obtain compact, powerful lower-limb prostheses that interact with amputees and the environment in a coordinated manner.

The initial efforts were focused on the design and control of transfemoral (TF, also known as above-knee) prostheses powered by pneumatic muscles, an extraordinary actuator with superb power-to-weight ratio. The first prototype incorporates powered knee and ankle joints in a volumetric profile similar to that of human leg. The unique feature is a single-acting-spring-return mechanism, in which a single pneumatic muscle drives the motion in the torque-demanding direction, while a set of mechanical springs drives the motion in the opposite direction. A finite-state impedance controller has been developed for this prosthesis, which was demonstrated to provide a natural gait. Based on previous success, a novel type of pneumatic muscle, namely double-acting sleeve muscle (DASM), was examined to replace traditional pneumatic muscle. Incorporating a second chamber, the DASM is able to provide additional extensional force without using return springs. Therefore, the prosthesis can be significantly simplified into a more compact and lightweight device.

Compared with pneumatic muscles, traditional cylinder-type actuators are more technologically mature. Therefore, the subsequent efforts were to develop a pneumatic cylinder-actuated TF prosthesis, which has great potential for real-world applications. All peripheral components were integrated, including a carbon fiber air tank as the energy source, and the prosthesis' capability of independent, untethered operation was demonstrated in human walking test.

In addition to the improvement of prosthetic design, control methods were also investigated. The results include an integrated walking – stair climbing controller and a sit-to-stand controller. Both were developed based on biomechanical analysis of the knee dynamics in human locomotion. In the walking – stair climbing control system, an improved finite state impedance controller was constructed, which incorporates a unique time function to enable gradual energy injection during weight acceptance phase. An intuitive thigh position-based switching condition was introduced to merge the walking and stair climbing controllers into one system. In the sit-to-stand controller, a similar controller was established, which eliminates the need for a state machine and significantly simplifies the controller tuning and implementation. The human testing was conducted with results demonstrating the effectiveness of both control systems.

DEDICATION

To my parents and my family

LIST OF ABBREVIATIONS AND SYMBOLS

PAM   Pneumatic artificial muscle

SPARKy   Spring ankle with regenerative kinetics

PID   Proportional integral derivative

MPKs   Microprocessor- controlled knees

DASM   Double acting sleeve muscle

IMU   Inertial measurement units

STS   Sit-to-stand

TF   Trans-femoral

CONTENTS

LIST OF TABLES

LIST OF FIGURES

1   INTRODUCTION

1.1   Motivation and previous work

There are about 2 million people living with limb loss in the United States and this number is projected to be over 3.6 million by the year 2050 [1]. Such dramatic change is caused by the aging population and higher rates of dysvascular conditions. Among these people, about 65% took the lower extremity amputation. However, majority of the commercial prostheses are passive devices which can only dissipate energy. As a result, amputees tend to adapt to inefficient and unbalanced walking gait, which consume them even more energy [2].Further, activities such as stair climbing and sit-to-stand are impossible for amputees because passive devices cannot provide enough torque and power. This issue motivated the development of powered lower-limb prostheses. In the following sub-section, commercial above-knee and below-knee prostheses will be discussed first, followed by research works in powered lower-limb prostheses.

1.1.1   Commercial above-knee prostheses

From purely mechanical joints to powered joints, each device has its own advantages and disadvantages, which depends on the user's activity and fitness level. Tang et al. provided a very comprehensive review of the current lower-limb prosthetic technologies [3].

The simplest form of above-knee prostheses is the single-axis knee in which the flexion and extension occur around a single axis. The advantages of these devices are simplicity, reliability, low maintenance and low cost. The adjustable friction cell was used to control the swing speed. These devices may also consist of elastic or spring loaded mechanism, in order to ensure full knee extension before heel strike during walking. The major issue with these devices is that the user could only walk at a single speed, thus limiting the mobility of the user.

In order to have a broader range of walking speed, the prosthesis began to use damper made of either a pneumatic or hydraulic cylinder to modulate the friction of the swing-phase, thus to achieve different speed. The amputee could manually adjust the damping level depending on their needs. The pneumatics is better for lower to moderate speed and hydraulic dampers are better for faster speeds due to their characteristics.

The state-of-the-art knee prosthetics is the microprocessor-controlled knees (MPKs) in which the damping level of the joints can be regulated automatically via a microprocessor. The OttoBock C-Leg® [4], which is the most popular and most clinically evaluated MPK so far, is modulating the damping through hydraulics. Such hydraulic system with two separate servo valves for flexion and extension movement provide better swing-phase flexion resistance, extension damping and stumble resistance. The microprocessor uses the sensor information to determine and control the valve to achieve desired resistance (damping) [5]. Several other MPKs are available on the market: the Ossur RHEO Knee® [6], the Freedom Innovations Plié® MPC Knee [7] and Endolite Orion2® [8]. The OttoBock C-Leg® 4 is shown in Figure 1-1 (a).

Figure 1-1: (a) OttoBock C-Leg® 4 (b) Ossur PowerKnee™

All of these knees are passive devices, which lack the ability to provide positive power at the joint. Currently, only one commercially available device exists which could generate power, the Ossur PowerKnee™, shown in Figure 1-1 (b). The positive power is applied to the knee joint using an electric motor, which assists users during all phases of walking, and also allows for other activities such as stair climbing. Control of the knee is achieved using sensors on the sound leg based on an echo control approach. However, the cost of this technology is not cheap, around $60,000 to $ 80,000, which is usually covered by the insurance, otherwise, the device is largely unavailable to the majority of amputees.

1.1.2 Commercial below-knee prostheses

Below-knee prostheses provide the primary purpose of serving as the anatomic foot and ankle for the amputee thus providing shock absorption and a stable weight bearing. There are four different designs of passive prosthetic feet. SACH (solid ankle cushion heel) feet have been applied to thousands of patients in the past decades because of its reliability for very low-activity amputees, which is shown in Figure 1-2 (a). This device consists of solid support structure

covered with functional foam and a synthetic heel wedge. During the heel strike, the cushioned heel compresses allowing the forefoot to move towards the floor to provide a comfortable heel strike. The amount of plantar flexion depends on the material of the heel and the weight of the amputee. But, patient cannot have a dorsiflexion due to the rigidity of the SACH foot.

The next level of articulated designs allows motion between the feet and shank which is further divided into two categories: single and multiple axes. Single axis designs, like the one in Figure 1-2 (b), allow for both plantar flexion and dorsiflexion of the foot, giving the person more stability during the stance phase of walking. Multi-axial designs, as shown in Figure 1-2 (c), allow movement about the ankle joint in multi-direction. The multi-axial compliance of the foot provides improved ground contact which could maintain balance, stability and comfort when walking on uneven surfaces. The toe lever can also provide improved support to the prosthetic limb during late stance.

Figure 1-2: (a) The SACH foot (Courtesy of Ohio Willow Wood); (b) Single-axis foot (Courtesy of Ohio Willow Wood); (c) Flex-Foot (Multi-axis) (Courtesy of Ossur); (d) Re-Flex Shock™ (Courtesy of Ossur)

Next level is the energy storing feet for more active users. These devices, such as the one in Figure 1-2 (d), use a composite spring in front to provide optimal shock absorption which reduces the impact to the patients. The vertical forces at heel contact are stored and the dynamic energy is returned back for users [6].

Till now, the most advanced passive prosthetic foot is the Ossur Proprio Foot®, shown in Figure 1-3 [6]. It utilizes the electrical motor to adjust the dosiflexion during the swing phase to increase ground clearance and reduce the risk of tripping and falling. However, it doesn't provide positive power in the push-off phase, which means it is still the passive or quasi-passive prosthetics.

Figure 1-3: Ossur Proprio Foot®

The first and only commercially available powered ankle-foot prosthetics is BiOM Ankle produced by BIONX Medical Technologies [9]. This prosthetic ankle, which is shown in **Figure 1-4**, is designed by Au, Herr et al. [10]. This prosthetic foot utilizes an electric motor in series with a spring to provide a positive net power at the ankle during the stance phase of a walking cycle. Some of the benefits are increased walking distance and speed, improved safety and

stability on variable terrain, reduced joint forces and easier climbing of ramps, hills and stairs [9]. Such technology is not cheap, which might cost about $52,000 [13].

Figure 1-4: BIONX BiOM Ankle

1.1.3   Lower-limb prostheses research

Different actuation methods have been explored including hydraulics, pneumatics and electrical motors. This section begins with discussion of knee prostheses, followed by ankle prostheses and then, integrated knee and ankle prostheses.

Lambrecht and Kazerooni developed a semi-active prosthetic knee which uses the hydraulic technology by adding power to the device with an electric motor driven pump [14]. The device is referred to as semi-active because during the majority of the walking gait cycle, the device functions as a passive energy storing device, similar to the aforementioned C-Leg®. The power added to the design could offer short-term power assistance for stair climbing activities.

The work by Waycaster developed a powered knee joint using two pneumatic artificial muscles (PAMs) as actuators [15]. The designed prosthesis could produce a maximum torque

about 150 N-m which allow for variable stiffness control. Experiments have demonstrated the joint position tracking performance.

Fite et al. developed a powered knee using a 150 W brushed DC motor actuating a ball screw assembly [16]. Such design could provide enough torque for stair climbing for an 85 kg user. However, a high power battery would be required for longer distance usage.

Versluys et al. designed and developed a powered foot prosthetic using Pleated Pneumatic Artificial Muscles and off board power [21]. The muscles are arranged in a slider-crank configuration. The antagonistically design utilizes three pneumatic muscles in which one is in front, the others are at the back. The design is capable to provide a peak torque of 200 N-m and also have the rotation motion in the frontal plane.

Sugar et al. developed the so-called spring ankle with regenerative kinetics (SPARKy) project [17-20], which is currently in its third phase called SPARKy 3. The goal of the research is to bring injured military personnel back to normal active duty. Such device needs to allow military personnel perform active tasks such as running, jumping to pass army physical fitness test. The current design utilizes motor powered ball screws to provide the positive net torque at the ankle joint. Two EC Powermax 30 motors were used due to the high power requirement for running and jumping. The current design also has two-degrees of freedom: plantar flexion and dorsiflexion in the sagittal plane and rotation of the ankle in the coronal plane (frontal plane). The springs were moved to the front of the keel instead of the back of the keel to minimize the volume of the design.

Sup et al. developed the first prosthesis with both knee and ankle joints using pneumatic cylinders as the actuators [22], as shown in Figure 1-5 (a). The prosthesis design could provide

required torque for a 75 kg user during walking. The initial prototype needs to be tethered to the pneumatic source. The next fully self-contained version by Sup et al. is replacing the pneumatic cylinders with motor-ball screw actuators [23]. The current design by Lawson et al. consists of a powered knee and a powered ankle connected by standard pylon [24], as shown in Figure 1-5 (b). Both joints are powered by brushless DC motor with a three-stage belt/chain speed reduction transmission. The author reports a maximum torque about 86 N-m for knee and a 110 N-m for the ankle (from motor).

(a)   (b)

Figure 1-5: (a) Pneumatic 2 Degree of Freedom prosthesis from Sup et al; (b) Electrical powered prosthesis from Lawson et al.

1.2 Objectives and organization

This dissertation consists four major objectives. The first objective is to develop a walking controller for the lowered leg prosthesis which was designed by T. Driver et al [25]. With the proposed controller, the prosthesis should be able to provide a walking gait similar to

that of a healthy person. The second objective is to design a powered knee prosthesis, using modified double-actuating sleeve muscle (DASM) [26], to examine the feasibility of DASM. The third objective is to develop a self-contained knee prosthesis to provide enough power for walking and stair climbing. The controller should make the transition from walking to stair climbing responsive and reliable. The final objective is to create the sit-to-stand (STS) controller to expand current impedance control framework. With this controller, the prosthesis should be able to detect the STS transition and perform the smooth STS movement for the amputees.

The dissertation is divided into six chapters, the remained is organized as follows: Chapter 2 presents the design and control of above-knee lower-limb prosthesis powered by pneumatic muscles; Chapter 3 presents the design of powered prostheses utilizing double-acting sleeve muscle (DASM) to replace the traditional pneumatic muscle; Chapter 4 presents the design and control of a self-contained knee prosthesis for level walking; Chapter 5 presents the integrated walking-stair climbing controller and finally, Chapter 6 presents initiation and controller of STS for the knee prosthesis.

References

[1]   Ziegler-Graham, K., MacKenzie, E.J., Ephriam, P.L., Travison, T.G., Brookmeyer, R. (2008). "Estimating the Prevalence of Limb Loss in the United States: 2005 to 2050." *Archives of Physical Medicine and Rehabilitation*, 89(3), 422-429.

[2]   Waters, R.L., Mulroy, S. (1999)."The energy expenditure of normal and pathologic gait." *Gait and Posture, 9*, 207-231.

[3]   Tang, P.C., Ravji, K., Key, J.J., Mahler, D.B., Blume, P.A., Sumpio, B. (2008). "Let Them Walk! Current Prosthesis Options for Leg and Foot Amputees." *Journal of the American College of Surgeons*, *206*(3), 548-560.

[4]   OttoBock. (2016). Retrieved from http://www.ottobockus.com/

[5]   Thiele, J., Westebbe, B., Kraft, M., & Bellmann, M. (2014). Designs and performance of microprocessor-controlled knee joints. *Biomedizinische Technik*, *59*(1), 65-77.

[6]   Ossur. (2016). Retrieved from http://www.ossur.com/americas

[7]   Freedom Innovations. (2016). Retrieved from http://www.freedom-innovations.com/

[8]   Endolite. (2016). Retrieved from http://www.endolite.com/products/orion2

[9]   BIONX. (2016). Retrieved from http://www.bionxmed.com/

[10]   Au, S.K., Weber, J., Herr, H. (2007). "Biomechanical design of a powered ankle-foot prosthesis." *Proceedings of the IEEE Intl. Conf. on Rehabilitation Robotics*, 298-303.

[11]   Au, S.K., Herr, H.M., (2008), "Powered Ankle-Foot Prosthesis: The importance of series and parallel motor elasticity." *IEEE Robotics and Automation Magazine*, 15 (3), 52-59.

[12]   Au, S.K, Weber, J., Herr, H. (2009), "Powered Ankle-Foot Prosthesis Improves Walking Metabolic Economy." *IEEE Transactions on Robotics*, 25 (1), 51-66.

[13]   Michael, F., (2014), "BiOM bionic ankle gives amputees natural movement." [The Boston Globe]. Retrieved from https://www.bostonglobe.com/business/2014/06/14/biom-bionic-ankle-gives-amputees-natural-movement/nfEuNYOUghcl9ChjuzF5BN/story.html

[14]   Lambrecht, B.G.A., Kazerooni, H. (2009). "Design of a Semi-Active Knee Prosthesis." *Proceedings of 2009 IEEE International Conference on Robotics and Automation*, 639-645.

[15]   Waycaster, G.C., (2010). "Design of a Powered Above Knee Prosthesis Using Pneumatic Artificial Muscles." Master's Thesis, University of Alabama, Tuscaloosa

[16]   Fite, K., Mitchell, J., Sup, F., Goldfarb, M. (2007). "Design and Control of an Electrically Powered Knee Prosthesis." *Proceedings of the IEEE Intl. Conf. on Rehabilitation Robotics*, 902-905.

[17]   Hitt, J., Holgate, M., Bellman, R., Sugar, T., Hollander, K. (2007), "The SPARKy (Spring Ankle with Regenerative Kinetics) Project: Design and Analysis of a Robotic Transtibial Prosthesis." *ASME International Design Engineering Technical Conference and Computers and Information in Engineering Conference.*

[18]   Hitt, J., Sugar, T., Holgate, M., Bellman, R., Hollander, K. (2009), "Robotic transtibial prosthesis with biomechanical energy regeneration." *Industrial Robot: An International Journal*, 36 (5), 441-447l

[19]   Bellman, R.D., Holgate, M.A., Sugar, T.G. (2008), "SPARKy 3: Design of an Active Robotic Ankle Prosthesis with Two Actuated Degrees of Freedom Using Regenerative Kinetics." *Proceedings of the 2nd Biennial IEEE/RAS-EMBS Internation Conference on Biomedical Robotics and Biomechatronics*, 511-516.

[20]   Hitt, J., Sugar, T. (2010), "Load Carriage Effects on a Robotic Transtibial Prosthesis." *Proceedings of the 2010 Intl. Conf. on Control Automation and Systems*, 139-142.

[21]   Versluys, R., Desomer, A., Lenaerts, G., Van Damme, M., Beyl, P., Van der Perre, G., Peeraer, L., Lefeber, D. (2008). "A Pneumatically Powered Below-Knee Prosthesis: Design Specifications and First Experiments with an Amputee." *Proceedings of the IEEE/RAS-EMBS Intl. Conf. on Biomedical Robotics and Biomechatronics*. 372-377.

[22]   Sup, F., Bohara, A., Goldfarb, M. (2008). "Design and Control of a Powered Transfemoral Prosthesis." *The Intl. Journal of Robotics Research*, 27(2), 263-273.

[23]   Sup, F., Varol, H.A., Mitchell, J. Withrow, T.J., Goldfarb, M. (2009). "Self-Contained Powered Knee and Ankle Prosthesis: Initial Evaluation on a Transfemoral Amputee." *Proceedings of the 11th IEEE Intl. Conf. on Rehabilitation Robotics*. 263-273.

[24]   Lawson, B., Mitchell, J., Truex, D., Shultz, A., Ledoux, E., & Goldfarb, M. (2014). "A robotic leg prosthesis: Design, control, and implementation." *IEEE Robotics And Automation Magazine*, 21(4), 70-81.

[25]   Driver, T. A. (2012). Innovation for powered prostheses utilizing pneumatic actuators (Doctoral dissertation, The University of Alabama TUSCALOOSA).

[26]   Zheng, H., & Shen, X. (2014). "Concept, Design, and Application of Sleeve Muscle Actuator." In *ASME 2014 International Design Engineering Technical Conferences and Computers and Information in Engineering Conference*.

2   DESIGN AND PRELIMINARY TESTING OF A PNEUMATIC MUSCLE-ACTUATED

TRANSFEMORAL PROSTHESIS

Providing powered joint actuation is a major focus of research in the lower-limb prosthesis area. The capability of actively powering the joints enables the prosthesis to meet the energetic requirements of locomotion, and thus provide higher performance in restoring the lost lower-limb functions in comparison with traditional passive prostheses. In this chapter, a powered transfemoral (above-knee) prosthesis is presented, in which the knee and ankle are powered with pneumatic muscle actuators. A new variable-radius pulley-based mechanism is utilized, which enables the free adjustment of actuation torque curve to better match the desired torque curve as dictated by the locomotive requirements. Additionally, a spring-return mechanism is also incorporated, which replaces the muscle actuator in the "weak" (less torque-demanding) direction with a set of mechanical springs. With this mechanism, both knee and ankle joints can be powered while maintaining a compact profile of the prosthesis. The design details are presented, and the prosthesis is able to provide sufficient torque for an 85 kg user in various locomotion modes. A prototype of the prosthesis has been fabricated and tested, with the preliminary results indicating that this prosthesis is able to provide a walking gait similar to that of a healthy person.

2.1   Introduction

For a healthy individual, the knee and ankle joints generate a significant amount of net power output to support his or her locomotion. On the contrary, the majority of existing transfemoral prostheses, however, are energetically passive. The inability to generate power on the knee and ankle poses a serious limitation to their performance in restoring locomotive functions, especially those requiring significant power output, such as walking upslope and upstairs [1,2]. Furthermore, even during level walking, transfemoral amputees fitted with traditional passive prostheses exhibit asymmetric gait, expend more metabolic energy [3], and exhibit considerably higher hip power and torque [1], compared with healthy subjects.

To obtain an energetically active transfemoral prosthesis, developing a compact and powerful actuation system is a key challenge. In the early research efforts by Flowers and Mann [4], an active knee joint was actuated with a hydraulic actuator, which offers the highest power density among traditional approaches. However, multiple drawbacks with hydraulics, such as leakage and lack of a compact supply, make it less attractive for prosthetic applications. Compared with hydraulics, electromechanical actuation is much easier to implement for prosthetic applications. As such, the majority of existing powered transfemoral prostheses are powered with electric motors. For example, Sup et al. developed a powered transfemoral prosthesis with powered knee and ankle, in which the joints are powered with motor-driven ball screw assemblies [5]; Martinez-Villalpando and Herr developed a powered knee prosthesis with two series-elastic actuators positioned in parallel in an agonist-antagonist arrangement [6]; Hoover et al. developed a myoelectric transfemoral prosthesis with the knee powered with a motor-driven ball screw assembly [7]. Additionally, Ossur, a leading orthopedics company, manufactured the Power Knee, which is the first commercial product in the powered

13

transfemoral prosthesis category. According to the available technical information, the Power Knee is also actuated with an electric motor. In addition to the electric motor-powered prostheses described above, fluid power actuators have also been utilized including the pneumatic cylinder-actuated transfemoral prosthesis by Sup et al. [8] and the hydraulically actuated semi-active knee prosthesis by Lambrecht and Kazerooni [9].

Unlike the approaches above, the powered transfemoral prosthesis in this chapter utilizes pneumatic muscle actuators to generate joint power output. Also known as the pneumatic artificial muscle and fluidic muscle, the pneumatic muscle mimics the functioning mechanism of biological muscles through an enclosed elastic tube, as shown in Figure 2-1. The pneumatic muscle enjoys multiple unique advantages compared with electromechanical actuators, including high power density and similar elastic characteristics to biological muscles. Furthermore, the pneumatic muscle can form a self-contained actuation system when combined with a compact pneumatic supply device [10]. This novel pneumatic supply utilizes a liquid propellant (monopropellant) as the energy-storing medium, which generates a high-pressure gaseous product in catalytic reactions. Based on the unique gas-generation process, this supply device is very simple in structure (pressurized tank combined with a catalyst pack), and can provide a large amount of energy to support a long duration of operation for the prosthesis. In the long term, this pneumatic supply device will be incorporated into the prototype described in this dissertation to form a completely self-contained prosthesis to serve the amputee users.
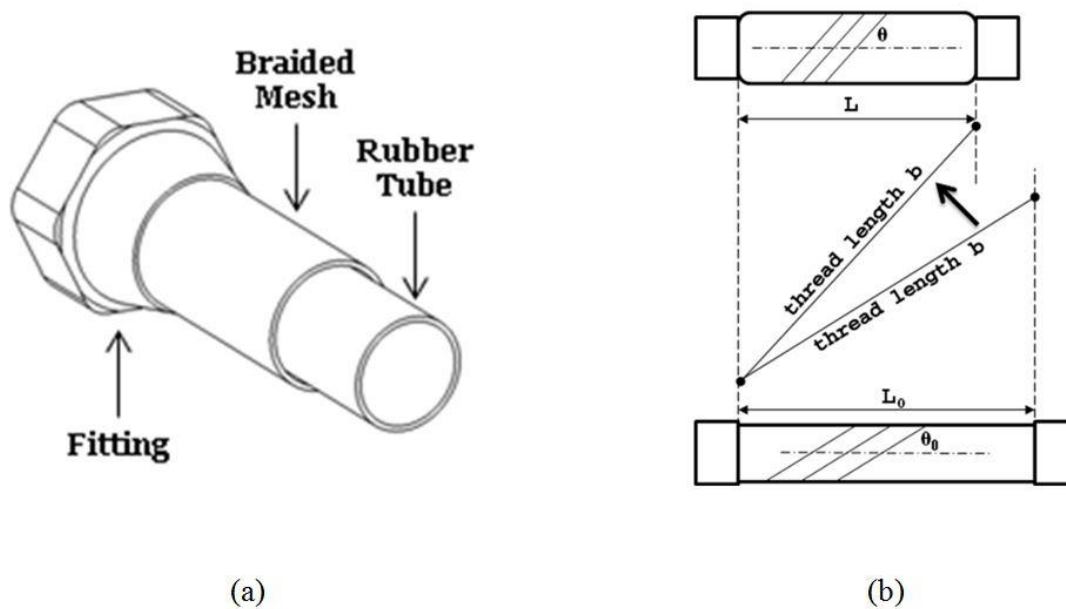
Figure 2-1: The structure (a) and functioning mechanism (b) of the pneumatic muscle

Based on the work by Waycaster et al. [11], the work presented in this chapter represents a significant step ahead by enabling the addition of powered ankle joint with a novel actuation mechanism. Biomechanical research indicates that the energetic behavior of the ankle in level walking is clearly and significantly positive, and stair ascending also requires a similar level of power output [2]. Despite the potential biomechanical benefits associated with a powered ankle, incorporating it in the prosthesis poses a significant design challenge. A pneumatic muscle is a single-acting actuator, and thus two actuators are required for the bi-directional actuation of a single joint. In the previous work, two actuators are used to drive the knee [11]. With the actuators occupying both the anterior and posterior space in the prosthesis, there is essentially no space available for ankle actuation. Motivated by this challenge, a new actuation mechanism is adopted, which enables the bi-directional actuation with only one actuator. The rest of the chapter is organized as follows: Section 2.2 presents the actuation mechanism; Section 2.3

presents the prosthesis design; Section 2.4 presents the experimental results; and Section 2.5 contains the conclusions of the chapter.

2.2 Actuation mechanism

For the prosthesis actuation system, a fundamental requirement is to provide comparable kinetic performance to biological joints. To meet the requirement, related biomechanical data are analyzed as a basis for determining the design specification. Level walking, as well as stair ascent/descent, are considered as the primary modes, for which the torque trajectories are plotted as functions of joint angle, as shown in Figure 2-2. Note that a major design goal for a powered prosthetic joint is to restore the kinetic functions of the corresponding biological joint. As such, these angle-torque trajectories can be used as the torque requirements associated with the corresponding locomotive modes.

From these curves in Figure 2-2, two important observations can be made:

1) The torque requirements are highly uneven, with the values changing significantly with the joint angles.
2) The torque requirements are highly asymmetric. For the knee, the torque for extension (positive in Figure 2-2a) dominates that for flexion. Similarly, for the ankle, the torque for plantar-flexion (positive in Figure 2-2b) dominates that for dorsi-flexion.
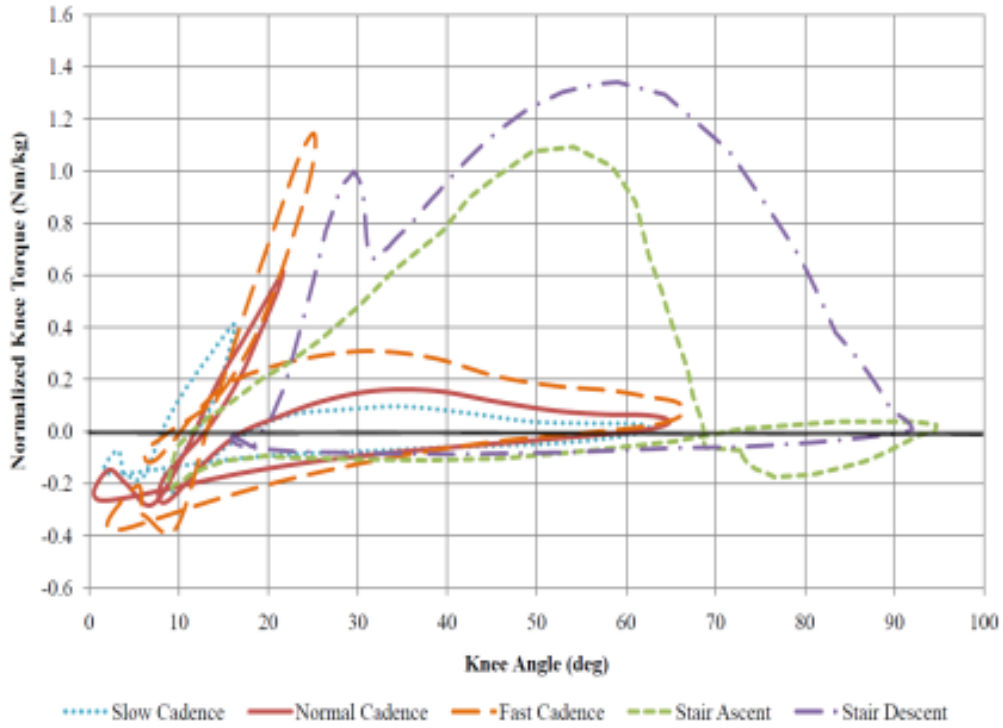
(a)
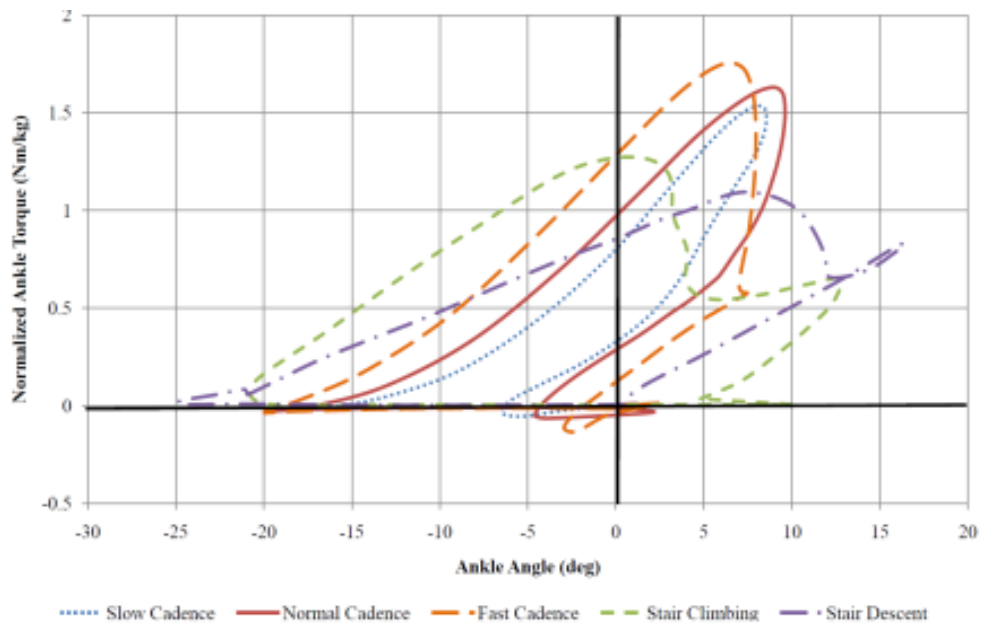
(b)

Figure 2-2: Body-weight-normalized joint torque trajectories for various locomotive modes: (a) Knee torque trajectories; (b) Ankle torque trajectories. The curves are plotted based on the level walking data from Winter [1] and the stair ascent/descent data from Riener et al. [2]

Based on these observations, a new actuation mechanism is created, with the schematic shown in Figure 2-3. As indicated in this figure, two new features are introduced:

1) <u>Variable-radius pulley.</u> Instead of being constant over the entire perimeter, the radius of the pulley is a function of the angular position: $r_P = r_P(\theta)$. By enabling the free adjustment of the effective moment arm as a function of the joint angle, this design feature provides a higher level of flexibility in shaping the torque curve.

2) <u>Single-acting actuation with spring return.</u> To meet the highly asymmetric torque requirements of the knee and ankle, the actuation torque in the weak direction can be provided with a mechanical spring (linear or torsional) while still providing the same capability of bi-directional actuation. Because of the lower torque requirement in the weak direction, the spring can be very small in dimension or even totally integrated into the joint design.
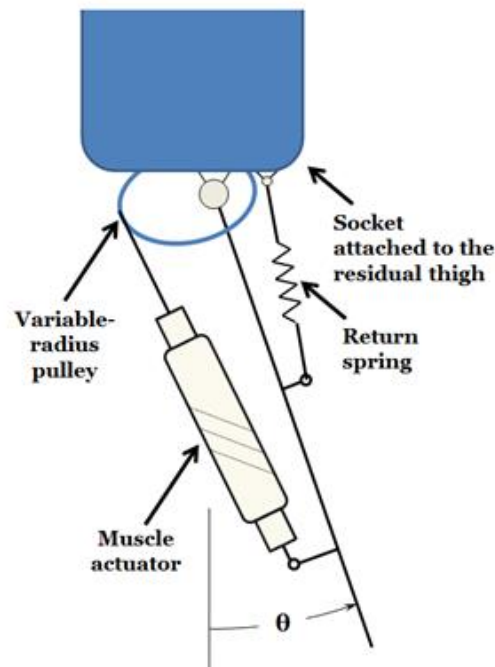
Figure 2-3: Schematic of the knee actuation mechanism

The basic design and control principles of the new actuation mechanism have been studied by Shen et al. [12]. In the knee actuation schematic (Figure 2-3), the variable-radius pulley is fixed to the thigh to enable the adjustment of the moment arm. As such, in the subsequent prosthesis design, the pulley will be rigidly connected to the pyramid connector, which is attached to the amputee's prosthetic socket in use.

Note that the two features described above can be used individually. The variable-radius pulley involves greater complexity in hardware implementation. Therefore, this design feature is not used for the ankle actuation, considering its smaller range of motion compared with the knee. The mechanism for ankle actuation is shown in Figure 2-4, in which the muscle actuator drives the ankle motion through the standard inverted crank-slider mechanism.
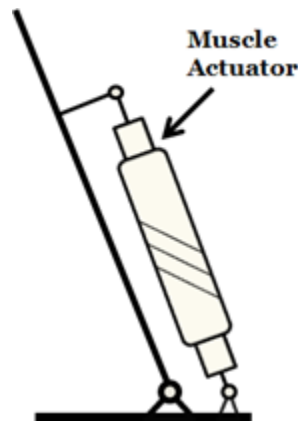
Figure 2-4: Schematic of the ankle actuation mechanism. Note that the return spring is incorporated in the prosthetic joint

2.3 Prosthesis design

After the determination of the actuation mechanism, prosthesis design is conducted to determine the parameters. Due to the prototype nature of the design, commercial off-the-shelf pneumatic muscle actuators (DMSP-40 series fluidic muscle, FESTO, Germany) are used.

Similarly, mature commercial products are also preferred for the selection of other major components. Under these constraints, the design objective is to meet the kinetic and kinematic requirements for the knee and ankle while minimizing the weight.

Since pneumatic muscle actuators expand radially when inflated, sufficient clearance in the radial direction must be provided to avoid interference. Providing sufficient clearance, however, enlarges the volumetric profile and makes the prosthesis bulky. To address this issue, an open-frame structure, as opposed to the traditional central-support structure, is utilized (Figure 2-5). Based on this structure, detailed design calculations are conducted to determine the design parameters of the prosthesis.
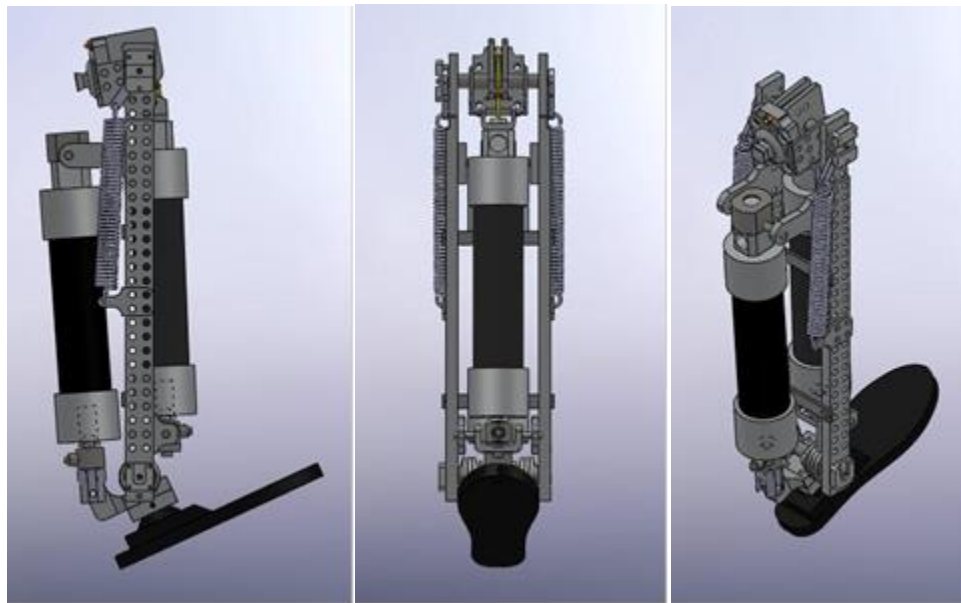
Figure 2-5: 3D model of the transfemoral prosthesis design

2.3.1 Design of the spring return mechanism

In the design calculations, the spring return mechanisms are considered first. For the knee, two linear springs are utilized, leveraging the higher flexibility associated with its kinetic

configuration (Figure 2-6). The torque provided by the linear spring can be expressed by the following equation

$$\tau = -r_{LS}(\theta) \cdot K_{LS} \cdot \left(L_{LS}(\theta) - L_{LS0} \right) \tag{2.1}$$
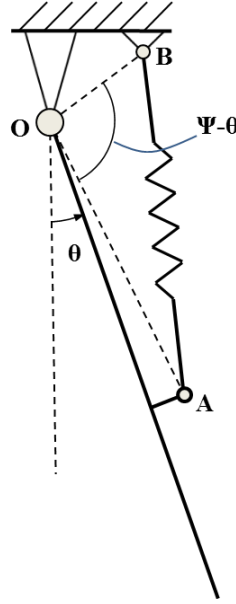
Figure 2-6: The linear spring-based return mechanism for the knee

where K_{LS} is the stiffness, L_{LS0} is the equilibrium length, $r_{LS}(\theta)$ is the moment arm of the spring force as a function of the joint position, and $L_{LS}(\theta)$ is the length of the spring. Note that the specific form of $r_{LS}(\theta)$ and $L_{LS}(\theta)$ can be easily obtained through trigonometry:

$$r_{LS}(\theta) = \frac{L_1 L_2 \sin(\psi - \theta)}{\sqrt{L_1^2 + L_2^2 - 2 L_1 L_2 \cos(\psi - \theta)}} \tag{2.2}$$

$$L_{LS}(\theta) = \sqrt{L_1^2 + L_2^2 - 2 L_1 L_2 \cos(\psi - \theta)} \tag{2.3}$$

where $L_1 = OA$, $L_2 = OB$, and $\psi = \angle AOB$ when $\theta = 0$, as shown in Figure 2-6. Here the design process is largely driven by practical concerns (e.g., limitation of available space), and the related parameters are shown in Table 2-1. The resultant torque curve is shown in Figure 2-7 in

a comparison with the torque requirement for the flexion of the knee. Note that the curve of torque requirement is obtained by combining the individual torque requirements corresponding to various locomotive modes, including level walking and stair ascent/descent. As can be seen in Figure 2-7, the curve of the available torque capacity is always higher than the curve of the required torque, indicating that the return springs are able to provide sufficient torque for the flexion of the knee in locomotion.

Table 2-1 Design parameters of the knee spring return mechanism

Parameter	Value	Unit
K	10.18	*N/mm*
L_1	213	*mm*
L_2	38	*mm*
L_{S0}	165.1	*mm*
ψ	135	*deg*
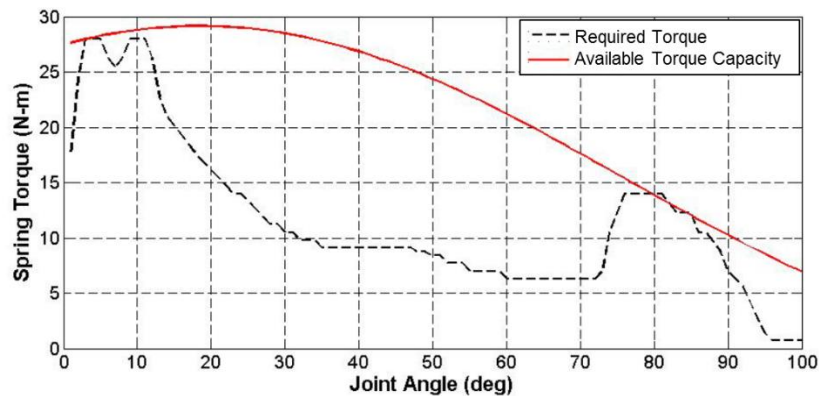
Figure 2-7: The available torque capacity provided by the spring-return mechanism (solid line in red), in comparison with the torque requirement (dashed line in black) for the flexion of the knee

For the ankle spring-return mechanism, torsion springs are selected to reduce the volumetric profile of the joint assembly. Related calculations show that if only a single pair of springs is used to provide the desired torque, the spring diameter would be large enough to cause

interference with other components. The solution is to use two pairs of torsion springs, with one

spring mounted inside the other on each side. The combined stiffness of the torsion springs is

0.47 N·m/deg, with an initial pretension of 3.18 N·m. The corresponding torque curve is shown

in Figure 2-8, compared with the desired torque for the dorsiflexion of the ankle. As shown in

this figure, the spring-return mechanism is able to provide the desired torque over the full range

of motion.
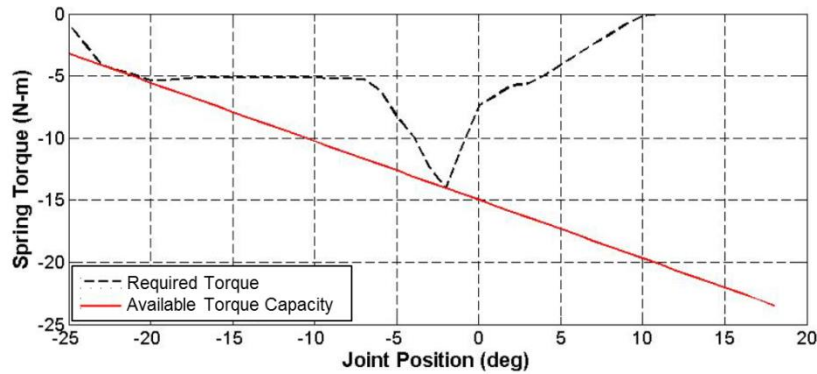
Figure 2-8: The available torque capacity provided by the spring-return mechanism (solid line in red), in comparison with the torque requirement (dashed line in black) for the dorsiflexion of the ankle

2.3.2   Design of the knee actuation mechanism

In the design of the knee actuation mechanism, the major challenge is to determine the

shape of the variable-radius pulley. Specifically, to define the profile of the variable-radius

pulley, a continuous function $r_P(\theta)$ is required, which entails an infinite number of unknown

variables. To address this issue, instead of utilizing an arbitrary curve, the pulley design in this

work is conducted based on a superellipse curve-based profile. Also known as the Lamé curve,

the superellipse can be defined by the following equation:

$$\left|\frac{x}{a}\right|^m + \left|\frac{y}{b}\right|^n = 1 \quad m, n > 0 \tag{2.4}$$

23

where a and b are known as the semi-diameters, and m and n are positive constants that determine the shape. For the definition of the pulley contour, the center position (r_0, θ_0), as well as the direction of major axis (φ), are also included as design parameters (Figure 2-9 a).
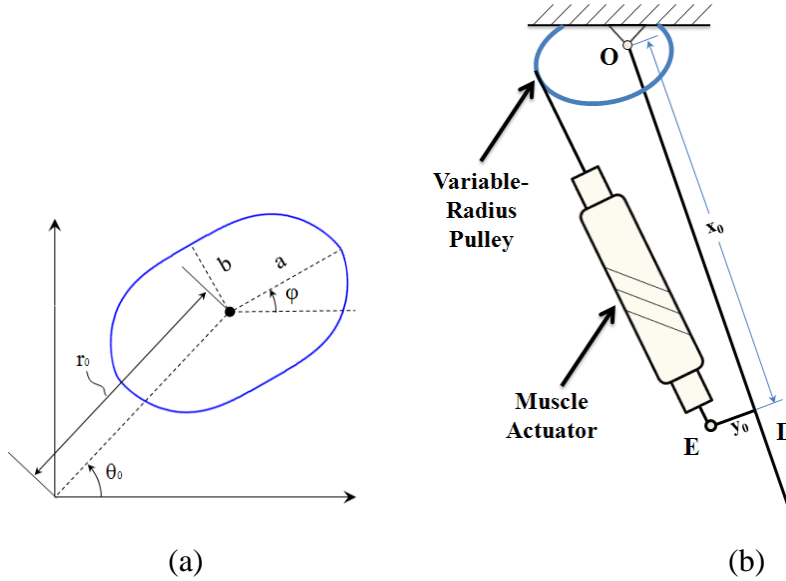
Figure 2-9: Definition of parameters for the superellipse (a) and the corresponding knee actuation mechanism (b)

The corresponding knee actuation mechanism is shown in Figure 2-9 b. In addition to the parameters related to the superelliptical function, the position of the pivot joint E (x_0, y_0) and the actuator resting length L0 are also included as design parameters. To determine the parameter values, a nonlinear optimization-based approach is developed, with the objective of minimizing the cumulative difference between the desired and available torque curve over the range of motion. The following cost function is defined to reflect this objective:

$$C(\mathbf{x}) = \int_{\theta_1}^{\theta_2} e(\mathbf{x}, \theta) d\theta \qquad (2.5)$$

24

where **x** is the vector of design parameters

$$\mathbf{x} = [a, b, m, n, \varphi, r_0, \theta_0, x_0, y_0, L_0]^T \tag{2.6}$$

and $e(\mathbf{x}, \theta)$ is the error function defined as

$$e(\mathbf{x}, \theta) = \begin{cases} \tau_a(\mathbf{x}, \theta) - \tau_d(\theta) & when \; \tau_a(\mathbf{x}, \theta) \geq \tau_d(\theta) \\ p_y \cdot [\tau_d(\theta) - \tau_a(\mathbf{x}, \theta)] & when \; \tau_a(\mathbf{x}, \theta) < \tau_d(\theta) \end{cases} \tag{2.7}$$

where $\tau_a(\mathbf{x}, \theta)$ is the available torque, $\tau_d(\theta)$ is the desired torque, and p_y is a penalty coefficient with the value greater than *1*. Note that the penalty coefficient p_y is introduced to highlight the fact that providing sufficient torque takes a higher priority than reducing excessive torque supply. Subsequently, the available torque can be expressed as the product of the actuation force $F(\mathbf{x}, \theta)$ and the corresponding moment arm $r(\mathbf{x}, \theta)$:

$$\tau_a(\mathbf{x}, \theta) = F(\mathbf{x}, \theta) \cdot r(\mathbf{x}, \theta). \tag{2.8}$$

In this equation, both the actuation force and moment arm are functions of the joint position and the design parameters, and the values of these functions are obtained through numerical approaches. Specifically, for a certain joint angle, the points on the perimeter of the pulley are searched to locate the tangential point, according to the criterion of largest distance from the center of rotation to the action line of the actuator force. Based on this point, the moment arm $r(\mathbf{x}, \theta)$ is determined as the distance from the rotation axis to the actuator action line, while the available force $F(\mathbf{x}, \theta)$ is obtained according to the muscle actuator force-length relationship (via the muscle actuator length determined from the tangential point).

After the optimization problem is defined, the MATLAB Optimization Toolbox is utilized to find the optimal solution. Using p_y=50, the optimization yields a set of design

parameters as shown in Table 2-2. The corresponding torque curve is shown in Figure 2-10, compared with the desired torque for the extension of the knee. As shown in this figure, the shape of the actuation torque curve is no longer monotonic as in the traditional antagonistic system, and thus poses a closer match to the shape of the desired torque curve. Also, the actuation torque is always greater than the desired torque, which indicates that the knee actuation mechanism is able to provide the desired torque over the full range of motion.

Table 2-2 Design parameters of the knee actuation mechanism.

| Parameter	Value	Unit
L_0	153	*mm*
x_0	330	*mm*
y_0	24.2	*mm*
φ	90	*deg*
m	3.48	
n	1.5	
a	29.86	*mm*
b	6.68	*mm*
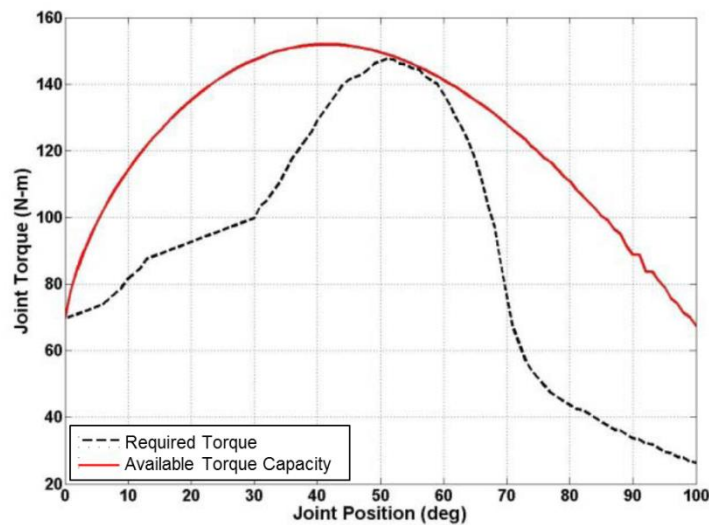
Figure 2-10: The available torque capacity provided by the knee actuation mechanism (solid line in red), in comparison with the torque requirement (dashed line in black) for the extension of the knee

26

2.3.3 Design of the ankle actuation mechanism

A similar optimization-based design approach is also applied to the ankle actuation mechanism. The formulation of the design problem is relatively simple with the inverted crank-slider mechanism. The definitions of the parameters are shown in Figure 2-11.
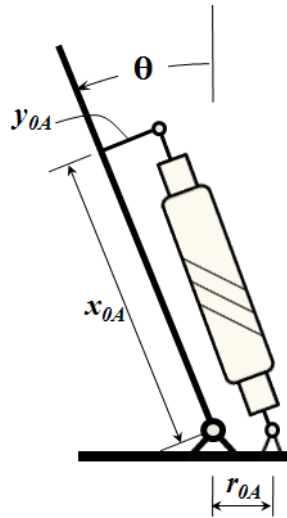
Figure 2-11: Definition of design parameters for the ankle actuation mechanism

In addition to the parameters shown in this figure, the initial length of the muscle actuator L_{0A} is also included as a design parameter. As such, the vector of design parameter is defined as:

$$\mathbf{x} = \left[x_{0A}, y_{0A}, r_{0A}, L_{0A} \right]^T \tag{2.9}$$

With a similar optimization approach as defined by Eqns. (2.5, 2.7, 2.8), a set of optimized design parameters are obtained, as shown in Table 2-3. The corresponding torque curve is shown in Figure 2-12, compared with the desired torque for the plantar-flexion of the ankle. As shown in this figure, the ankle actuation mechanism is able to provide the desired torque over the full range of ankle motion.

Table 2-3 Design parameters of the ankle actuation mechanism.

| Parameter	Value	Unit
L_{0A}	141	*mm*
x_{0A}	292.5	*mm*
y_{0A}	64.5	*mm*
r_{0A}	45	*mm*
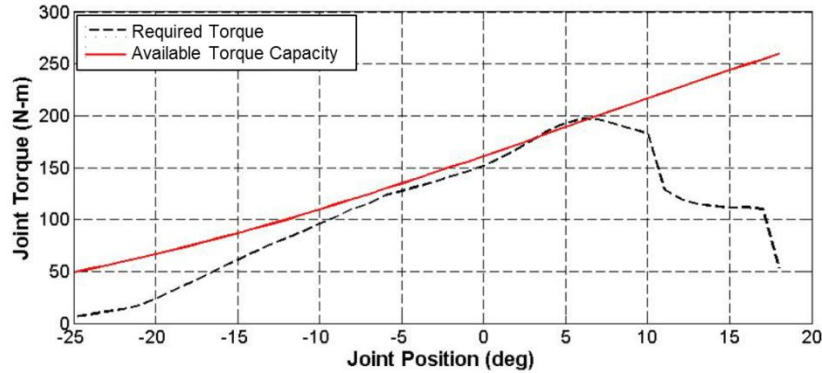
Figure 2-12: The available torque capacity provided by the ankle actuation mechanism (solid line in red), in comparison with the torque requirement (dashed line in black) for the plantar-flexion of the ankle

2.3.4   The complete prosthesis package

Using the design parameters above, a prosthesis prototype has been designed and fabricated (Figure 2-13).   Standard interface is incorporated to make use of a commercial prosthetic foot (Lo Rider, Otto Bock, Germany), and multiple sensors are incorporated for the control purpose.   Specifically, rotary potentiometers (RDC503, ALPS Electric, Japan) are attached to the joints to measure the joint motion; load cells (WMC2000, Interface Inc., Scottsdale, AZ, USA) are mounted in line with the muscle actuators to measure actuation forces; and force-sensing resistors (FSR400, Interlink Electronics, Camarillo, CA, USA) are mounted under the prosthetic foot to detect critical events in the gait, including heel strike and toe off.   In this preliminary prototype, the control valves (MPYE-5-1/8LF-010-B, FESTO, Germany) are currently implemented off-board.   In the future, the commercial pneumatic muscles will be

replaced with a custom integrated design, which incorporates the valve and sensor in the dead space inside the actuator. Furthermore, a compact liquid propellant-based pneumatic supply will also be incorporated, as described in Section 2.1. Leveraging the high energy density of liquid propellant, such supply device is expected to provide sufficient energy supply to support the desired long duration of operation for practical transfemoral prosthesis.

Figure 2-13: Photos of the prosthesis prototype

2.4   Preliminary testing

After the prosthesis prototype was fabricated, the walking experiments were conducted for a preliminary evaluation of the prosthesis's rehabilitation effects. To reduce the risk, a healthy person served as the test subject, who was fitted with the prosthesis through a custom able-body adaptor (Figure 2-14). Modified from a commercial knee immobilizer, the adaptor locks the knee joint of the test subject and transfers the load to the prosthesis through a standard pyramid connector. In the testing, the prosthesis was tethered to the external pressure source nitrogen) at 653 kPa (94.7 psi). Locomotive testing was conducted on a treadmill, which provides a controlled walking speed and enhanced safety features, including custom handrails and overhead suspension harness.
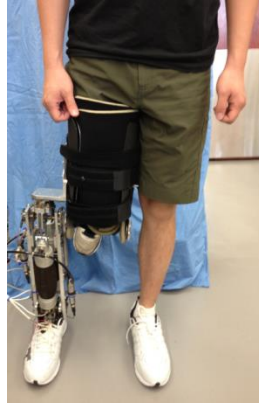
Figure 2-14: A healthy subject fitted with the prosthesis through an able-body adaptor

For the real-time control of the prosthesis motion, the impedance-based control approach is adopted [8]. In this controller, a gait cycle is divided into a finite number of phases, each of which possesses distinct dynamic characteristics. Furthermore, each state is also triggered from a set of highly definitive conditions, which can be easily detected with sensor signals, facilitating the real-time implementation of the controller. For the walking, a cycle is divided into four states, with the definition and switching conditions illustrated in Figure 2-15.
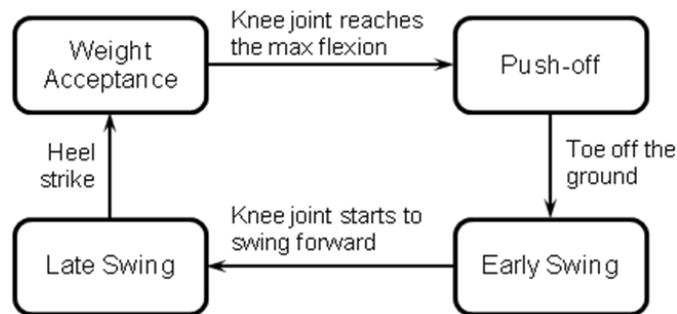
Figure 2-15: Definition of the states and triggering conditions

Based on the definition of states, the dynamic behavior within each state can be characterized with artificial impedance (i.e., artificial spring + artificial damper):

$$\tau = k_1\left(\theta - \theta_e\right) + k_2\left(\theta - \theta_e\right)^3 + b\dot{\theta} \tag{2.10}$$

where k_1 and k_2 are the linear and cubic stiffness values, respectively, b is the damping, and θ_e is the equilibrium position. For the real-time implementation, curve fitting of related biomechanical data [8] can be used to determine the starting values for the impedance parameters, and the optimal parameters were obtained after repeated tuning experiments.

In the walking experiments, the controller was implemented in a desktop computer running the MATLAB Simulink Real-Time Workshop. Since a healthy subject was used in the experiments, the trajectories of his biological knee and ankle joints were recorded during his normal walking (without the prosthesis). In the tuning of the controller parameters, the trajectories of the prosthetic joints are compared with the recorded biological joint trajectories, forming an objective evaluation of the gait quality. Additionally, visual observation and the feedback from the test subject also played important roles for the adjustment of control parameters. Figure 2-16 displays a comparison between the trajectories of the prosthetic joints versus those of the biological joints. It can be seen that, for both knee and ankle, the joint trajectories are very close to each other. The trajectories of the biological joints are slightly smoother, while the prosthetic joint trajectories display more obvious transition between adjacent phases, presumably because of the use of the finite-state impedance controller. In spite of the slight difference, the similar shapes of the trajectories indicate that the prosthesis provides a similar locomotive behavior to the biological lower limb, and thus is able to effectively restore the lost locomotive functions for an amputee user.
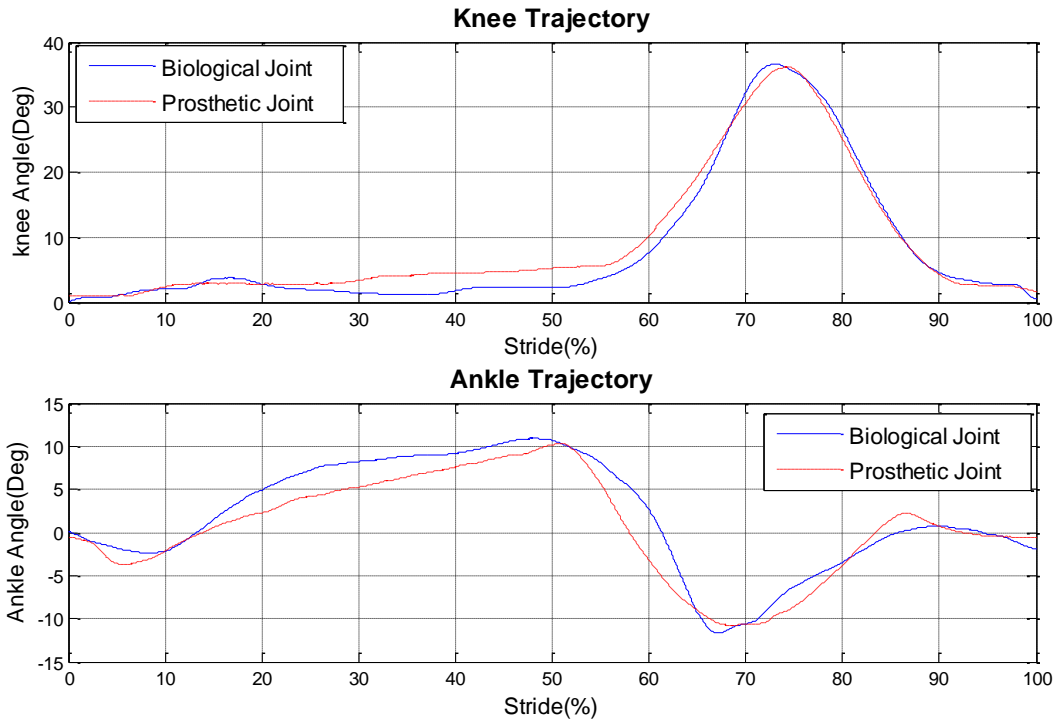
Figure 2-16: Comparison of the trajectories of the biological joints versus the prosthetic joints

2.5 Conclusions

This work presents a unique robotic transfemoral prosthesis design that utilizes pneumatic muscle actuators to drive the prosthetic knee and ankle joints. To enable the actuation of both joints without generating an excessively large prosthesis profile, this new design utilizes a new actuation mechanism with two important features: variable-radius pulley and single-acting-spring-return mechanism. The former enables the free adjustment of actuation torque curve, reducing the unnecessary torque supply in a wide range of joint angle; the latter reduces the number of actuator for each joint from two to one, while still maintaining the bi-directional actuation capability. Details of the prosthesis design are provided, including the spring return mechanisms for the knee flexion and ankle dorsi-flexion, as well as the pneumatic muscle

32

actuation mechanisms for the knee extension and ankle plantar-flexion. Based on the design, a prosthesis prototype has been fabricated and tested. Results from walking experiments demonstrated that the prosthesis is able to provide a walking gait similar to that of a healthy person.

2.6   Acknowledgement

References

[1]   Winter, D.A. (1991) *The Biomechanics and Motor Control of Human Gait: Normal, Elderly and Pathological*. 2nd edition, Waterloo, ON, University of Waterloo Press.

[2]   Riener, R., Rabuffetti, M., and Frigo, C. (2002) "Stair ascent and descent at different inclinations." *Gait and Posture*, no. 15, pp. 32-44.

[3]   Waters, R., Perry, J., Antonelli, D., and Hislop, H. (1976) "Energy cost of walking amputees: the influence of level of amputation." *Journal of Bone and Joint Surgery*, vol. 58A, pp. 42-46.

[4]   Flowers, W.C., and Mann, R.W. (1977) "Electrohydraulic knee-torque controller for a prosthesis simulator." *ASME Journal of Biomechanical Engineering*, vol. 99, no. 4, pp. 3-8.

[5]   Sup, F., Varol, H.A., Mitchell, J., Withrow, T.J., and Goldfarb, M. (2009) "Preliminary evaluations of a self-contained anthropomorphic transfemoral prosthesis." *IEEE/ASME Transactions on Mechatronics*, vol. 14, no. 6, pp. 667-676.

[6]   Martinez-Villalpando, E.C. and Herr, H. (2009) "Agonist-antagonist active knee prosthesis: A preliminary study in level-ground walking." *Journal of Rehabilitation Research & Development*, vol. 46, no. 3, pp. 361-374.

[7]   Hoover, C.D., Fulk, G.D., and Fite, K.B. (2012) "The design and initial experimental validation of an active myoelectric transfemoral prosthesis." *ASME Journal of Medical Devices*, vol. 6, p. 011005.

[8]   Sup, F., Bohara, A, and Goldfarb, M. (2008) "Design and control of a powered transfemoral prosthesis." *The International Journal of Robotics Research*, vol. 27, no. 2, pp. 263-273.

[9]   Lambrecht, B.G.A. and Kazerooni, H. (2009) "Design of a semi-active knee prosthesis." *Proceedings of 2009 IEEE International Conference on Robotics and Automation*, Kobe, Japan, pp. 639-645.

[10]   Shen, X. and Christ, D. (2011) "Design and control of chemo-muscle: A liquid-propellant-powered muscle actuation system." *ASME Journal of Dynamic Systems, Measurement, and Control*, vol. 133, no. 2, p. 021006.

[11]   Waycaster, G., Wu, S.-K., and Shen, X. (2011) "Design and control of a pneumatic artificial muscle actuated above-knee prosthesis." *ASME Journal of Medical Devices*, vol. 5, p. 031003.

[12]   Shen, X., Waycaster, G., and Wu, S. (2013) "Design and control of a rariable-radius pulley-based pneumatic artificial muscle actuation system." *International Journal of Robotics and Automation*, vol. 28, no. 4, pp. 389-400.

3 DOUBLE-ACTING SLEEVE MUSCLE: CONCEPT AND EXAMPLE APPLICATION IN POWERED PROSTHESES

(IMECE. **2015**, 51052)

Pneumatic muscle actuator is a type of muscle-like actuator that mimics human skeletal muscle action through an airtight elastic tube. This unique type of actuator is able to generate a large output force with a very lightweight structure, and thus has been used in various robotic systems. In this chapter, the authors further expand the performance and functionality of pneumatic actuator by introducing a unique modification to the actuator structure. Specifically, a telescoping insert is integrated to the center of the actuator. This insert serves dual purposes. First, by eliminating the central space in the pneumatic muscle, this structural change increases the force output and reduces the energy consumption of the actuator. Second, the insert incorporates an additional pneumatic chamber at the center of the actuator, which enables the actuator to generate an extension force and become a double-acting actuator. Comparative experimental results demonstrated the advantages of the new actuator over the traditional pneumatic muscle with respect to the actuation force over the entire range of motion. Furthermore, a design example, knee actuation mechanism in a powered leg prosthesis, is presented to illustrate the application of the new actuator. To provide the desired performance, a double-acting sleeve muscle drives the knee joint through an inverted crank-slider mechanism. A graphic comparison shows that the actuation system is able to provide sufficient torque to support a 75 kg user's level walking and stair climbing.

3.1 Introduction

In the long history of engineering practice, humans have been taking inspiration from nature to solve challenging problems. Humans themselves also serve as the source of inspiration in a lot of cases. For example, robotic actuators can be developed by mimicking the structure or functioning mechanism of human skeletal muscles. Such efforts have generated a variety of muscle-like actuators, including pneumatic muscle actuators [1], piezoelectric actuators [2], shape memory alloy actuators [3], dielectric elastomer actuators [4], etc. Among these actuators, pneumatic muscle is a mature and highly competitive choice for robotic actuation, especially for biologically inspired robotic systems and devices. Also known as McKibben muscle and fluidic muscle, the pneumatic muscle simulates the functioning mechanism of biological skeletal muscles through the pressurizing of an air-tight tube surrounded by an inextensible mesh. With the interior volume pressurized, the tube expands radially and contracts axially, generating a contraction force to the external load. With this structure, the pneumatic muscle possesses multiple unique advantages, including simple structure, high power density, and similar elastic characteristics to biological skeletal muscles. Researchers have reported the power density values ranging from 1 kW/kg [5] to 10 kW/kg [6], significantly higher than the typical value for electric motors (~0.1 kW/kg as reported by Isermann and Raab [7]). The advantage in power density enables a large power output within a compact package, and thus makes the pneumatic muscle a highly competitive actuation approach for the robotic systems with strict weight and volumetric constraints. Moreover, the actuation force decreases with the contraction, which can be utilized to simulate the elastic behavior of biological skeletal muscles [8]. With these unique characteristics, pneumatic muscle has seen extensive use in robotic systems. For example,

37

pneumatic muscle has been used to drive lower-limb prosthetic devices [9] and rehabilitation exoskeleton systems [10, 11].

Despite the performance advantages described above, the pneumatic muscle still has weaknesses that affect its efficacy in use. A pneumatic muscle has a large internal volume, which causes multiple issues, e.g., slow dynamic response and high energy consumption. Furthermore, the pneumatic muscle is a single-acting actuator, generating contraction force only. As such, two actuators are required for a single degree of freedom, increasing the complexity and weight/volume of the robotic system.

To address these issues, a new variation of the traditional pneumatic muscle, namely double-acting sleeve muscle (DASM), is presented in this chapter. This new variation expands the performance and functionality of pneumatic muscle by introducing a unique modification to the actuator structure. Specifically, a telescoping insert is integrated to the center of the actuator. By eliminating the central space in the pneumatic muscle, this structural change increases the force output and reduces the energy consumption of the actuator. Furthermore, the insert incorporates an additional pneumatic chamber at the center of the actuator, which enables the actuator to generate an extension force and become a double-acting actuator. The inspiration of the new double-acting sleeve muscle is presented in the subsequent section, followed by the details of the actuator design as well as an example application of powered leg prosthesis.

3.2   Inspiration of DASM

The basic concept of DASM is inspired by the working principle of the traditional pneumatic muscle. Pneumatic muscle generates power output through the shortening of the flexible membrane under internal gas pressure. In this process, the internal volume also

38

increases, as a result of the radial expansion. Applying the principle of virtual work, the following equation can be obtained:

$$dW_{out} = dW_{in} \tag{3.1}$$

where W_{out} and W_{in} are the input work and output work, respectively. dW_{out} can be further expressed as

$$dW_{out} = -FdL \tag{3.2}$$

where F is the contraction force, and L the length of the elastic section of the muscle. dW_{in} can be expressed as

$$dW_{in} = (P - P_{atm})dV \tag{3.3}$$

where P is the actuator internal pressure, P_{atm} is the atmosphere pressure, and V is the internal volume. Combining the three equations above, the force output can be expressed as:

$$F = (-dV/dL) \cdot (P - P_{atm}) \tag{3.4}$$

As indicated by this equation, the contraction force F is proportional to the gauge pressure $(P - P_{atm})$, with the coefficient of proportionality as $(-dV/dL)$. Therefore, in order for the pneumatic muscle to generate a contraction force output, the internal volume V needs to expand when the muscle length L reduces, providing a positive value of $(-dV/dL)$. To gain further insight into the actuation process, the internal volume V can be divided into two parts, including V_1, a cylindrical volume at the center of the muscle, whose diameter is equal to that of the muscle' end connectors; and V_2, a ring-shaped volume surrounding V_1 (Figure 3-1).
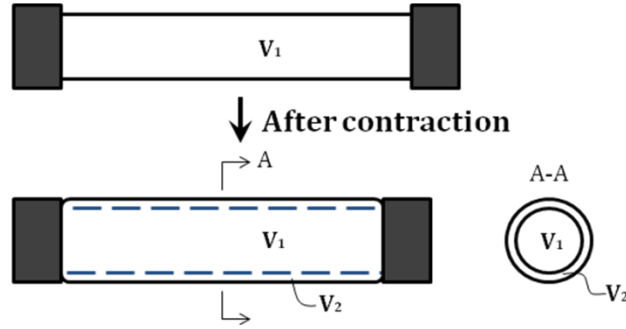
Figure 3-1: Dividing the internal volume into two parts: V_1 and V_2. Note that V_2 is negligible at the equilibrium state.

Note that V2 is negligible at the equilibrium state. Both V1 and V2 changes with the length of the actuator, and thus the total contraction force can be expressed as the sum of F1 and F2:

$$F = F_1 + F_2 \tag{3.5}$$

where F1 and F2 are the contributions of the changes of V1 and V2, respectively:

$$F_1 = \left(-\frac{dV_1}{dL} \right) \cdot \left(P - P_{atm} \right) \tag{3.6}$$

$$F_2 = \left(-\frac{dV_2}{dL} \right) \cdot \left(P - P_{atm} \right) \tag{3.7}$$

To further analyze the contributions of these volume changes, V_1 can be expressed as the product of the fixed cross-sectional area $A_C = \frac{1}{4} \pi D^2$ (D is the diameter of the muscle end connector) and the muscle length L, and thus decreases with the shortening of the muscle. Consequently, the contribution of V_1 to the contraction force is always negative, as indicated by the following equation:

$$\frac{dV_1}{dL} = \frac{1}{4}\pi D^2 > 0 \implies F_1 = \left(-\frac{dV_1}{dL}\right) \cdot (P - P_{atm}) = -A_C(P - P_{atm}) < 0 \qquad (3.8)$$

On the other hand, V_2 expands with the shortening of the pneumatic muscle, and thus contributes positively to the generation of the output force:

$$\frac{dV_2}{dL} < 0 \implies F_2 = \left(-\frac{dV_2}{dL}\right) \cdot (P - P_{atm}) > 0 \qquad (3.9)$$

Based on these two equations, it can be inferred that the total contraction force F is always less than F_2, due to the fact that the negative F_1 always reduces the total force output. This conclusion can be better explained with a simple force analysis as shown in Figure 3-2. Among the two forces applied to the moving end of the pneumatic muscle, F_2 is the contraction force generated by the membrane, while F_1 is the extension force applied to the end connector due to the internal air pressure. When these forces are applied simultaneously, F_1 partially cancels out F_2, resulting in a loss of the actuator force capacity. This observation inspired the basic concept of double-acting sleeve muscle actuator, which incorporates a cylindrical insert at the center of the muscle actuator with the purpose of eliminating F_1.
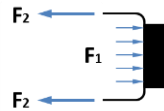
Figure 3-2: Contributions of V1 and V2 to the contraction force: F1 is extension force applied to the end connector due to the internal pressure, and F2 is extension force by the membrane.

3.3 Single-acting sleeve muscle

Inspired by analysis above, the Driver et al. has developed two variations of the traditional pneumatic muscle, both named as *Sleeve Muscle*, with the objective of eliminating the

central volume V_1 and its negative contribution to the actuation force. The earlier type, *Single-Acting Sleeve Muscle* (SASM), incorporates a rigid cylindrical bar or tube that is inserted into the center of the muscle actuator (Figure 3-3) [12].

cylindrical insert
with internal air
pathway
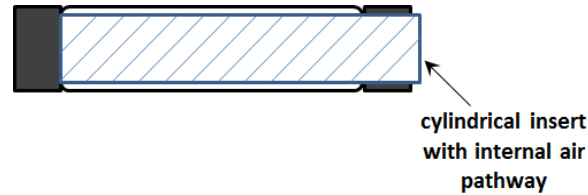
Figure 3-3: Schematic of the SASM.

A major challenge in developing the SASM is that the length of the unwanted central volume changes with the actuator length. To avoid possible motion interference of the moving end of the muscle actuator versus the rigid insert, the moving end is modified into a hollow structure that slides on the surface of the rigid insert, as seen in Figure 3-3. Additionally, a built-in air pathway is incorporated into the cylindrical insert to enable the access to the volume between the insert and the flexible membrane. With the insert occupying the central volume, the SASM increases the actuator force capacity compared with an identical pneumatic actuator (without the insert):

$$\Delta F = -F_1 = \frac{1}{4}\pi D_I^2 \left(P - P_{atm}\right)$$

(3.10)

where D_I is the outer diameter of the insert, which needs to be slightly less than the muscle end-connector diameter D to ensure the structural strength of the moving end. From Eq. (3.10), it can be deduced that, under a certain internal pressure, the magnitude of force increase is a constant, i.e., not affected by the contraction of the muscle. As such, this effect is especially important in

the large-contraction region, where the contraction force is much less than that at the equilibrium state. A comparison of the force curves is shown in Figure 3-4.
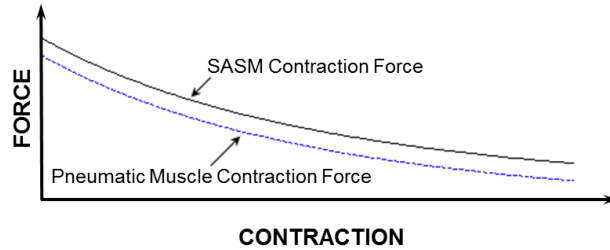
Figure 3-4: Comparison of force outputs under the same internal pressure.

In addition to the greater force capacity, the SASM also features a significant reduction in energy consumption compared with the traditional pneumatic muscle. This can be attributed to two factors: 1) The internal volume has been significantly reduced after incorporating the insert, and 2) With the greater force capacity, the SASM requires a lower air pressure to generate the desired force output, also contributing to the energy saving. According to a comparison experiment, the reduction of energy consumption ranges from 20% to 37%, depending on the percentage of muscle contraction [12].

3.4 Double-acting sleeve muscle

The SASM described above is able to provide enhanced performance. However, the rigid insert, with its fixed length, also requires special treatment when the SASM is used in a robotic system. Also, the single-acting nature of the pneumatic muscle remains unchanged: the SASM still lacks the capability to generate an extension force. Motivated by these issues, Zheng et al. developed the second type of Sleeve Muscle, named as *Double-Acting Sleeve Muscle* (DASM) [13]. Unlike the SASM, the DASM does not eliminate the V_1 in the traditional

pneumatic muscle. Instead, the DASM is developed by isolating V_1 from V_2, such that both contraction and extension forces can be provided. The schematic of DASM is shown in Figure 3-5.
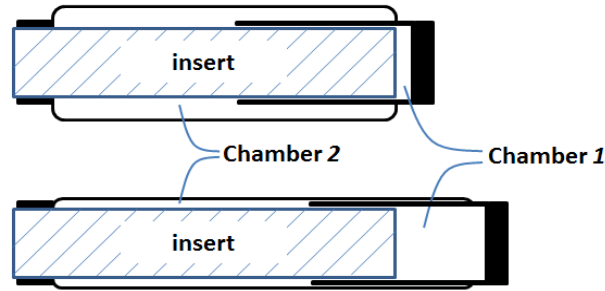
Figure 3-5: Schematic of the DASM.

As shown in Figure 3-5, the DASM incorporates two separate volumes through a telescoping structure. Near the moving end of the actuator is Chamber 1, which is formed with a cylindrical rigid shell sliding on the surface of a rigid insert. One end of the cylindrical shell is closed, and it also serves as the connection element for load transfer. Chamber 2 is the space between the flexible membrane and the insert/shell, which is essentially the same inflatable space as in the SASM. Note that the membrane is connected to the cylindrical shell, such that the contraction force can also be transferred to the moving end. With this unique structure, the DASM features two separate chambers that can be individually pressurized or exhausted for contraction and extension, providing a truly bi-directional robotic actuator.

Based on the schematic in Figure 3-5, the force output can be expressed as a function of the pressures in the chambers. For the membrane pulling force, various theoretical or empirical

models have been established with different levels of complexity and accuracy. To avoid losing

generality in force calculation, assume the membrane force model takes the following form:

$$F_{PM} = F_{PM}(P, L) \tag{3.11}$$

in which P is the internal air pressure and L is the length of the actuator. For the DASM, the

pressure applied to the membrane is the Chamber 2 pressure P_2. Also, compared with the

traditional pneumatic muscle, the DASM provides an increase in the force output as expressed

by Eqn. (3.10). As such, the contraction force of the DASM F_C can be expressed as:

$$F_C = F_{PM}(P_2, L) + \frac{1}{4}\pi D_I^{\ 2}(P_2 - P_{atm}) \tag{3.12}$$

To calculate the extension force, the cross-sectional area of Chamber 1 is a constant

$\frac{1}{4}\pi D_I^{\ 2}$. As such, the extension force can be expressed as:

$$F_E = \frac{1}{4}\pi D_I^{\ 2}(P_1 - P_{atm}) \tag{3.13}$$

in which P_1 is the Chamber 1 pressure. Combining Eqns. (3.12) and (3.13), the force output of

the DASM is:

$$F_{DASM} = F_{PM}(P_2, L) + \frac{1}{4}\pi D_I^{\ 2}(P_2 - P_1) \tag{3.14}$$

for which the contraction force is considered as positive. Based on this equation, a comparison

of the force capacity of the DASM versus the traditional pneumatic muscle is shown in Figure

3-6. From this figure, one can clearly see the increased contraction force capacity (positive) and

the newly added extension force capacity (negative) provided by the DASM, indicating the unique performance provided by this new muscle actuator.
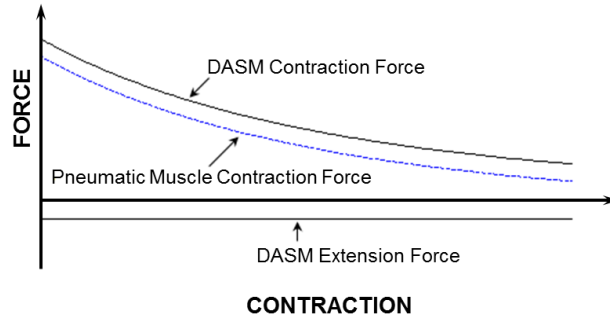
Figure 3-6: Force capacity of the DASM in comparison with that of the traditional pneumatic muscle.

To demonstrate the performance of the DASM, a prototype has been designed and tested [13]. This prototype was developed based on a commercial pneumatic muscle (DMSP-40-180N-RM-CM, FESTO, Germany). Both ends of this commercial product were drilled through to accommodate the insert structure in the center, as shown in Figure 3-7 a. To attach a rigid shell to the moving end, a commercial pneumatic cylinder (Model 124-R, Bimba Manufacturing, University Park, IL, USA) was selected and modified. Specifically, on the rodless end of this single-acting cylinder is an aluminum connector. After cutting the stainless steel body shell to the desired length (Figure 3-7b), the aluminum connector was fitted into the through hole in the muscle actuator to form the moving end. Teflon tape and adhesive were used to provide the required sealing effect. On the stationary end, a solid aluminum insert is mounted to the through hole, and it provides the required air pathways to access the two chambers (Figure 3-7c). Also, two U-Cups, mounted in slots located close to the end of the insert, provide the sliding seal between the chambers during operation.

(a)   (b)

(c)   (d)
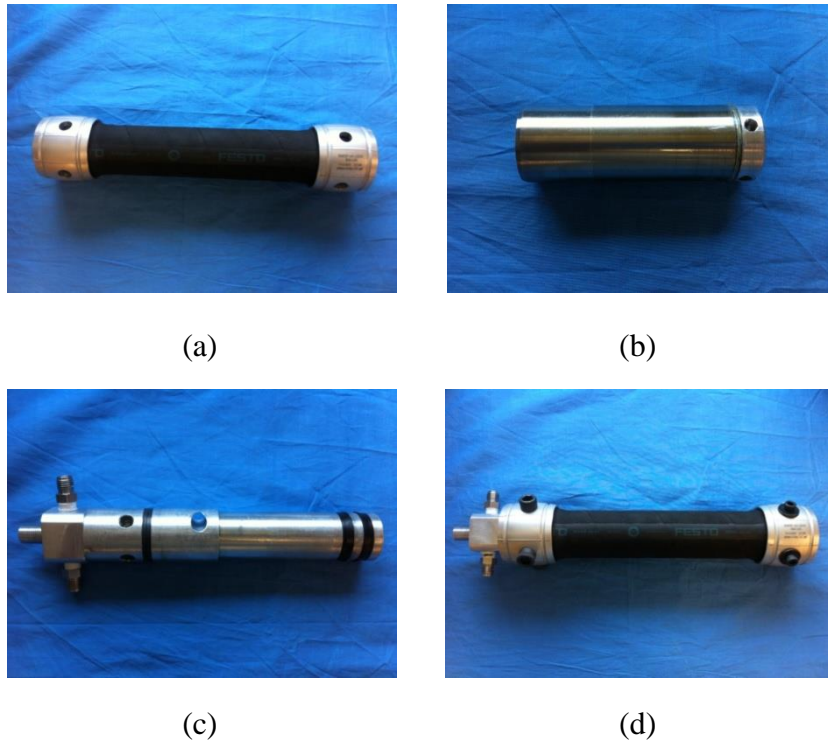
Figure 3-7: The DASM prototype: (a) modified commercial pneumatic muscle; (b) aluminum connector with stainless steel shell; (c) solid aluminum insert mounted on the stationary end; (d) the assembled actuator prototype

A typical set of data collected in the experiments are shown in Figure 3-8. The focus of the experiments is to demonstrate the bi-directional actuation capability, and verify the force model Eqn. (3.14). In the figure, the force-length curve of the pneumatic muscle (dashed lines in blue) was experimentally determined. Based on these curves, the theoretical force curves for contraction and extension (dashed lines in black) are calculated according to Eqn. (3.14). As can be seen in the figure, the measured contraction force by DASM displays a consistent increase over the entire range of motion compared with that provided by the traditional pneumatic muscle. Also, the DASM is able to provide an extension force that the traditional pneumatic muscle is not able to provide (the flat curves with negative values). Since the extension force is provided by the telescoping insert with a constant cross-sectional area, the magnitude of the

47

force is unaffected by the actuator length. Furthermore, the measured curves display a close

match to the theoretic curves, demonstrating the validity of the pressure-force equation (3.14).
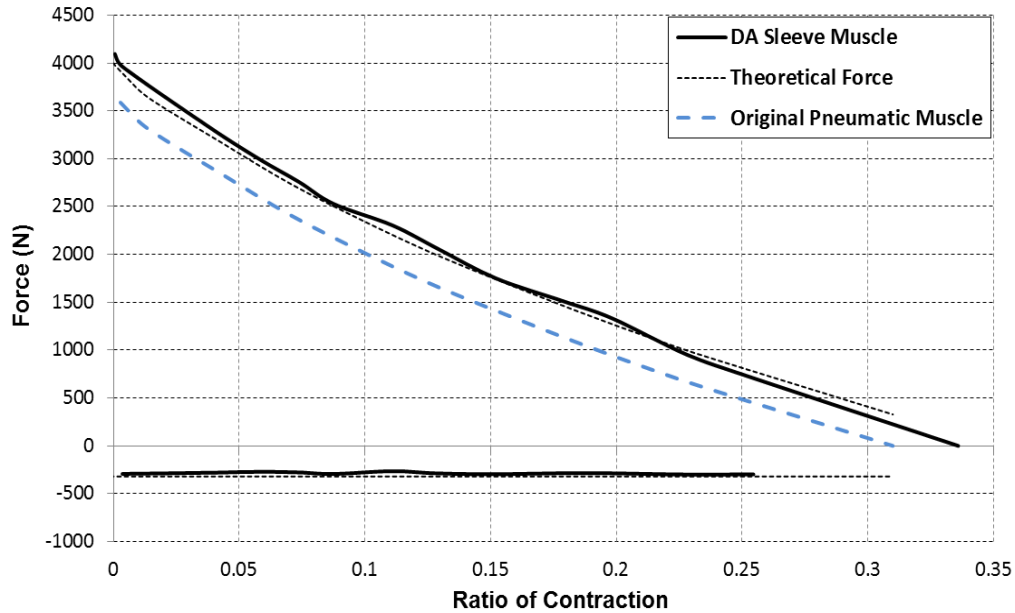
Figure 3-8: Measured and theoretically calculated force outputs of the DASM in comparison with the force output of the original pneumatic muscle under the gauge pressure of 414 KPA (60 PSI)

3.5 Application in leg prostheses

Compared with the traditional pneumatic muscle, the DASM retains the muscle-like functioning mechanism, and provides an increased force capacity and a unique capability of generating an extension force. As such, the DASM can potentially become a highly competitive choice for the actuation of robots and robotic devices, especially those with strict limitation on the weight and size. Robotic leg prosthesis is a typical example for such intended application. Currently, the majority of existing above-knee leg prostheses are energetically passive (i.e. unpowered), and the actuation technology is a major limiting factor for the development of powered leg prostheses. The inability to generate power on the knee and ankle poses a serious limitation to their performance in restoring locomotive functions, especially those requiring

significant power output, such as walking upstairs/upslope, running, and jumping [14-18]. Furthermore, even during level walking, lower limb amputees fitted with traditional passive prostheses exhibit asymmetric gait, expend more metabolic energy [19], and exhibit a significantly higher amount of hip power and torque [14], in comparison with healthy subjects.

For the actuation of the leg prosthesis, the major requirement is to provide sufficient torque capacity to support the user's locomotion. Torque trajectories in biological leg joints (knee and ankle) are highly asymmetric in locomotion. For example, the knee generates a significantly higher torque for extension than that for flexion. This clearly matches the asymmetric force capacity of the DASM. In this work, a knee actuation system is developed in the standard inverted crank-slider mechanism to demonstrate the application of the DASM, as shown in Figure 3-9. DASM is placing at the anterior portion of the prosthesis. The contraction of the DASM results in the extension of the knee which makes full use of the greater force capacity in this direction.

(a)   (b)
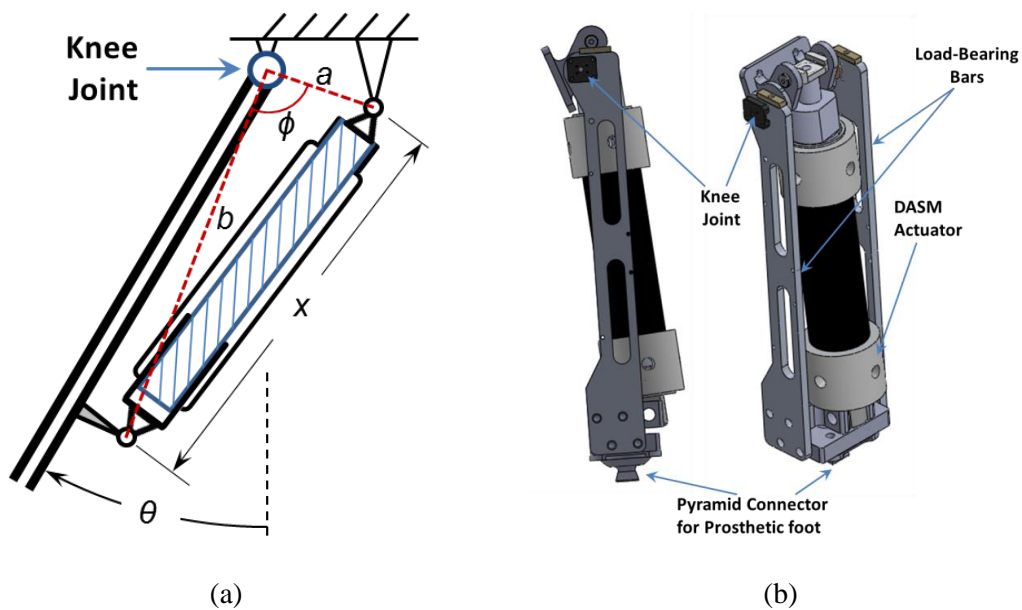
Figure 3-9: Schematic (a) and solid model (b) of the DASM-actuated knee prosthesis

49

For the calculation of the torque capacity of the DASM-actuated knee joint, the configuration in Figure 3-9 a is essentially a triangle, in which a and b are the two segments with constant lengths, ϕ is the angle between these segments, and x is the length of the variable (i.e., actuated) segment. As such, the variable segment length x can be expressed as a function of ϕ:

$$x = \sqrt{a^2 + b^2 - 2ab\cos\phi} \tag{3.15}$$

Based on this equation, the torque τ can be expressed as a function of the actuation force F and the angle ϕ:

$$\tau = F\left(\frac{dx}{d\phi}\right) = F\left(\frac{ab\sin\phi}{\sqrt{a^2 + b^2 - 2ab\cos\phi}}\right) \tag{3.16}$$

The actuator used in this design is modified from a FESTO DMSP-series pneumatic muscle, with the membrane equilibrium length at 140 mm. The maximum actuation force of the original pneumatic muscle is determined according to the manufacturer's literature, which serves as the values of F_{PM} in Eqn. (3.14). Note that it is a function of the actuator length. Using Eqn. (3.14), the actuation forces (both contraction and extension) of the DASM can be calculated as functions of the actuator length. Subsequently, Eqn. (3.16) can be used to determine the knee actuation torques for extension and flexion.
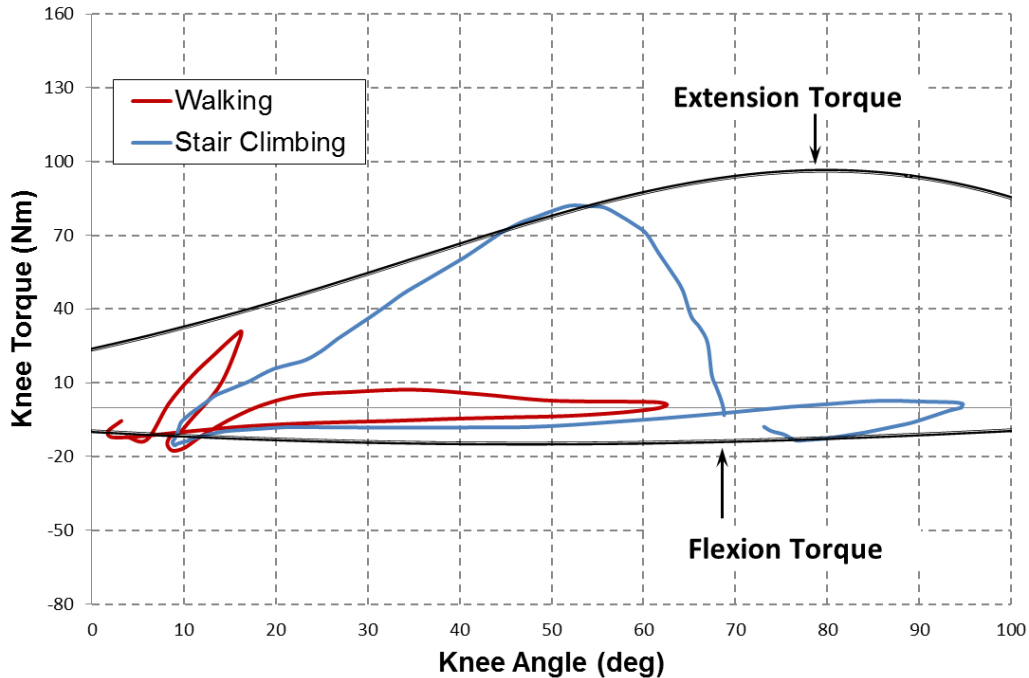
Figure 3-10: Comparison of the actuator torque capacity versus the required torque curves for walking and stair climbing

To determine the values of the design parameters a, b and ϕ (when $\theta = 0$), a graphic comparison is conducted on the joint angle-torque plane, since both the actuation torque (provided by the DASM) and the desired torque (for locomotion) are function of the joint angle. Specifically for the desired torque, joint torque data from existing biomechanical studies are adopted. Two common modes of locomotion, including level walking and stair climbing, are determined as the target modes, with the corresponding data by Winter [14] (for level walking) and Riener et al. [17] (for stair climbing). From these data, the torque trajectories are plotted for both modes for a 75 kg user, indicating the torque requirement for the actuation system design (Figure 3-10). Also shown in Figure 3-10 are the available actuation torques for knee extension and flexion. These curves are generated according to the following set of design parameters, which are obtained through an iterative design calculation process: $a = 21.6$ mm, $b = 256$ mm, $\phi = 38°$ (when $\theta = 0$). It can be clearly observed from this figure that the actuator is able to provide

51

sufficient torque for walking and stair climbing within the majority of the joint range of motion, demonstrating the effectiveness of the prosthetic joint design.

3.6 Conclusions

This chapter presents the concept and example application of a new muscle actuator, namely double-acting sleeve muscle (DASM). To introduce the rationale for this new actuator, an analysis was conducted on the traditional pneumatic muscle, in which the internal volume of the traditional pneumatic muscle was divided into two parts and the contribution of each part was analyzed. The conclusion of this analysis led to the basic concept of DASM, which uses a telescoping insert to provide an enhanced contraction force capacity and an added extension force. To demonstrate the DASM's robotic use, the powered knee joint of a leg prosthesis was used as an application example. Using the DASM in an inverted crank-slider mechanism, the actuation system is able to provide sufficient torque to support a 75 kg user's level walking and stair climbing, which has been demonstrated in a graphic comparison between the required knee torque trajectories for walking and stair climbing versus the extension/flexion torque capacities provided by the actuation system.

3.7 Acknowledgements

References

[1]   Schulte, H.F., 1961. "The characteristic of the McKibben artificial muscle." *The Application of External Power in Prosthetics and Orthotics*, Washington, D.C., National Academy of Sciences – National Research Council, Publication 874: Appendix H, pp. 94-115.

[2]   Secord, T.W., Ueda, J., and Asada, H.H., 2008. "Dynamic analysis of a high-bandwidth, large-strain, PZT cellular muscle actuator with layered strain amplification." *Proceedings of IEEE International Conference on Robotics and Automation*, pp. 761-766.

[3]   Ikuta, K., 1990. "Micro/miniature shape memory alloy actuator." *Proceedings of the IEEE/RSJ International Conference on Intelligent Robots and Systems*, pp. 2156-2161.

[4]   Baughman, R.H., 1996. "Conducting polymer artificial muscles." *Synthetic Metals*, vol. 78, no. 3, pp. 339-353.

[5]   Caldwell, D.G., Medrano-Cerda, G.A, and Goodwin, M.J., 1995. "Control of pneumatic muscle actuators." *IEEE Control Systems*, vol. 15, no. 1, pp. 40-48.

[6]   Hannaford, B. and Winters, J.M., 1990. "Actuator properties and movement control: biological and technological models." in *Multiple Muscle Systems: Biomechanics and Movement Organization*, chapter 7, pp. 101-120, Springer-Verlag, New York.

[7]   Isermann, R. and Raab, U., 1993. "Intelligent actuators – Ways to autonomous systems." *Automatica*, vol. 29, no. 5, pp. 1315-1331.

[8]   Klute, G.K., Czerniecki, J.M., and Hannaford, B., 2002. "Artificial Muscles: Actuators for Biorobotic Systems." *The International Journal of Robotics Research*, vol. 21, no. 4, pp. 295-309.

[9]   Versluys, R., Desomer, A., Lenaerts, G., Van Damme, M., Berl, P., Van der Perre, G., Peeraer, L., and Lefeber, D., 2008. "A Pneumatically Powered Below-Knee Prosthesis: Design Specifications and First Experiments with an Amputee." in Proceedings of the *Second Biennial IEEE/RAS-EMBS International Conference on Biomedical Robotics and Biomechatronics*, Arizona, USA, pp. 19-22.

[10]   Sawicki, G.S. and Ferris, D.P., 2009. "A pneumatic powered knee-ankle-foot orthosis (KAFO) with myoelectric activitation and inhibition." *Journal of NeuroEngineering and Rehabilitation*, vol. 6, no. 23.

[11] Ferris, D.P., Czerniecki, J.M., and Hannaford, B., 2005. "An ankle-foot orthosis powered by artificial pneumatic muscles." *Journal of Applied Biomechanics*, vol. 21, no. 2, pp. 189-197.

[12] Driver, T. and Shen, X., 2013. "Sleeve muscle actuator: Concept and prototype demonstration." Journal of Bionic Engineering, vol. 10, no. 2, pp. 222-230.

[13] Zheng, H. and Shen, X., 2013. "Double-acting sleeve muscle actuator for bio-robotic systems." *Actuators*, vol. 2, pp. 129-144.

[14] Winter, D.A., 1991. *The Biomechanics and Motor Control of Human Gait: Normal, Elderly and Pathological.* 2nd edition, Waterloo, ON, University of Waterloo Press.

[15] Jacobs, R., Bobbert, M.F., van Ingen Schenau, G.J., 1996. "Mechanical output from individual muscles during explosive leg extensions: the role of biarticular muscles." *Journal of Biomechanics*, vol. 29, no. 4, pp. 513-523.

[16] Nagano, A., Ishige, Y., and Fukashiro, S., 1998. "Comparison of New Approaches to Estimate Mechanical Output of Individual Joints in Vertical Jumps." *Journal of Biomechanics*, vol. 32, no. 10, pp. 951-955.

[17] Riener, R., Rabuffetti, M., and Frigo, C., 2002. "Stair ascent and descent at different inclinations." *Gait and Posture*, no. 15, pp. 32-44.

[18] Nadeau, S., McFadyen, B.J., and Malouin, F., 2003. "Frontal and sagittal plane analyses of the stair climbing task in healthy adults aged over 40 years: What are the challenges compared to level walking?" *Clinical Biomechanics*, vol. 18, no. 10, pp. 950-959.

[19] Waters, R., Perry, J., Antonelli, D., and Hislop, H., 1976. "Energy cost of walking amputees: the influence of level of amputation." *Journal of Bone and Joint Surgery*, vol. 58A, pp. 42-46.

4   DESIGN AND PRELIMINARY TESTING OF A SELF-CONTAINED KNEE

PROSTHESIS WITH PNEUMATIC ACTUATION

(IAES *Int. J. Robotics and Automation*, **2016**)

For a powered lower-limb prosthesis, a fundamental requirement is to provide the desired joint power and torque to support the amputee user's locomotion. Considering the limited weight and space, such requirement poses a significant challenge to the design of such prosthetic devices. In this chapter, the design of a powered knee prosthesis is presented, which addresses this challenge by using a pneumatic actuator to power the prosthetic joint, leveraging the multiple advantages of this high-power-density actuator. Through kinetic calculation, the powered knee is able to provide sufficient torque in level walking and stair climbing for an 85 kg user, as demonstrated by a graphical comparison on the joint angle-torque plane. The prosthesis is also instrumented with multiple sensors and a servo valve to enable the locomotive control. Furthermore, a compressed air tank and a microprocessor-based controller are incorporated to form a self-contained prosthetic device ready for untethered use. Implementing a finite-state impedance control, the powered knee prosthesis is able to provide a natural walking gait as demonstrated in the treadmill walking experiments conducted on a human subject.

4.1   Introduction

Experiencing a lower limb amputation is a major life-changing event for amputees. To help them overcome the difficulties associated with limb loss, a lower-limb prosthesis should ideally provide comparable functions like its biological counterpart. From an energetic

perspective, lower-limb joints generate a significant amount of power and torque to support a healthy individual's locomotion. Existing lower-limb prostheses, however, are largely passive devices. Passive devices are simple, lightweight, and inexpensive, and they are able to provide natural swing motion in walking. Despite such advantages, the passive devices' inability to generate power in the prosthetic joints poses a serious limitation to their performance in restoring locomotive functions, especially those requiring significant power output, such as walking upstairs/upslope, running, and jumping [1-5]. Furthermore, even during level walking, transfemoral (i.e. above-knee) amputees fitted with traditional passive prostheses exhibit asymmetric gait, expend more metabolic energy [6], and exhibit a significantly higher amount of hip power and torque [1], in comparison with healthy subjects. Actively-powered transfemoral prostheses, in comparison, have the potential of restoring the biological knee functions in such challenging motion modes. The active prostheses, in general, are heavier and more expensive than passive devices, which limit the population that can benefit from them, but they still attract heavy research interest with the unique biomechanical advantages associated with the actively powered joints.

To develop an actively-powered transfemoral prosthesis, a compact and powerful actuation system is a key component. In the early research efforts by Flowers and Mann [7], a powered knee joint was actuated with a hydraulic actuator, which offers the highest power density among traditional approaches. However, multiple drawbacks with hydraulics, such as leakage and lack of a compact supply, make it less attractive for prosthetic applications. Compared with hydraulics, electro-mechanical actuation does not rely on working fluid in operation, significantly reducing the difficulty of implementation in prosthetic devices. As such, the majority of existing powered transfemoral prostheses are powered with electric motors [8-

14]. For example, Sup et al. developed a transfemoral prosthesis, in which the knee and ankle are powered with DC motor – ball screw assemblies [11]; Martinez-Villalpando and Herr developed a powered knee prosthesis with two series-elastic actuators positioned in parallel in an agonist-antagonist arrangement [12]; Hoover et al. developed a myoelectric transfemoral prosthesis, in which the powered knee is controlled with an electromyography (EMG) - based motion controller [13]. Additionally, Ossur, a leading orthopedics company, manufactured the Power Knee, the first commercially available powered transfemoral prosthesis. According to the available technical information, the Power Knee is also actuated with an electric motor.

Compared with these existing works, the transfemoral prosthesis presented in this chapter is pneumatically powered, and thus enjoys multiple advantages associated with this actuation approach. A pneumatic cylinder generates linear translation with significant force capacity, and thus can be used to drive a robotic joint with a simple inverted crank-slider mechanism. In comparison, an electric motor generates high-speed rotation with limited torque output, and thus requires a high-gear-ratio transmission to generate the desired joint torque. Furthermore, benefiting from the compressibility of the working fluid, a pneumatic actuator entails a physically-existing impedance, which provides necessary buffering protection against the impacts in locomotion (e.g. heel strike-caused impact to the knee). This eliminates the need of using additional elastic components, a common practice for motor-actuated system (e.g. in a series-elastic actuator). Last but not least, pneumatic actuators can be used in conjunction with liquid fuel-based pneumatic supply to form a compact, fully self-contained actuation system. Specifically, a unique class of liquid fuel, namely monopropellant, generates the required high-pressure gas product through catalytic reaction. This unique approach has been experimentally demonstrated to provide an order of magnitude improvement in actuation performance,

compared with traditional battery-DC motor systems [14,15]. Rather than using this actuation system directly, the authors have developed a self-contained pneumatic knee prosthesis, utilizing a commercially carbon-fiber air tank as the pneumatic supply to expedite the research process. This prosthesis prototype was developed based on the experience obtained in developing similar prosthetic and orthotic devices by the authors' group [16-18]. Note that, pneumatics also suffers from a few weaknesses. Compared with electromagnetic motor systems, pneumatic systems require more components with a more complex configuration, the noise level is higher, and they are more difficult to control with strong nonlinearity. Compared with hydraulic systems, pneumatic systems have lower force capacities due to the lower pressure in the working fluid. However, in the authors' opinion, the aforementioned advantages outweigh these weaknesses, and pneumatic actuation can still be a competitive actuation approach for transfemoral prostheses. Note also that, although pneumatic actuation has been attempted for transfemoral prosthesis actuation, existing prototypes have been limited to tethered devices without onboard pneumatic supply [19]. In the future, the air tank can be replaced with a propellant cartridge and catalyst pack to provide a longer duration of operation while maintaining the kinetic and kinematic performance of the current prosthesis prototype.

4.2   Prosthesis design

For the design of the prosthesis, the objective is to provide the desired torque and power capacity while keeping the prosthesis lightweight for practice use by amputee users. Based on this objective, the specifications of the prosthesis design were determined according to the human biomechanical and anatomical data. Subsequently, the actuation mechanism and the overall layout of the prostheses were established, and design parameters are determined to provide the desired torque capacity.

4.2.1 Design specifications

According to human biomechanics study, the knee provides a significant amount of power during the motion modes that involve vertical body movement. A typical example is stair climbing, for which the knee supplies the majority of the required power [4]. For an 85 kg individual, the peak torque during stair climbing can be as high as 93 N-m, and the peak power can be as high as 220 W. As a result of such high kinetic requirements, stair climbing is considered as one of the most challenging motion modes for transfemoral amputees fitted with traditional passive prostheses. Even during level walking, although the net power over a gait cycle is negative, the knee still needs to generate a peak torque of 52 N-m for a healthy individual [1]. Unable to provide the desired torque and power, a passive prosthesis user usually suffers from issues such as asymmetric gait, elevated energy consumption, and greater hip power in locomotion. To help a tranfemoral amputee to overcome such difficulties in his/her real life, the design of the powered prosthesis in this chapter aims to provide the desired power and torque capacity in locomotion, with level walking and stair climbing as the target motion modes.

In addition to the required kinetic performance factors, the weight limit of the device is another major design specification. Amputee users prefer lightweight prosthetic devices. Powered prostheses, however, tend to be heavier than unpowered devices due to the added weight for the actuation and control components. To establish a reasonable goal for the device weight, the corresponding limb segment is taken as the reference. The shank and foot accounts for approximately 6.1% of the total body weight [20], equivalent to 5.2 kg for an 85kg person. As such, 5.2 kg is taken as the upper limit for the weight of the device, and meanwhile minimizing the device weight still remains a major goal in the design process.

4.2.2 Actuation mechanism design

To minimize the risk in developing this powered prosthesis prototype, off-the-shelf commercial components are preferred in the selection of major components, including the actuator and various sensors in the device. As the basis of the actuation mechanism design, a double-acting pneumatic cylinder with a bore size of 38 mm (1.5 inch) from BIMBA Manufacturing (University Park, IL, USA) is chosen as the actuator. Under the supply pressure of 2 MPa, it is able to generate an extension force of 2.36 kN and a contraction force of 2.16 kN. To convert the linear motion into the rotation of the joint, the standard inverted crank-slider mechanism is utilized (Figure 4-1).
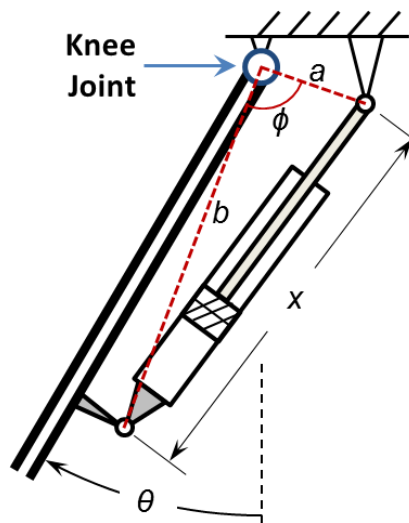
Figure 4-1 The actuation mechanism of the powered knee joint

The detailed design of the actuation mechanism aims to provide sufficient power and torque, as described in the previous section. Note that human locomotion is a relatively slow motion, and thus it is usually not a challenging problem to provide sufficient joint velocity, considering the high speed action provided by the pneumatic cylinder (with the maximum speed of 1000 mm/s when oil-free air is used, according to [21]). As such, the emphasis of design is

placed on the torque capacity calculation. As shown in Figure 4-1, the configuration of the mechanism can be represented by a triangle, in which *a* and *b* are the two segments with constant lengths, ϕ is the angle between these segments, and *x* is the length of the variable (i.e., actuated) segment. As such, the variable segment length *x* can be expressed as a function of ϕ:

$$x = \sqrt{a^2 + b^2 - 2ab\cos\phi} \qquad (4.1)$$

Based on this equation, the torque τ can be expressed as a function of the actuation force *F* and the angle ϕ:

$$\tau = F\left(\frac{dx}{d\phi}\right) = F\left(\frac{ab\sin\phi}{\sqrt{a^2 + b^2 - 2ab\cos\phi}}\right) \qquad (4.2)$$

As can be clearly seen from this equation, the moment arm length varies according to the joint angular position. Similarly, the torque requirement (as dictated by the locomotive needs) is also a function of the joint angle. To ensure a sufficient amount of torque supply over the entire range of motion, the design parameters are determined based on the graphical comparison conducted on the joint angle-torque plane (Figure 4-2). Specifically, for each motion mode, the torque curve is drawn by combining the corresponding joint angle trajectory and torque trajectory (both are given as functions of the percentage of the gait cycle), with data from related biomechanical literature ([1] for level walking and [4] for stair climbing). The available actuation torque, on the other hand, covers a certain range as defined by the maximum extension torque (positive) and the maximum flexion torque (negative). For the determination of the design parameters, the actuation torque range is expected to cover both torques curves to ensure ample torque supply. Furthermore, the powered knee joint is expected to provide sufficient

range of motion (0~95°), with the upper and lower limits determined according to the biomechanical data as well.
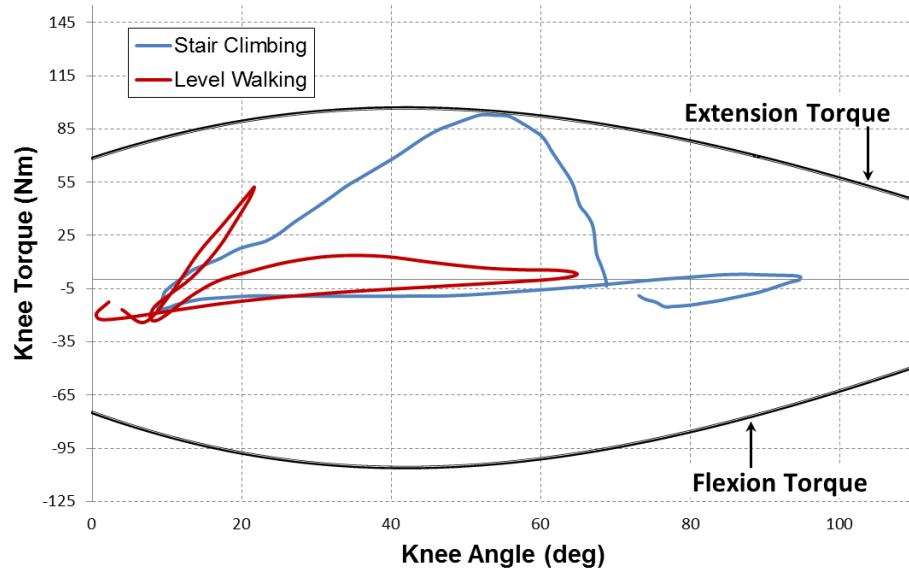
Figure 4-2 Comparison of the biomechanical torque curves versus the torque capacity of the powered knee joint

With an iterative design process, the design parameters were determined, as shown in Table 4-1.   The resulting torque capacity is also shown in Figure 4-2, as defined by the maximum extension and flexion torque curves.   From the comparison of the actuation torque capacity versus the desired torque curves, it can be clearly seen that the actuation system is able to provide sufficient torque to support the locomotion of an 85 kg individual.   Also, the powered knee joint provides a range of motion of 0~110°, exceeding the aforementioned requirement for locomotion.   The higher upper limit enables the user to bend the knee more to provide extra flexibility and comfort at the seated position.

Table 4-1 Design parameters of the knee prosthesis prototype

Parameter	Value	Unit
a	158	*mm*
b	46	*mm*
ϕ (when θ=0)	98	°

4.2.3   Overall design of the prosthesis

In the design process, a major challenge is to incorporate an off-the-shelf air tank into the prosthesis as the onboard pneumatic supply. The specific model of the air tank is Dura Pro SLP from Ninja Paintball (Crystal Lake, IL, USA), which has a volume of 0.74 L (45 in^3) that can be charged to 31 MPa. The large outer diameter (~94 mm) makes it difficult to fit the tank into the prosthesis. To solve this problem, the traditional central tubular supporting structure is replaced with an open-frame structure. This structure consists of two lateral supporting bars bearing the load applied by the prosthesis user, leaving the central space open to accommodate the air tank and the pneumatic actuator (Figure 4-3). As a result, the profile of the prosthesis is minimized to facilitate its practical use by amputee users. Besides, the flat surfaces of the supporting bars can be used as the basis for mounting various peripheral components in the prosthesis system.
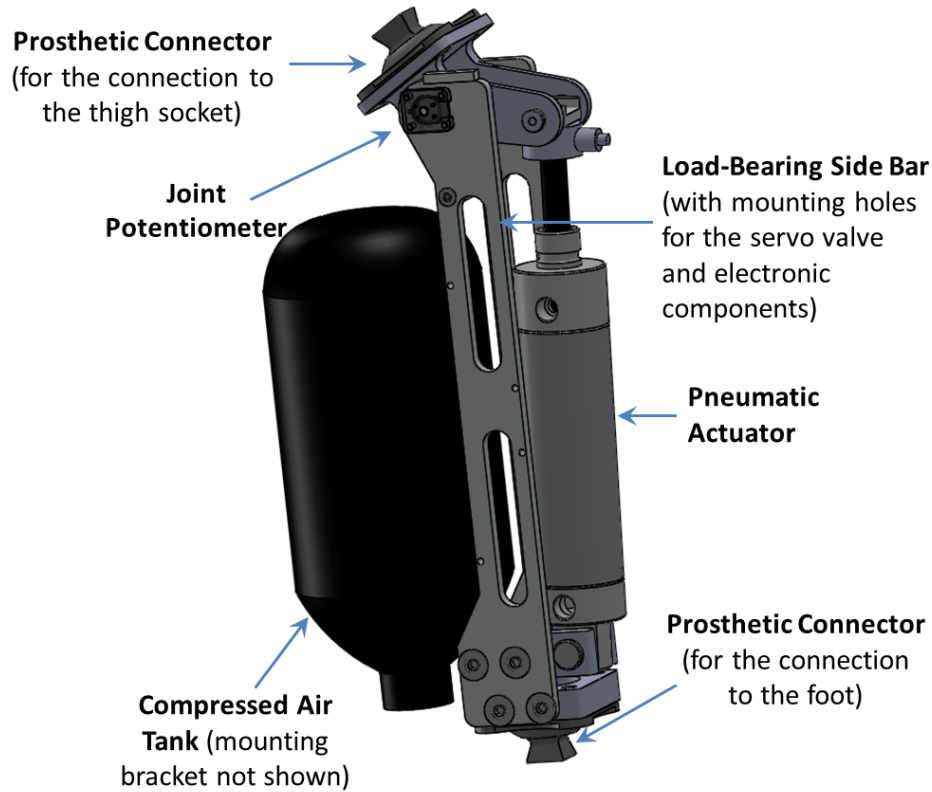
Figure 4-3 Solid model of the major components of the prosthesis

As a self-contained robotic device, the powered prosthesis incorporates various electronic and mechanical components for the control purpose. A high-speed proportional pneumatic valve (ZS-V-13000, Enfield Technologies, Shelton, CT, USA) is used to regulate the air flows to the pneumatic actuator. A compact tension/compression load cell (ELPF-500-T3E, Measurement Specialties, Hampton, VA, USA) is mounted inline with the actuator to measure the actuation force. A rotary potentiometer (RDC503, ALPS Electric, Japan) is embedded into the prosthetic joint to measure the joint angle. Additionally, to detect the important events in locomotion (e.g. heel strike and toe off), a pair of force-sensing resistors ((FSR400, Interlink Electronics, Camarillo, CA, USA) are mounted under the prosthetic foot to measure the ground contact force at the heel and toe. The signals generated from these sensors are collected by a microcontroller

(PIC16LF1709, Microchip Technology Inc., Chandler, AZ, USA), on which the prosthesis controller is implemented (details described in the subsequent section). Subsequently, the microcontroller generates the control command to the pneumatic valve to obtain the desired motion.

Note that the device presented in this chapter is a knee prosthesis, which only includes a powered knee joint. The knee prosthesis, on the other hand, is short enough (0.27 m in height) such that it can be used in conjunction with a powered ankle-foot prosthesis to form a complete transfemoral prosthesis. To reduce the complexity of the preliminary testing, the knee prosthesis is currently mounted with a commercial prosthetic foot (Lo Rider, Otto Bock, Germany) through an extension pylon. Figure 4-4 shows a unilateral transfemoral amputee fitted with the prosthesis.
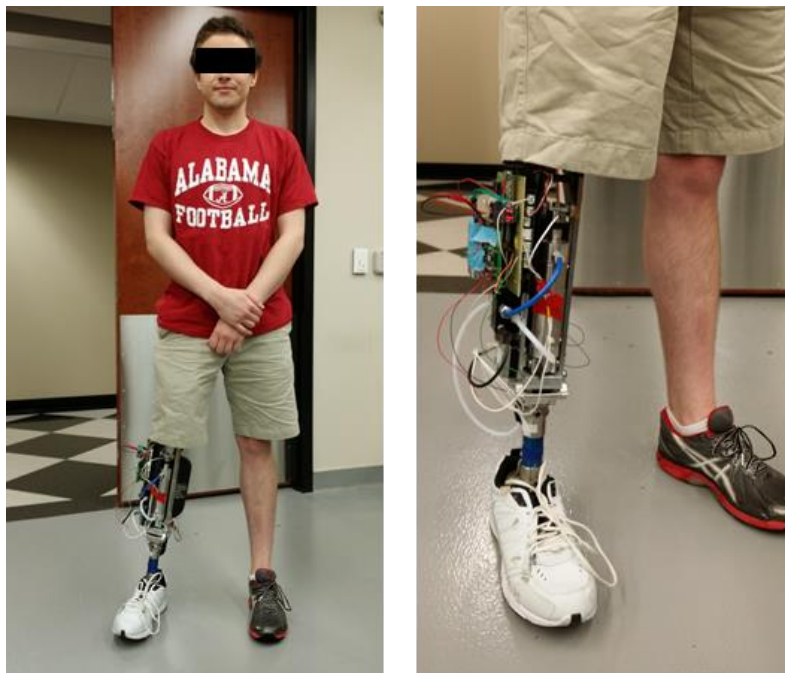
Figure 4-4 A transfemoral amputee fitted with the knee prosthesis

Last but not least, the authors experimentally measured the weight of the prosthesis since reducing prosthesis weight is a major target of the design. The prosthesis body weighs 2.27 kg, including the prosthetic connectors but excluding the prosthetic foot and the pneumatic tank. The prosthetic foot assembly, including an extension pylon and a regular running shoe, weighs 1.06 kg. The carbon-fiber air tank assembly, including the pressure regulator, weights 1.13 kg. The total weight of the prosthesis, including all the components above, is 4.46 kg, less than the 5.2 kg upper limit. In the future, the prosthesis weight can be further reduced by using lightweight material for load-bearing structure, and lightweight custom components (air tank, prosthetic foot, etc.) when such components become available.

4.3   Prosthesis control

As a human-assistive robotic device, the powered prosthesis is expected to function like its biological counterpart and generate a natural motion well-coordinated with the human body. Early works in transfemoral prosthesis control were focused on an "echo control" scheme, in which the knee motion of the unaffected side is recorded and serves as the motion command for the prosthetic joint with a half-stride delay. Echo control is able to provide symmetric reciprocating leg motion, but its effectiveness is challenged by multiple weaknesses. For example, the control is not done in a real-time manner (i.e. with a half-stride time delay), and the position-controlled prosthetic joint precludes the interaction with the user. To address these issues, Sup et al. developed a finite-state impedance control approach, with the innovation of regulating the dynamic behavior of the prosthetic joints in locomotion instead of dictating the joint trajectories [19]. With the new control philosophy, this approach is able to provide effective motion control while enabling user interaction with the prosthesis, a highly important feature for any robotic device serving human assistive purposes.

Adopting the finite-state impedance control framework, the prosthesis controller in this work is similar to that by Sup et al., but with details modified to adapt to the specific design of the powered knee prosthesis. Note that the current controller is developed for walking only, and the prosthesis control for stair climbing will be investigated in the future. As the first step of controller development, a state machine is established with four distinct states, representing the four phases in a gait cycle (Figure 4-5).
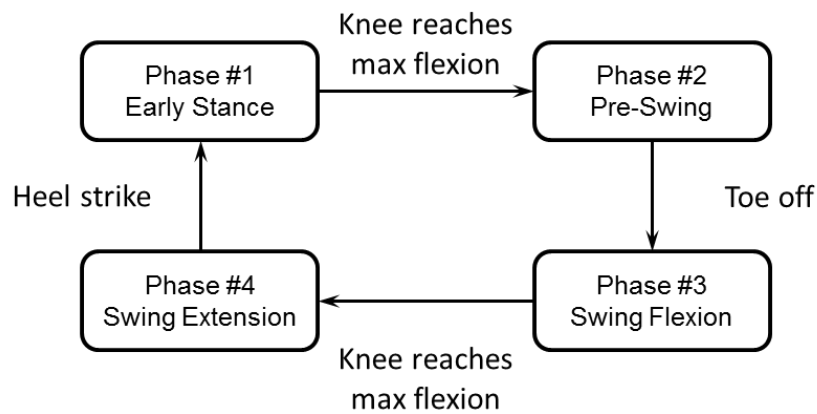
Figure 4-5 States and transitional conditions of the state machine

(1) Early Stance (ES). Triggered by heel strike, ES marks the start of a gait cycle. During this state, the knee maintains a high impedance to absorb the energy of ground contact and a stable support of the human body. As a result, the knee bends slightly after the initial ground contact occurs, and keeps absorbing energy until the maximum flexion is reached.

(2) Pre-Swing (PS). PS starts when the knee flexion reaches the maximum. This phase is usually associated with the generation of power to obtain the impetus for the forward motion.

(3) Swing Flexion (SF). Triggered by the toe-off, SF is associated with the flexion of the knee while the leg swings forward.

(4) Swing Extension (SE). SE starts when the knee starts to swing forward. In this mode, the knee will go back to the initial position, ready for the heel strike of the next gait cycle.

Note that each of the four states features a unique dynamic behavior, which forms the basis of motion control with the specific state. For the control implementation, the dynamic behavior is characterized with an impedance representation, i.e., the combination of an artificial spring and artificial damper, as expressed by the following equation:

$$\tau_d = -K(\theta - \theta_e) - B\dot{\theta} \tag{4.3}$$

where τ_d is the desired actuation torque, θ is the joint angle, $\dot{\theta}$ is the joint velocity, K is the stiffness of the implemented artificial spring, θ_e is the equilibrium position of the spring, and B is the damping value of the implemented artificial damper. The control parameters K, θ_e and B take a certain set of values corresponding to the current state, while the kinematic variables θ and $\dot{\theta}$ are measured with the rotary potentiometer embedded in the prosthetic joint. From an energetic point of view, the artificial impedance includes an energetically conservative artificial spring and an energetically dissipative artificial damper. As such, within each state, the prosthetic joint always dissipates energy, and thus eliminates the major cause of instability in the interaction (unwanted energy injection). On the other hand, from a global perspective, the prosthesis still remains energetically active by introducing a certain amount of energy into the system. This is achieved via the shift of the equilibrium point of the artificial spring, associated with the transition between consecutive states. This "globally active, locally passive" is expected to minimize the risk of instability while generating the desired power input to support the user's locomotion.

The state machine (Figure 4-5), combined with impedance-based joint behavior representation (Eq. 4.3), generates the desired actuation torque command for the powered knee joint. To obtain this desired actuation torque, the torque command, as calculated from (3), is converted to the desired actuation force according to the actuation mechanism shown in Figure 4-1. The following equation is derived for this purpose:

$$F_d = \tau_d \left(\frac{\sqrt{a^2 + b^2 - 2ab\cos\phi}}{ab\sin\phi} \right) \tag{4.4}$$

The desired force, as calculated by the above equation, is compared with the measured actuation force to generate the error signal $e = F_d - F$. Based on this error signal, the standard Proportional-Integral-Derivative (PID) control is applied to obtain the valve command for the real-time implementation of the controller. The control gains were tuned in the experiments to generate a quick response without jeopardizing stability in operation.

4.4   Experimental results

After finishing the design of the prosthesis, the authors have fabricated a self-contained prototype with all peripheral components integrated. As a preliminary evaluation of the prosthesis performance, treadmill walking experiments have been conducted to evaluate the prosthesis' performance in restoring an amputee user's locomotion functions. The experimental protocol is approved by the Institutional Review Board of the University of Alabama. A unilateral amputee participated in the study. The male participant was 21 years old, 178 cm in height, and weighed 57 kg.

In the experiments, repeated tuning was conducted to obtain the control parameters with satisfactory performance. As a quantitative evaluation of the gait quality, the trajectory of the

prosthetic joint was compared with the standard joint trajectory in biomechanical literature (such as [1]). Additionally, visual observation and feedback from the test subject were also used for the adjustment of control parameters. The control parameters obtained from the tuning are summarized in Table 4-2. A typical sequence of snapshots of the walking gait is shown in Figure 4-6. Figure 4-7 displays a comparison between the angular trajectories of the prosthetic joint versus the biological joint, utilizing the standard biomechanical data in [1]. As shown in the figure, the prosthetic joint trajectory is smooth and close matches the standard joint trajectory. It is worth mentioning that the prosthesis controller does not directly control the joint trajectory. Instead, the trajectory in walking is generated as a result of the dynamic interaction between the user and the prosthesis, and thus serves as a good indication of the gait quality in the experiment. As such, the close match of the prosthetic joint trajectory to the standard biomechanical trajectory indicates the prosthesis is able to provide a stable and comfortable walking experience for the user, which has been verified by the oral feedback from the test subject.

Table 4-2 Parameters of the prosthesis controller

State	K (N-m/deg)	B (N-m-s/deg)	θ_0 (deg)
ES	2	0.01	2
PS	1	0.01	30
SF	0.34	0.01	48
SE	0.5	0.005	-12
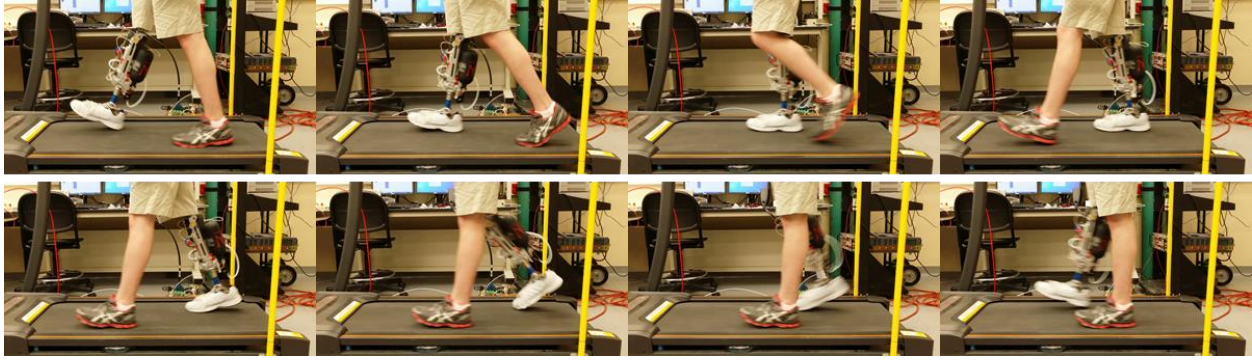
Figure 4-6 A sequence of snapshots of the walking gait (from left to right, top to bottom)
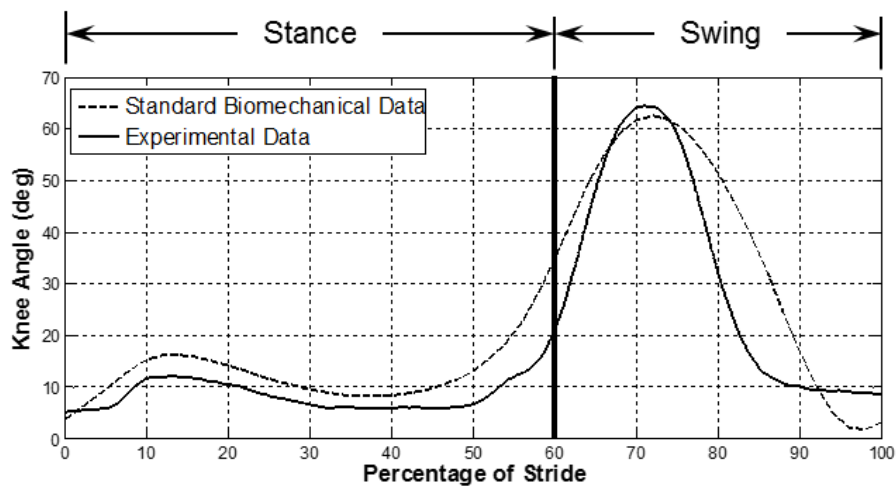
Figure 4-7 Comparison of the trajectory of the prosthetic knee joint versus the standard knee trajectory of healthy subjects in level walking (data from [1])

4.5 Conclusions

This chapter presents a unique robotic knee prosthesis design that utilizes a pneumatic actuator to drive the prosthetic knee joint. The pneumatic actuator was selected because of its excellent actuation performance, combining large force and power outputs with a compact, light-weight package. Through the design calculation based on an inverted crank-slider mechanism, the design parameters were determined. A graphical comparison was conducted between the desired joint torque (required for level walking and stair climbing) and the torque capacity

provided by the actuator. The resulted figure indicates that the powered knee is able to provide sufficient torque output for an 85 kg user in these important, energetically demanding locomotive modes. The prosthesis also incorporates the necessary peripheral components (servo valve, air tank, etc.) and sensors (load cell and potentiometer) to make it a completely self-contained device, with the total weight below the desired weight target. A prosthesis control algorithm has also been developed and tuned. Through the experiments conducted on an amputee user, the prosthesis has been demonstrated to provide a knee trajectory similar to that in the walking of healthy subjects, suggesting a natural walking experience for the prosthesis user.

4.6 Acknowledgement

References

[1]   Winter, D.A. (1991) *The Biomechanics and Motor Control of Human Gait: Normal, Elderly and Pathological.* 2nd edition, Waterloo, ON, University of Waterloo Press.

[2]   Jacobs, R., Bobbert, M.F., van Ingen Schenau, G.J. (1996) "Mechanical output from individual muscles during explosive leg extensions: the role of biarticular muscles." *Journal of Biomechanics*, vol. 29, no. 4, pp. 513-523.

[3]   Nagano, A., Ishige, Y., and Fukashiro, S. (1998) "Comparison of New Approaches to Estimate Mechanical Output of Individual Joints in Vertical Jumps." *Journal of Biomechanics*, vol. 32, no. 10, pp. 951-955.

[4]   Riener, R., Rabuffetti, M., and Frigo, C. (2002) "Stair ascent and descent at different inclinations." *Gait and Posture*, no. 15, pp. 32-44.

[5]   Nadeau, S., McFadyen, B.J., and Malouin, F. (2003) "Frontal and sagittal plane analyses of the stair climbing task in healthy adults aged over 40 years: What are the challenges compared to level walking?" *Clinical Biomechanics*, vol. 18, no. 10, pp. 950-959.

[6]   Waters, R., Perry, J., Antonelli, D., and Hislop, H. (1976) "Energy cost of walking amputees: the influence of level of amputation." *Journal of Bone and Joint Surgery*, vol. 58A, pp. 42-46.

[7]   Flowers, W.C., and Mann, R.W. (1977) "Electrohydraulic knee-torque controller for a prosthesis simulator." *ASME Journal of Biomechanical Engineering*, vol. 99, no. 4, pp. 3-8.

[8]   Popovic, D. and Schwirtlich, L. (1988) "Belgrade active A/K prosthesis." in de Vries, J. (Ed.), *Electrophysiological Kinesiolog*y, Interm. Congress Ser. No. 804, Excerpta Medica, Amsterdam, The Netherlands, pp. 337–343.

[9]   Hata, N. and Hori, Y., (2002) "Basic research on power limb using gait information of able-side leg." *7th International Workshop on Advanced Motion Control*, pp. 540-545.

[10]   Fite, K., Mitchell, J., Sup, F., and Goldfarb, M. (2007) "Design and control of an electrically powered knee prosthesis." *Proceedings of the 2007 IEEE 10th International Conference on Rehabilitation Robotics*, pp. 902-905.

[11]   Sup, F., Varol, H.A., Mitchell, J., Withrow, T.J., and Goldfarb, M. (2009) "Preliminary evaluations of a self-contained anthropomorphic transfemoral prosthesis." *IEEE/ASME Transactions on Mechatronics*, vol. 14, no. 6, pp. 667-676.

[12]   Martinez-Villalpando, E.C. and Herr, H. (2009) "Agonist-antagonist active knee prosthesis: A preliminary study in level-ground walking." *Journal of Rehabilitation Research & Development*, vol. 46, no. 3, pp. 361-374.

[13]   Hoover, C.D., Fulk, G.D., and Fite, K.B. (2012) "The design and initial experimental validation of an active myoelectric transfemoral prosthesis." *ASME Journal of Medical Devices*, vol. 6, p. 011005.

[14]   Goldfarb, M., Barth, E. J., Gogola, M. A., & Wehrmeyer, J. A. (2003). Design and energetic characterization of a liquid-propellant-powered actuator for self-powered robots. *Mechatronics, IEEE/ASME Transactions on*, *8*(2), 254-262.

[15]   Fite, K. B., & Goldfarb, M. (2006). Design and energetic characterization of a proportional-injector monopropellant-powered actuator. *Mechatronics, IEEE/ASME Transactions on*, *11*(2), 196-204.

[16]   Wu, S.-K., Driver, T., and Shen, X. (2012) "Design and control of a pneumatically actuated lower-extremity orthosis." *ASME Journal of Medical Devices*, vol. 6, no. 4, p. 041004.

[17]   Wu, M., Driver, T., Wu, S.-K., and Shen, X. (2014) "Design and preliminary testing of a pneumatic muscle-actuated transfemoral prosthesis." *ASME Journal of Medical Devices*, vol. 8, no. 4, p. 044502.

[18]   Wu, M., Zheng, H., and Shen, X. (2015) "A pneumatically actuated knee prosthesis." *ASME Journal of Medical Devices*, vol. 9, no. 3, p. 030911.

[19]   Sup, F., Bohara, A, and Goldfarb, M. (2008) "Design and control of a powered transfemoral prosthesis." *The International Journal of Robotics Research*, vol. 27, no. 2, pp. 263-273.

[20]   Clauser, C. E., McConville, J. T., & Young, J. W. (1969). *Weight, volume, and center of mass of segments of the human body*. ANTIOCH COLL YELLOW SPRINGS OH.

[21]   Beater, P. (2007) *Pneumatic Drives: System Design, Modelling and Control*. Springer-Verlag Berlin Heidelberg.

5   WALKING – STAIR CLIMBING CONTROL FOR POWERED KNEE PROSTHESES

(*Proceedings of The ASME Dynamic Systems And Control Conference,* **2016**)

Recent progresses in powered lower-limb prostheses have the potential of enabling amputee users to conduct energetically demanding locomotive tasks, which are usually beyond the capability of traditional unpowered prostheses. Realizing such potential, however, requires responsive and reliable control of the power provided by prosthetic joints. In this chapter, an integrated walking-stair climbing control approach is presented for transfemoral prostheses with powered knee joints. Leveraging the similarities between walking and stair climbing, this new approach adopts the general finite-state impedance control framework. Furthermore, important modifications are introduced to model the biomechanical characteristics that are beyond the capability of standard impedance control. The transition between the walking and stair-climbing modes is triggered through the real-time measurement of the spatial orientation of the user's thigh, which provides a reliable indicator of the user's intention of making such transition. This new control approach has been implemented on a powered knee prosthesis, and its effectiveness was demonstrated in human subject testing.

5.1   Introduction

For individuals with mobility-related disabilities, climbing upstairs is a highly challenging task in their daily life. This is especially true for transfemoral (i.e., above-knee) amputees, considering the significant role played by the biological knee in stair climbing. Due to the upward motion of the body center-of-gravity, the knee has to expend a substantial amount of

torque and power to lift the human body in stair climbing. Biomechanical studies indicate that the knee generates a peak torque of 1.1 N-m/kg (normalized to the body weight) [1], or 82.5 N-m for an 85 kg person. This value almost doubles the peak torque for level walking (0.615 N-m/kg according to Winter [2]). Furthermore, the peak power generation by the knee in stair climbing reaches 2.5 W/kg, or 213 W for an 85 kg person, far exceeding that in level walking (0.75 W/kg according to Winter [2]). The loss of knee function seriously affects the mobility of transfemoral amputees in such energetically-demanding motion modes.

Traditionally the lost limb functions for transfemoral amputees are replaced with passive prosthetic devices, which lack the ability of generating positive power output in the prosthetic joints. These passive prostheses are capable of restoring the walking functions for the amputee users, despite the existence of a few common problems (greater energy expenditure [3], higher hip torque [2], etc.). However, energetically demanding locomotive modes, such as stair climbing and upslope walking, are beyond the capability of such devices. This significant deficiency motivated researchers to take on the challenge of developing powered transfemoral prostheses. The pioneering work in this area was conducted by Flowers and Mann, which uses a hydraulic actuator to actuate the knee joint [4]. However, multiple drawbacks with hydraulics, such as leakage and lack of a compact supply, make it less attractive for prosthetic applications. Currently, most powered transfemoral prostheses are actuated with electric motors [5-10], e.g. Sup et al. developed a powered knee and ankle prosthesis with both joints powered with DC motor – ball screw assemblies [8]; Martinez-Villalpando and Herr developed a powered knee prosthesis with two series-elastic actuators positioned in parallel in an agonist-antagonist arrangement [9]; Hoover et al. developed a myoelectric transfemoral prosthesis, in which the powered knee is controlled with an EMG-based motion controller [10]. Additionally, Ossur, a

leading orthopedics company, manufactured the Power Knee, the first commercially available powered transfemoral prosthesis. According to the available technical information, the Power Knee is also actuated with an electric motor. In addition to these motor-powered devices, pneumatically-actuated prostheses have also been developed by researchers including the authors' group, for example, the prototypes powered with pneumatic cylinders [11] and muscle actuators [12].

Most of the powered prostheses mentioned above are able to provide sufficient joint torque and power required for stair climbing. Making full use of such capability, however, requires an effective and reliable controller to regulate the joint power delivery in motion. Currently, walking controller for powered prostheses have been well established. Typical approaches include echo control, which controls the prosthetic joint to track the recorded sound-side motion with a half-cycle delay [13]; and finite-state impedance control, which implements an artificial impedance within each phase of the gait cycle [11]. Electromyography has also been attempted in obtaining the user's motion intent and generating the corresponding motion command [14]. Some of the walking control approaches have been adapted for stair climbing control. For example, Lawson et al. developed a stair ascent/descent controller for powered transfemoral prostheses, based on the aforementioned finite-state impedance control framework [15]; Hoover et al. developed a myoelectric stair ascent controller, which regulates the knee torque directly based on the measured EMG signals [16].

Different from these existing works, the control approach in this chapter is an integrated walking – stair climbing control system, which not only provides natural locomotive experience for an amputee user within each mode, but also enables the user to switch between these locomotive modes in a natural and responsive manner. Furthermore, the individual controller for

each motion mode is developed based on a comprehensive analysis and modeling of the biomechanical characteristics of the biological knee, which contains important augmentation to the existing impedance control framework. The details on the biomechanical analysis and modeling are provided in the subsequent section, following by the control system design and the results of the human subject testing of the proposed control system.

5.2   Biomechanical modeling of human walking and stair climbing

Biomechanics in human walking and stair climbing are topics of intense interest from the research community, and a large body of data are available through various studies. Ideally, a prosthesis controller should replicate the biomechanical characteristics displayed in human locomotion, providing the amputee user a control experience similar to that of biological limbs. However, replicating the kinematic and kinetic data in prosthesis control is unfeasible, not only because of the poor repeatability and large inter-subject variability, but also because of the interactive nature of the human locomotion. The biomechanics in human locomotion is a result of interaction between the human limb segments/joint, the rest of the human body, and the environment. Enforcing a prerecorded joint motion or torque trajectory precludes such interaction, generating a poor experience for the prosthesis user.

To obtain effective control in human-robot interaction, a widely accepted control theory is impedance control [17].

Instead of enforcing a motion or torque/force trajectory, an impedance controller implements an artificial impedance (artificial spring combined with artificial damper), which is essentially a relationship between force/torque and motion. This control framework has been widely used in robot control for a variety of purposes such as obstacle avoidance in robotic

manipulation. In recent years, impedance control, in conjunction with the finite-state machine approach, has been successfully introduced into lower-limb prosthesis control [11].

Impedance control, however, has its limitation stemming from its inherent dynamic characteristics. The dominant element in the artificial impedance, virtual mechanical spring, generates a force in the opposite direction as the displacement:

$$\tau_{spring} = -K(\theta - \theta_e) \tag{5.1}$$

where K is the stiffness of the virtual spring and θe is the equilibrium point of the virtual spring. Such condition can be met for the majority of phases during a gait cycle, but exceptions still exist and they have to be treated differently. In the remainder of this section, the biomechanics of the knee is analyzed for both walking and stair climbing, applying the augmented impedance control approach that complements the impedance control with a time-based torque function.

5.2.1   Biomechanical modeling of walking

To understand and model the way humans regulates knee torque during walking, a graphical approach is adopted. As the basis of this work, existing biomechanical data from Winter [2] are utilized to generate a trajectory on the knee angle-torque plane, as shown in Figure 5-1. Specifically, Figure 5-1a is the trajectory of knee angle, and Figure 5-1b is the trajectory of the knee torque. For each data point of stride percentage, the corresponding joint angle and torque can be paired to locate a point on the joint angle-torque plane. Connecting all such points in sequence, a joint angle-torque trajectory can be obtained, as shown in Figure 5-1c.

It is important to understand the sign convention used in Figure 5-1. As shown in Figure 5-2, the knee angle is defined as the angle of flexion from the knee-straight position. As such,

knee flexion results in the increase of the joint angle. Conversely, the knee torque is defined as the extensional torque, which has the effect of extending the knee. The reason behind such definition is the significant amount of torque for knee extension in human locomotion, which dominates the torque for knee flexion. As such, defining the extensional torque positive renders the figure more readable. Such definition, however, also dictates that the angle-torque curve for a virtual spring extend to the upper-right corner, i.e., with a positive slope. Virtual spring-based modeling of the biomechanical data must meet this requirement to be valid.
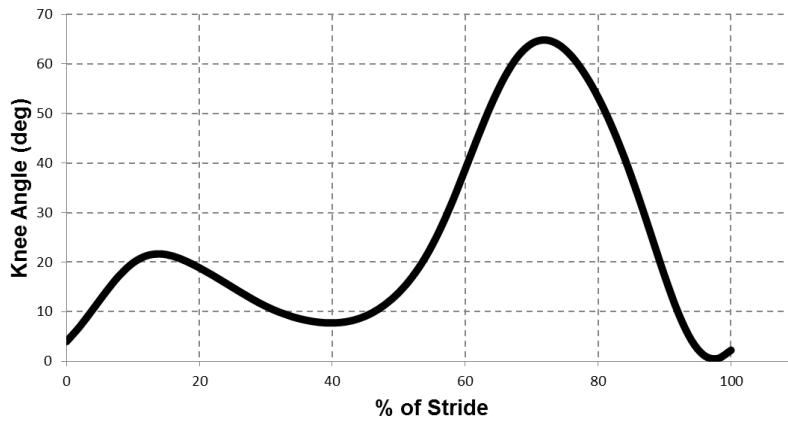
(a)
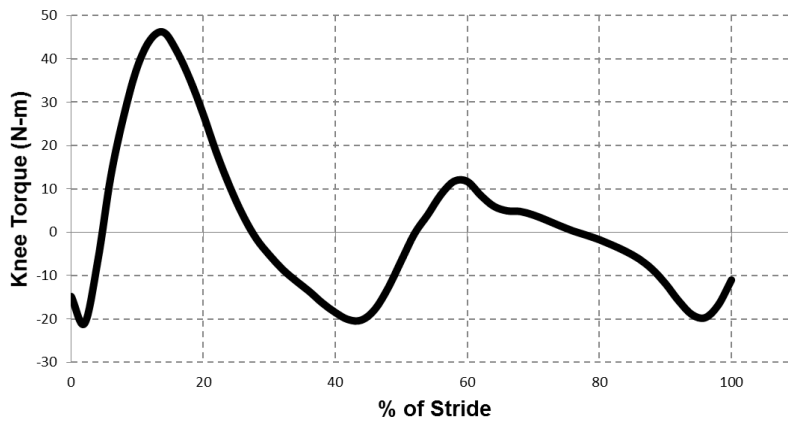
(b)
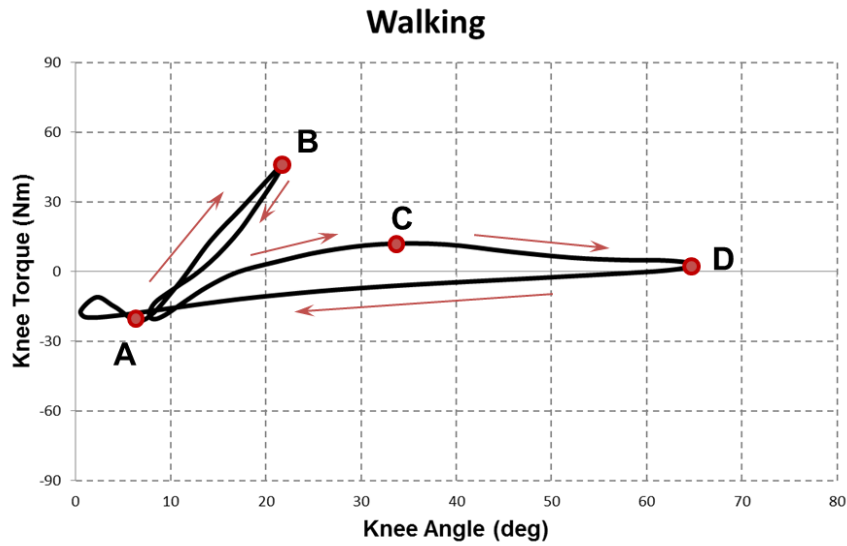
(c)

Figure 5-1 Angle trajectory (a), torque trajectory (b), and angle-torque trajectory (c) of the knee in level walking
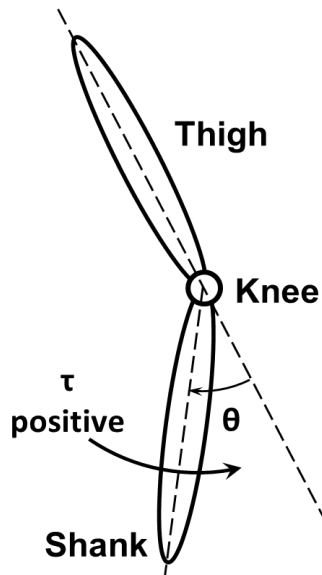
Figure 5-2 Sign convention of the knee angle and torque

Subsequently, piece-wise segmentation is conducted to divide the gait cycle into a number of phases, each with a set of distinct dynamic characteristics. Following is a list of important points (most of which are also transitional points between phases):

Point A: Heel strike, marking the beginning of a gait cycle.

Point B: Maximum knee flexion during weight acceptance.

Point C: Toe-off, marking the transition from stance to swing.

Point D: Maximum knee flexion during swing.

And the gait phases are defined correspondingly:

Phase #1: Early Stance (A → B → A). During this first phase of the gait cycle, the knee deflects slightly under the initial ground contact to absorb the impact energy. In this process, the joint maintains high stiffness to avoid the collapse of the knee and provide stable support to the human body. Such dynamic behavior can be clearly identified in the angle-torque curve (Figure 5-1c). At Point A (heel strike), the knee is slightly flexed (~5°) with a small flexional torque (~20 N-m). After the heel strike, the knee displayed further flexion under the dynamic load until reaching the maximum flexion (Point B). In this process, the joint torque increases in value and reaches the maximum extensional torque of ~46 N-m. Subsequently, the knee starts to extend with the knee torque decreasing proportionally with the joint angle. At the end of this phase, the joint angle and torque return to approximately the same values as at the heel strike. The biomechanical joint behavior within this phase can be modeled with a very stiff virtual spring, as shown in Figure 5-3. For a 75 kg subject, the spring stiffness is approximately 5 N-m/deg with the equilibrium at ~12°.

Phase #2: Pre-Swing (A → C). In this phase, the knee experiences fast flexion to prepare for the subsequent swing phase. Under the flexional torque in the joint as well as the dynamic load of walking, the knee accelerates in its flexion at the beginning of this phase. The flexional torque starts at the maximum value and decreases with the joint angle. After the torque reduces

to zero, the flexion continues and the joint torque turns extensional. The extensional torque increases with the joint angle. The biomechanical joint behavior within this phase can be modeled with a soft virtual spring, with the stiffness of ~1 N-m/deg and equilibrium at 24°.

Phase #3: Swing flexion (C → D). In this phase, the knee continues to flex until reaching the maximum flexion in the gait cycle. Note that the joint torque decreases with the joint angle in this phase. Such behavior cannot be modeled with a virtual spring. On the other hand, the joint torque is opposite to the joint motion, and eventually reduces to zero when the joint motion stops. The dynamic behavior, therefore, is largely dissipative, and thus can be modeled with a mild virtual damper. Based on the biomechanical data by Winter [2], the peak joint velocity is ~5 rad/s, and the damping coefficient can be calculated as ~2.4 N-m-s/rad.

Phase #4: Swing extension (D → A). In this phase, the knee experiences fast extension to return to the original position of the gait cycle, preparing for the start to the next gait cycle. In this process, the knee generates a flexional torque that increases with the extension of the knee. Such behavior can be modeled with a mild virtual spring, with the stiffness of ~0.4 N-m/deg and the equilibrium at ~65°.
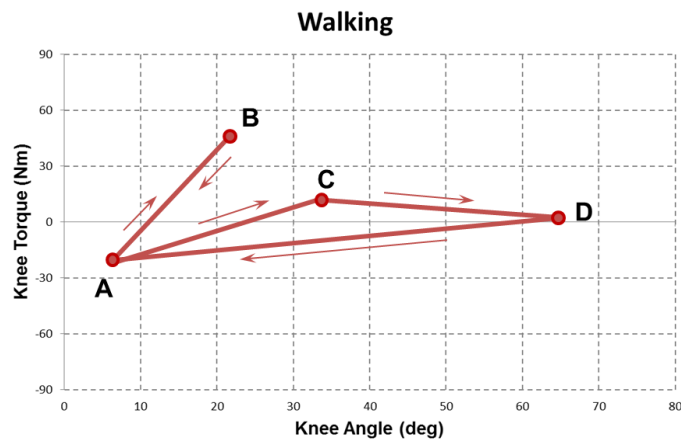
Figure 5-3 Modeling of the knee dynamic behavior in walking

5.2.1   Biomechanical modeling of stair climbing

A similar graphic approach is used to model the biomechanical behavior of the knee in stair climbing. Stair climbing is similar to walking in that the motion is cyclic with similar sequence of phases. Stair climbing, however, is significantly more challenging for lower-limb amputees because of the upward movement of body center-of-gravity (COG). Such body COG motion requires the knee to contribute significant amount of power and torque to lift the human body in stair climbing. Based on the biomechanical data from Riener et al. [1], knee angle and torque trajectories are plotted, as show in Figure 5-4a and 4b. Combining these plots, a joint angle-torque trajectory is generated, as shown in Figure 5-4c. Based on this trajectory, a few critical points are identified that segment the gait cycle into different phases. The following is a list of such critical points:

Point A: ground contact, marking the start of the gait cycle.

Point B: maximum extensional torque.

Point C: knee straight, when the knee is extended to the maximum.

Point D: maximum knee flexion.

These critical points divide the gait cycle into a number of states with distinct dynamic characteristics:

Phase #1: Weight Acceptance (A → B). In this phase, the knee generates a gradually increasing extension torque to allow the support leg to accept the weight of the human body. At ground contact, the knee torque is approximately zero, while at the peak the knee torque can reach over 80 N-m. Furthermore, the knee extends slightly when the extensional torque

84

increases, indicating that energy is gradually injected into the knee (as opposed to the complete injection at the phase transition). Such behavior cannot be modeled with virtual impedance, which is dissipative in nature. To address this problem, an alternative time-function approach is utilized. Based on the desired speed of weight acceptance, the knee torque increases as a function of time, and reaches the maximum at the end of this phase:

$$\tau_t = G(t - t_0) \tag{5.2}$$

where t is the current time, t_0 is the starting time, and G is a positive constant.
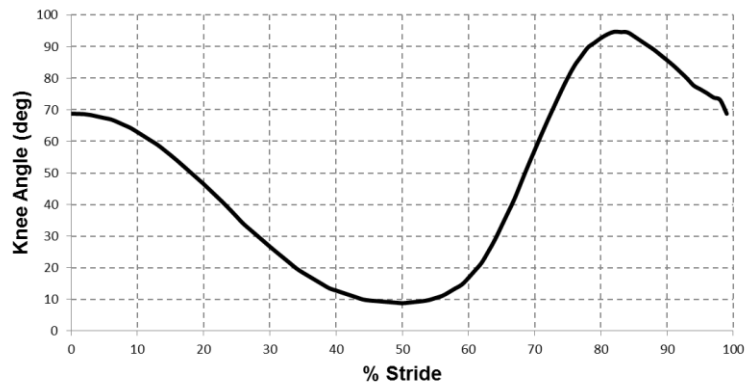
(a)
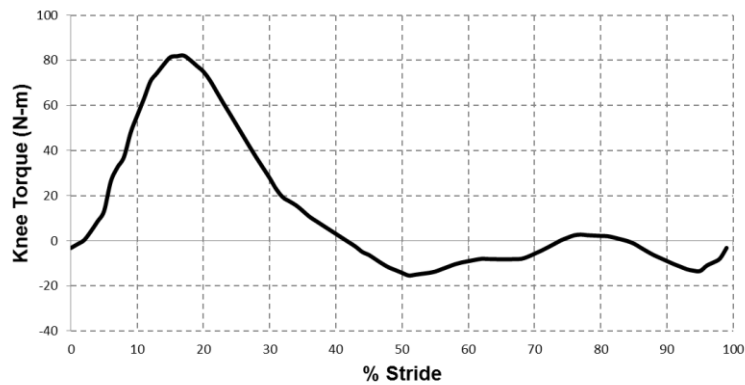
(b)
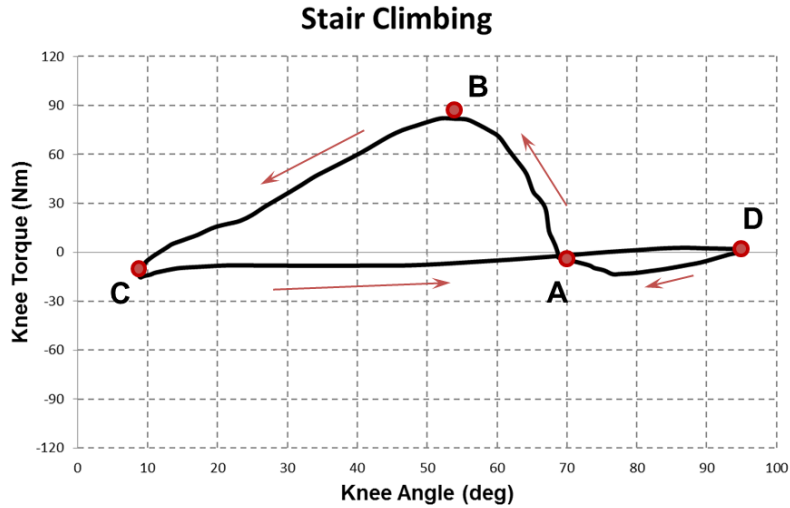
(c)

Figure 5-4 Angle trajectory (a), torque trajectory (b), and angle-torque trajectory (c) of the knee in stair climbing

To simplify the tuning, a proportional function is used, as shown in the equation above. The joint motion during this phase has a nearly constant velocity, and thus the angle-torque trajectory modeled with the time function can be expressed with a straight line segment, as shown in Figure 5-5.
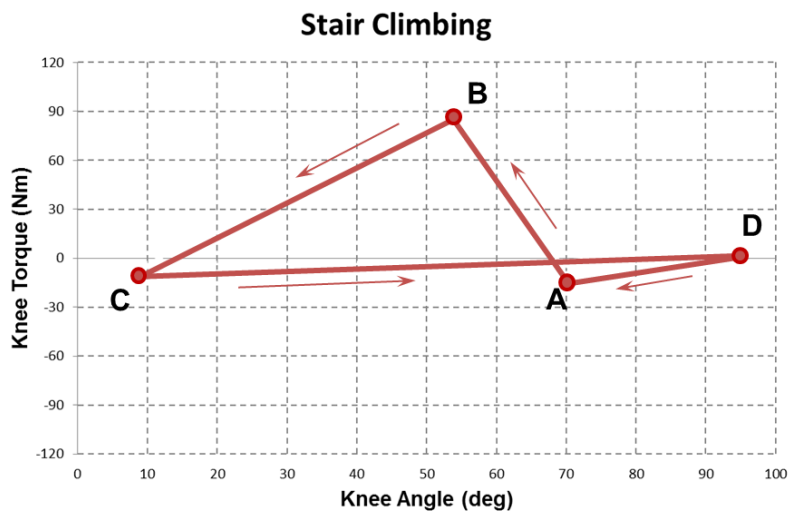
Figure 5-5 Modeling of the knee dynamic behavior in stair climbing

86

Phase #2: Push-Off (B → C). After reaching the maximum joint torque, the knee starts to extend to lift the human body up the stair. In this process, the extensional torque in the knee decreases with the joint extension, and reduces to a negative value (i.e., becomes a low flexional torque) at the end of this phase. The dynamic behavior in this phase can be modeled with a relatively stiff virtual spring, with the stiffness at 2 N-m/deg and the equilibrium at ~14°.

Phase #3: Swing Flexion (C → D). Shortly after the knee reaches the straight position, the swing phase starts. The knee torque starts from a mild flexional torque of ~15 N-m, and gradually reduces to almost zero at the end of this phase. Under the joint torque as well as the torque of gravity, the joint experiences rapid flexion until reaching the final angle of ~95°. The dynamic behavior in this phase can be modeled with a soft virtual spring, with the stiffness at 0.1 N-m/deg and the equilibrium at ~95°.

Phase #4: Swing Extension (D → A). In this last phase of the gait cycle, the knee swings back (i.e., extends) by approximately 30°, with the purpose of providing the correct posture to prepare for the subsequent landing of the foot. In this process, the knee generates a flexional torque that increases during the majority of this phase. At the end of this phase, the torque gradually reduces to zero. The dynamic behavior of the knee in this phase is largely dissipative, allowing the foot position to be regulated in the desired way. As such, it can modeled with a soft virtual spring combined with a mild virtual damper. To simplify the modeling representation, the angle-torque curve in this phase is a straight line segment, while the Phase 1 curve is extended downward slightly to account for the decreasing torque at the end of this phase, as shown in Figure 5-5.

5.3 Walking-stair climbing control system design

Considering the purpose of the knee prosthesis in restoring the lost functions of the amputee user's biological knee, the prosthesis controller is expected to emulate how a human controls his/her biological knee in locomotion. The biomechanical modeling presented in the previous section, therefore, serves as the basis of the subsequent control system design. The control system is comprised of a walking controller, a stair climbing controller, and a gait mode switching mechanism, with the details presented below.

5.3.1 Walking controller

Based on the biomechanical modeling of the knee's dynamic behavior in walking, impedance characterization can be applied in all four phases in the gait cycle. As such, the walking controller is developed by combining a finite state machine with an impedance controller within each state. The states of the controller, as well as the switching conditions, are depicted in Figure 5-6.
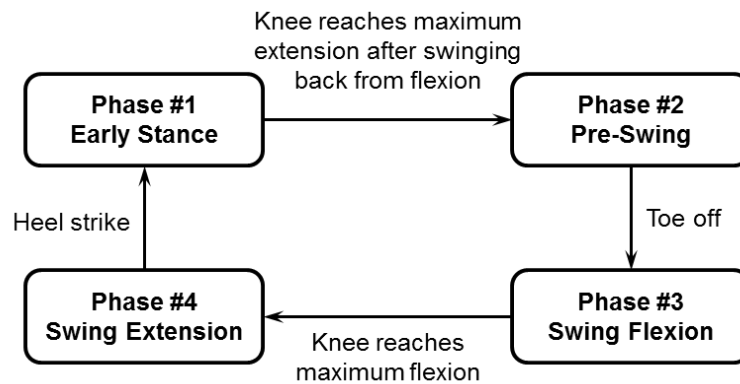
Figure 5-6 State diagram of the walking controller

Characteristics of the impedance controllers can be summarized as follows: 1) in Early Stance, the controller implements a very stiff virtual spring to provide stable support under the dynamic loading of ground contact, complemented with a relatively strong damper to damp out

the impact in the process; 2) in Pre-Swing, a soft virtual spring combined with a mild damper is implemented to provide resistance to the rapid knee flexion, keeping the swing speed under control; 3) in Swing Flexion, a mild virtual damper is implemented to slow down the flexion and prepare for the subsequent motion reversal; 4) in Swing Extension, a soft virtual spring combined with a mild damper is implemented to provide resistance to the rapid knee extension, keeping the motion in motion to prepare for the heel strike in the subsequent gait cycle.

5.3.2   Stair climbing controller

Unlike the biomechanics in walking, stair climbing involves a phase (Weight Acceptance) that cannot be modeled with impedance characterization. The dynamic behavior in this phase, therefore, is represented by time-based ramp-up function. Furthermore, the ramp-up function can be combined with the impedance controller in the subsequent phase (Push-Off), and thus the two phases can be implemented as a single phase in the controller. The state diagram of the stair climbing controller is shown in Figure 5-7.
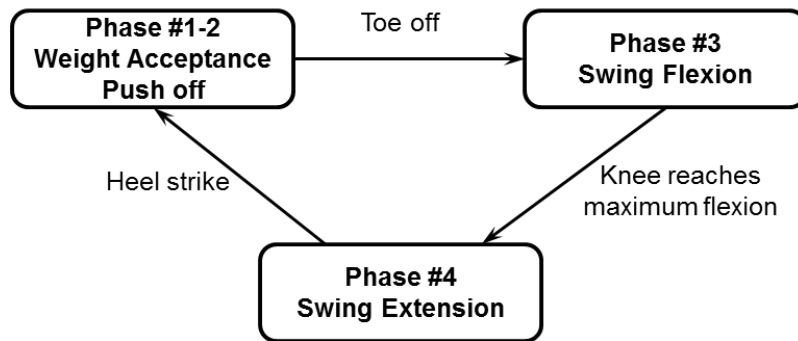
Figure 5-7 State diagram of the stair climbing controller

Specifically for the "Phase #1-2" in Figure 5-7, the ramp-up impedance controller can be expressed by the following equation:

$$\tau_{ru-imp} = R\left(\frac{t-t_0}{T}\right)\tau_{imp}\left(\theta, \dot{\theta}\right) \tag{5.3}$$

In Eq. (6.3), $\tau_{imp}(\theta, \dot{\theta})$ is the impedance function as defined by the following equation:

$$\tau_{imp} = K(\theta - \theta_e) + B\dot{\theta} \tag{5.4}$$

where B is the damping coefficient of the virtual damper, and $R\left(\dfrac{t-t_0}{T}\right)$ is the ramp-up function

defined as follows:

$$R\left(\frac{t-t_0}{T}\right) = \begin{cases} \dfrac{t-t_0}{T} & when \ \dfrac{t-t_0}{T} < 1 \\ 1 & otherwise \end{cases} \tag{5.5}$$

where, t_0 is the starting time, t is the current time, and T is the length of the ramp-up period. During the ramp-up period, the function outputs a value proportional to the elapsed time. After the ramp-up period, the output remains at 1, and thus the controller becomes the standard impedance controller. T is a tunable parameter that can be adjusted according to the gait speed. Also, the impedance parameters, including the virtual spring stiffness and virtual damping coefficient, are also tunable parameters. In this phase, the controller implements moderate virtual spring that reduces the torque output when the knee extends, complemented with a moderate virtual damper to keep the extension speed under control.

The other two states in the controller can both be implemented with the standard impedance controller. In Swing Flexion, a very soft virtual spring is implemented, while in Swing Extension, a virtual spring slightly stiffer than that in Swing Flexion is implemented, complemented with a mild virtual damper. A smooth swing motion can be obtained through experimental tuning of the control parameters in the impedance controller.

5.3.3   Walking – stair climbing transition mechanism

From the biomechanical analysis in the previous section, it can be clearly seen that these gait modes have strong similarities in various aspects. The major difference, apparently, is the

upward motion of the human body in stair climbing, which is not present in walking. On the joint and limb motion level, successful foot landing on the next step in stair climbing requires the thigh to be lifted significantly higher than in walking. Biomechanical data on the hip motion also support this observation. In walking, the hip angle goes up to approximately 25º in swing [2], while in stair climbing, the hip angle can go up to 70º or higher [1]. The significant difference in the hip motion can be used as clear indicator for the mode transition between walking and stair climbing. In the control implementation, a threshold value θ_T for the thigh spatial position (with respect to the vertical direction) can be found through repeated experimental tuning to serve as the transitional condition. The complete control system diagram is shown in Figure 5-8. Note that, due to the limitation of the available testing facility, only the unidirectional transition from walking to stair climbing can be tested, but the method can be easily extended to the transition in the opposite direction.
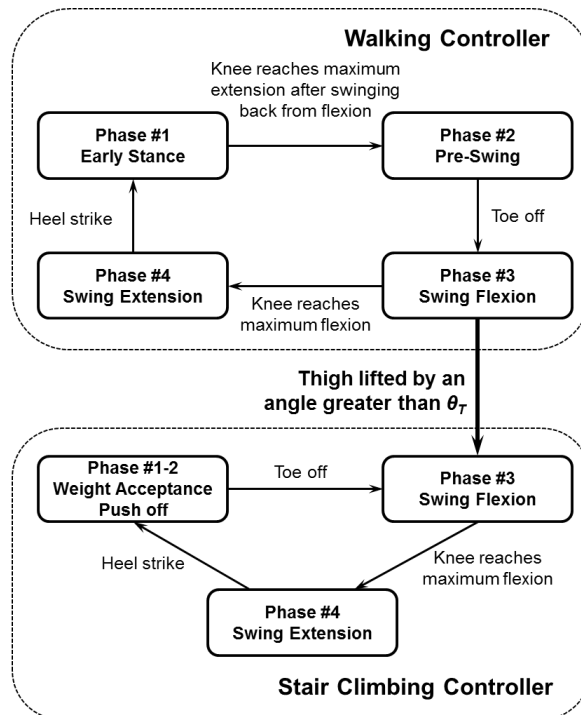
Figure 5-8 State diagram of the complete control system

5.4   Preliminary testing results

To demonstrate the effectiveness of the walking – stair climbing controller, the authors conducted a set of human subject experiments at the HUman-centered BioRobotics (HUB-Robotics) Laboratory at The University of Alabama. The human subject participated in the testing was a 21-year-old male unilateral amputee, 178 cm in height, and weighed 57 kg. He was fitted with a powered knee prosthesis prototype developed at HUB-Robotics, namely Alabama Powered Prosthetic Limb – Knee (APPL-K), shown in Figure 5-9.
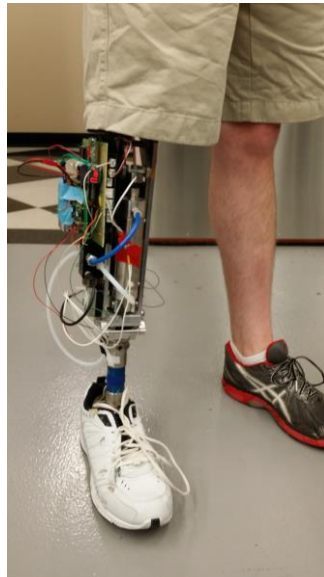
Figure 5-9 The powered knee prosthesis APPL-K fitted to the test subject

The version of the powered knee prosthesis APPL-K used in this study was powered by a pneumatic cylinder, and the details can be found in the previous publication [18,19]. Pneumatic actuator is used to reduce the weight and complexity of the device while providing the desired torque and power to support the amputee user's locomotion. When a 300 psi pneumatic supply is used, the actuator is able to an extension force of up to 2.36 kN and a contraction force of up to 2.16 kN. Depending on the joint angle, the torque capacity of powered knee ranges from 49~106 N-m in flexion and 45~97 in extension, providing sufficient torque for walking and stair

climbing for a 75 kg user. For the control purpose, a compact load cell is mounted in line with the actuator to measure the force output, a rotary potentiometer is embedded into the prosthetic joint to measure the joint angle, and a servo valve is also incorporated into the prosthesis to enable the control of the output force (and hence the actuation torque) in real time. Human testing of the APPL-K in walking has been conducted, with the results showing natural walking gait and user interaction in treadmill walking [19].

To implement the walking – stair climbing control system presented in this chapter, the prosthesis is also equipped with two additional sensors to provide necessary signals for state transitions. The first is a custom ground contact force load cell designed by the Center for Intelligent Mechatronics at Vanderbilt University [20], which provides reliable detection of important events in the gait, e.g., heel strike and toe off. The other sensor is a 6-degree-of-freedom inertial measurement unit(IMU), including a 3-dof accelerometer and a 3-dof gyroscope. The IMU is mounted on the prosthesis, providing the capability of measuring the spatial orientation of the prosthesis in the sagittal plane. Combining the prosthesis orientation with the joint angle measured with the rotary potentiometer, the prosthesis controller can calculate the thigh orientation, serving the purpose of triggering mode transition in the desired way.

Due to the limitation of available equipment, the data collected in the testing were all based on the sensors embedded in the prosthesis, primarily the joint angle and torque trajectories. Figure 5-10 shows a typical knee trajectory obtained in the experiments, which covers a complete cycle of walking, a mixed cycle of walking/stair climbing, and a complete cycle of stair climbing. The desired mode transition (at ~55% of the motion progress) was correctly identified and executed. Figure 5-11 shows a sequence of screenshots taken from the testing video. It can be clearly observed that the new prosthesis control system was able to generate natural motion

within each motion mode and trigger desired mode transition according to the user's thigh motion, which was further confirmed by the test subject's oral feedback.
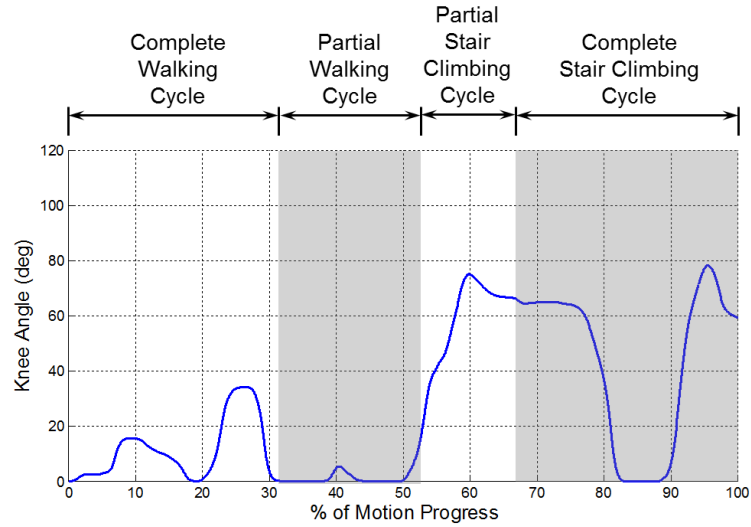
Figure 5-10 Knee angle trajectory in testing
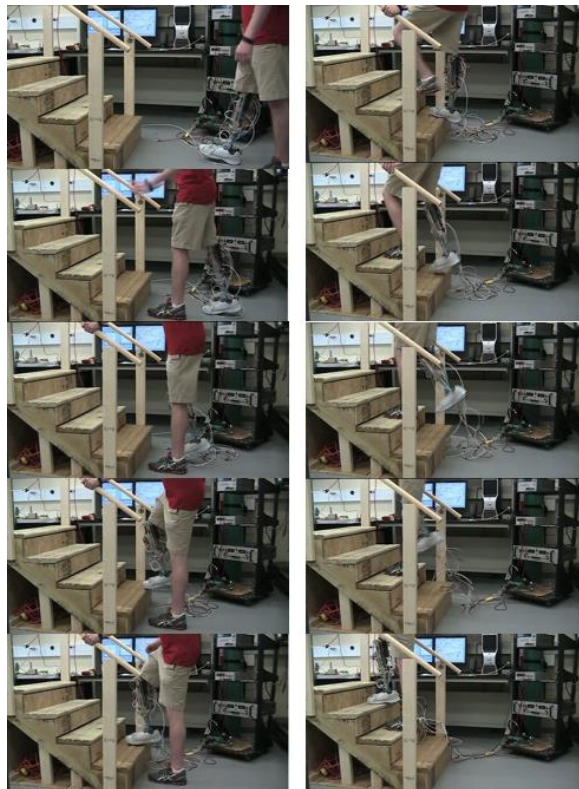
Figure 5-11 A sequence of screenshots of the testing video (from top to bottom, left to right)

5.5 Conclusions

This chapter presents a new walking and stair climbing control system for powered knee prostheses. With the objective of emulating how humans control the biological knee, this new control system was developed by analyzing and modeling the biomechanical data in walking and stair climbing. In addition of using the traditional impedance modeling technique, a new time-based function was introduced to model the phase that requires graduate energy injection, which is beyond the capability of impedance modeling. Subsequently, finite-state controllers for walking and stair climbing were developed, along with a thigh spatial position-based mode-transition mechanism. Preliminary human testing demonstrated the effectiveness of the proposed control system in generating natural motion in each motion mode and triggering mode transitions reliably.

5.6 Acknowledgements

References

[1] Riener, R., Rabuffetti, M., and Frigo, C., 2002. "Stair ascent and descent at different inclinations." *Gait and Posture*, no. 15, pp. 32-44. Riener, R., Rabuffetti, M., and Frigo, C., 2002. "Stair ascent and descent at different inclinations." *Gait and Posture*, no. 15, pp. 32-44.

[2] Winter, D.A., *The Biomechanics and Motor Control of Human Gait: Normal, Elderly and Pathological.* 2nd ed., Waterloo, ON, University of Waterloo Press, 1991.

[3] Waters, R., Perry, J., Antonelli, D., and Hislop, H., 1976. "Energy cost of walking amputees: the influence of level of amputation." *Journal of Bone and Joint Surgery*, vol. 58A, pp. 42-46.

[4] Flowers, W.C., and Mann, R.W., 1977. "Electrohydraulic knee-torque controller for a prosthesis simulator." *ASME Journal of Biomechanical Engineering*, vol. 99, no. 4, pp. 3-8.

[5] Popovic, D. and Schwirtlich, L., 1988. "Belgrade active A/K prosthesis." in de Vries, J. (Ed.), *Electrophysiological Kinesiolog*y, Interm. Congress Ser. No. 804, Excerpta Medica, Amsterdam, The Netherlands, pp. 337–343.

[6] Hata, N. and Hori, Y., 2002. "Basic research on power limb using gait information of able-side leg." *7th International Workshop on Advanced Motion Control*, pp. 540-545.

[7] Fite, K., Mitchell, J., Sup, F., and Goldfarb, M., 2007. "Design and control of an electrically powered knee prosthesis." *Proceedings of the 2007 IEEE 10th International Conference on Rehabilitation Robotics*, pp. 902-905.

[8] Sup, F., Varol, H.A., Mitchell, J., Withrow, T.J., and Goldfarb, M., 2009. "Preliminary evaluations of a self- contained anthropomorphic transfemoral prosthesis." *IEEE/ASME Transactions on Mechatronics*, vol. 14, no. 6, pp. 667-676.

[9] Martinez-Villalpando, E.C. and Herr, H., 2009. "Agonist-antagonist active knee prosthesis: A preliminary study in level-ground walking." *Journal of Rehabilitation Research & Development*, vol. 46, no. 3, pp. 361-374.

[10] Hoover, C.D., Fulk, G.D., and Fite, K.B., 2012. "The design and initial experimental validation of an active myoelectric transfemoral prosthesis." *ASME Journal of Medical Devices*, vol. 6, p. 011005.

[11] Sup, F., Bohara, A, and Goldfarb, M., 2008. "Design and control of a powered transfemoral prosthesis." *The International Journal of Robotics Research*, vol. 27, no. 2, pp. 263-273.

[12] Waycaster, G., Wu, S.K. and Shen, X., 2011. "Design and control of a pneumatic artificial muscle actuated above-knee prosthesis." *Journal of Medical Devices*, vol. 5, no. 3, p.031003.

[13] Grimes, D. L., Flowers, W. C., and Donath, M., 1977. "Feasibility of an Active Control Scheme for Above Knee Prostheses." *ASME Journal of Biomechanical Engineering*, vol. 99, no. 4, pp. 215-221.

[14] Wu, S.K., Waycaster, G. and Shen, X., 2011. "Electromyography-based control of active above-knee prostheses." *Control Engineering Practice*, vol. 19, no. 8, pp.875-882.

[15] Lawson, B.E., Varol, H.A., Huff, A., Erdemir, E. and Goldfarb, M., 2013. "Control of stair ascent and descent with a powered transfemoral prosthesis." *Neural Systems and Rehabilitation Engineering, IEEE Transactions on*, vol. 21, no. 3, pp.466-473.

[16] Hoover, C.D., Fulk, G.D. and Fite, K.B., 2013. "Stair ascent with a powered transfemoral prosthesis under direct myoelectric control." *Mechatronics, IEEE/ASME Transactions on*, vol. 18, no. 3, pp.1191-1200.

[17] Hogan, N., 1985. "Impedance control: An approach to manipulation." *Journal of dynamic systems, measurement, and control*, *107*(1), pp.1-24.

[18] Wu, M., Zheng, H., and Shen, X., 2015. "A pneumatically actuated knee prosthesis." *ASME Journal of Medical Devices*, vol. 9, no. 3, p. 030911.

[19] Wu, M. and Shen, X., 2016. "Design and preliminary testing of a self-contained knee prosthesis with pneumatic actuation." *International Journal of Robotics and Automation*, in press.

[20] Lawson, B.E., Mitchell, J.E., Truex, D., Shultz, A., Ledoux, E., and Goldfarb, M., 2014. "A robotic leg prosthesis: Design, control, and implementation." *IEEE Robotics & Automation Magazine*, vol. 21, no. 4, pp. 70-81.

6   SIT-TO-STAND CONTROL OF POWERED KNEE PROSTHESES

Standing up from a seated position is a very common activity in people's daily life. However, for transfemoral (i.e., above-knee) amputees fitted with traditional passive prostheses, the sit-to-stand (STS) transition is also highly challenging, due to the inability of the prosthetic joints in generating torque and power output. In this chapter, a new STS control approach for powered lower-limb prostheses is introduced, which is able to regulate the power delivery of the prosthetic knee joint to obtain natural STS motion similar to that displayed by healthy subjects. Mimicking the dynamic behavior of the knee in both phases of the STS, a unified control structure provides the desired control actions by combining an impedance function with a time-based ramp-up function. The former provides the gradual energy release behavior desired in the rising phase, while the latter provides the gradual energy injection behavior desired in the loading phase. This simple and intuitive control structure automates the transition between the loading and rising phases, eliminating the need for explicit phase transition and facilitating the implementation in powered prostheses. Human testing results demonstrated that, by regulating the power provided by the prosthesis, this new control approach is able to generate a natural standing-up motion, which is well coordinated with the user's healthy-side motion in the STS process.

6.1   Introduction

Standing from a seated position is a common, yet dynamically challenging task in people's daily life. Due to the vertical ascent of the body center of gravity, sit-to-stand (STS)

98

transition requires high torque from the knee, far exceeding the joint torque in walking. Various biomechanical studies reported knee peak torques in STS as high as 2.2 Nm/kg (e.g., [1]), while the typical peak torque in natural walking is only 0.615 Nm/kg [2] (both body weight normalized). As a result, STS transition poses a major barrier to the mobility of individuals with lower limb motor impairments, including the transfemoral (TF) amputees (i.e., individuals suffering from above-knee amputations). A related study showed that unilateral TF amputees suffer from high asymmetry in ground reaction forces (53~69%) and knee moments (110~124%), while the asymmetry for healthy controls is limited to less than 7% [3]. Note that, although a powered TF prosthesis (Power Knee) was used in this study, it generated resistance in the STS and thus produced similar results as the passive devices in the study (C-Leg and Mauch SNS). The inability of existing prostheses in generating enough knee torque and regulating the torque delivery in the STS seriously affects the mobility of the large population of TF amputees in their daily life.

Motivated by this significant performance deficiency of traditional passive TF prostheses, researchers have expended substantial efforts in developing powered devices. The pioneering work in this area was conducted by Flowers and Mann, which uses a hydraulic actuator to actuate the knee joint [4]. However, multiple drawbacks with hydraulics, such as leakage and lack of a compact supply, make it less attractive for prosthetic applications. Currently, most powered transfemoral prostheses are actuated with electric motors [5-10], e.g. Sup et al. developed a powered knee and ankle prosthesis with both joints powered with DC motor – ball screw assemblies [8]; Martinez-Villalpando and Herr developed a powered knee prosthesis with two series-elastic actuators positioned in parallel in an agonist-antagonist arrangement [9]; Hoover et al. developed a myoelectric transfemoral prosthesis, in which the powered knee is

99

controlled with an EMG-based motion controller [10]. Additionally, Ossur, a leading orthopedics company, manufactured the aforementioned Power Knee, the first commercially available powered transfemoral prosthesis. According to the available technical information, the Power Knee is also actuated with an electric motor. In addition to these motor-powered devices, pneumatically-actuated prostheses have also been developed by researchers including the authors' group, for example, the prototypes powered with pneumatic cylinders [11] and muscle actuators [12].

The powered prostheses mentioned above are able to actively generate joint torque and power for dynamically challenging tasks such as STS transition. Making full use of such capability, however, requires an effective and reliable controller to regulate the joint power delivery in motion. Currently, walking controller for powered prostheses have been well established. Typical approaches include echo control, which controls the prosthetic joint to track the recorded sound-side motion with a half-cycle delay [13]; and finite-state impedance control, which implements an artificial impedance within each phase of the gait cycle [11]. Electromyography has also been attempted in obtaining the user's motion intent and generating the corresponding motion command [14]. STS control, however, is much less investigated. The Center for Intelligent Mechatronics at Vanderbilt University developed a multi-mode controller for powered knee and ankle prostheses, in which STS is incorporated as a transitional motion between sitting and standing states [15,16]. However, no details were provided on the rationale of the controller structure or the determination of the control parameters.

In the research presented in this chapter, this dissertation developed a new control approach to regulate the power and torque delivery in the STS process. As the basis of this approach, an analysis of the biomechanical behavior of the knee in the STS was conducted,

providing the inspiration for the proposed controller structure. Subsequently, curve fitting was conducted to evaluate the validity of the new controller structure, utilizing the existing biomechanical data of the STS motion. This new approach was implemented in a powered knee prosthesis developed in HUman-centered BioRobotics (HUB-Robotics) Laboratory at The University of Alabama, generating qualitative and quantitative results to evaluate its effectiveness.

6.2   Knee biomechanical behavior-inspired STS controller

Biomechanics in STS is a heavily investigated topic with a large body of data generated from numerous studies. Ideally, an STS controller should replicate the biomechanical behavior of the knee in this process, providing the prosthesis user a nature control experience. However, exactly replicating the kinetic and kinematic trajectories of the biological knee is unfeasible. Human locomotion is a highly interactive process, in which the human lower limbs interact with the rest of the human body and the environment to obtain coordinated motion. Enforcing the kinetic/kinematic trajectories in the prosthetic knee precludes such interaction, resulting in a poor experience for the amputee users. Results of the biomechanical data, on the other hand, provides insight to the dynamic behavior of the knee and thus can be used as the inspiration for the prosthesis controller.

Unlike cyclical motion modes such as walking, STS is a typical transitional motion with clearly defined start (seated position) and end (standing position). The typical joint position and torque trajectories are shown in Figure 6-1(data from [1]). The entire process can be divided into two phases with distinct dynamic characteristics, separated by the instant of Seat-Off (SO):

(1) Loading phase (from Start to SO): with the body weight shifted from the seat to the lower limb, the knee torque increases rapidly to support the body weight and initiate the upward motion. In this phase the knee position remains almost constant until the final portion of the phase, and the torque increases at a nearly constant rate after the initial dormant period.

(2) Rising phase (from SO to End): after reaching the maximum value, the knee torque reduces with the joint extension, and settles at a steady-state value after the standing position is reached.
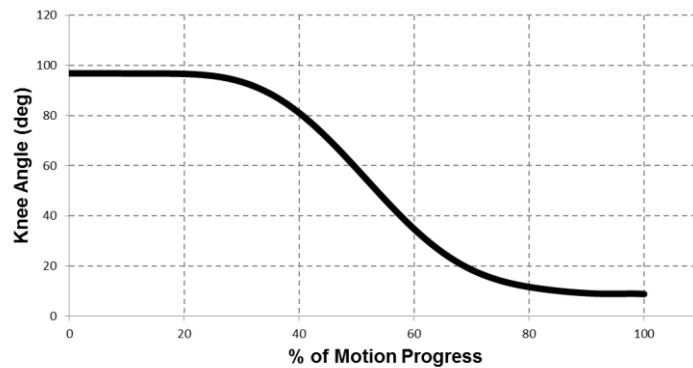
(a)
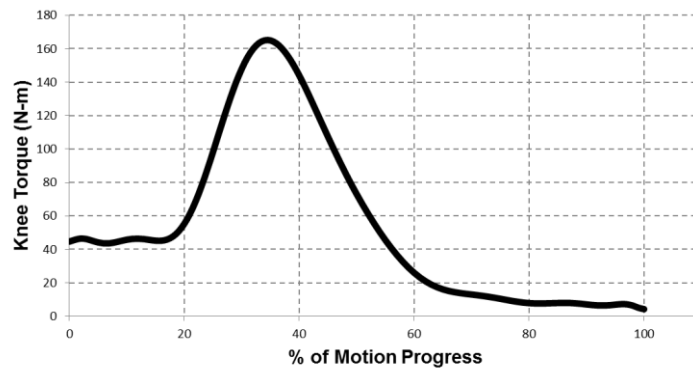
(b)

Figure 6-1 Knee position (a) and torque (b) trajectories in the STS motion, plotted for a 75 kg person with the data from [1]

Such segmentation of the STS motion can be clearly seen in Figure 6-1. For a powered knee prosthesis to generate natural motion in this process, the controller should follow the same strategy, generating a knee torque that changes in a way similar to the biological joint torque trajectory. To facilitate the implementation in powered prostheses, the STS controller structure should be adequately simplified while retaining the essence of human biological control. Furthermore, considering the significant inter-subject variation among amputee users, subject-specific tuning is an indispensable step in fitting a powered prosthesis. Ideally, the number of control parameters should be minimized, and all parameters should have clearly defined physical meanings to make the tuning process intuitive and easy to understand. Based on the multiple requirements above, this chapter proposes a control structure consisting of a time-based ramp-up function for gradual loading of the knee combined with an impedance function for automatic adjustment of knee torque according to the motion progress:

$$\tau = R\left(\frac{t - t_0}{T}\right)\tau_{imp}\left(\theta, \dot{\theta}\right) \tag{6.1}$$

In this equation, the impedance function τ_{imp} is defined as:

$$\tau_{imp} = K(\theta - \theta_e) + B\dot{\theta} \tag{6.2}$$

where θ is the joint position (measured from the knee straight position), $\dot{\theta}$ is the joint angular velocity, K is the stiffness of the virtual spring, θ_e is the equilibrium point of the virtual spring, and B is the damping value of the virtual damper. The ramp-up function $R\left(\frac{t - t_0}{T}\right)$ is defined as

$$R\left(\frac{t - t_0}{T}\right) = \begin{cases} \dfrac{t - t_0}{T} & when\ t_0 \le t \le t_0 + T \\ 1 & when\ t > t_0 + T \end{cases} \tag{6.3}$$

where t is current time point, t_0 is the starting time point of the ramp-up period, and T is the length of the ramp-up period.

The impedance function, as the major part of the controller, simulates the dynamics of a mechanical spring combined with a viscous damper. A mechanical spring is energetically conservative, while a viscous damper is dissipative. As such, the simulated spring-damper combination is purely passive, guaranteeing the stability in the control process. The passivity, on the other hand, dictates that all the required artificial mechanical energy (in the form of artificial spring deflection) to be introduced at the onset of STS motion, such that sufficient power output can be provided while lifting the user in the upward motion. Consequently, the torque output of the spring-damper combination immediately reaches the maximum at the motion onset, as opposed to the gradual increase as shown in the biomechanical data.

The time-based ramp-up function is then introduced to address this problem. As Eq. (6.3) shows, the value of the function increases linearly from 0 to 1 within the ramp-up period, and stays at 1 afterwards. As such, it only takes effect in the ramp-up period, providing the gradual energy injection required in the loading phase. It is worth mentioning that the use of the ramp-up function eliminates the need for explicit phase transition from loading to rising as a result of the limited effective period, which significantly simplifies the implementation of controller.

To validate the controller structure shown by Eqs. (6.1)~(6.3), curve fitting was conducted based on the biomechanical data of knee position/velocity and torque in the STS for a 75 kg subject [1]. Matlab Curve Fitting Toolbox was utilized to obtain the optimal set of values for K, θ_e, B, and T with least error from the biomechanical data. Figure 6-2 shows the

comparison of the fitted knee torque curve versus the knee torque trajectory plotted from biomechanical data. The close match between the two curves indicates that the proposed controller structure is able to replicate the dynamic behavior of the biological knee joint in the STS motion with very small error.
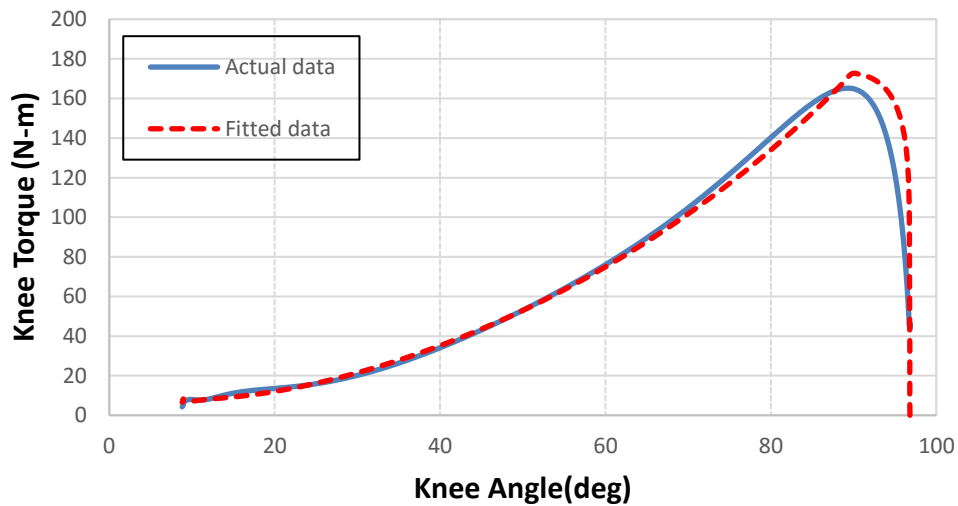
Figure 6-2 Comparison of the fitted knee torque curve vs biomechanical knee torque curve in the STS for a 75 kg subject

Finally, to initiate the control action, the axial load in the prosthesis combined with the knee joint angle serves as the indicator for the user's readiness for the STS motion. When the user prepares for standing up, he/she first bend the knees by a large angle (usually greater than 90º) such that the feet can be directly underneath the body center of mass. Subsequently, the weight is gradually shifted to the feet, increasing the axial load born by the prosthesis. Based on such biomechanical process, the trigger condition is set as: the prosthesis axial load greater than a certain threshold F_T, and the prosthesis knee angle also greater than a certain threshold θ_T. This

simple yet effective triggering condition can be easily implemented by using the embedded sensors in the prosthesis, and provides an intuitive and reliable way to initiate the STS motion.

6.3   Human testing results

To demonstrate the effectiveness of the STS controller, the authors conducted a set of human subject experiments at the HUman-centered BioRobotics (HUB-Robotics) Laboratory at The University of Alabama. The human subject participated in the testing was a 22-year-old male unilateral amputee, 178 cm in height, and weighed 57 kg. He was fitted with a powered knee prosthesis prototype developed at HUB-Robotics Lab, namely Alabama Powered Prosthetic Limb – Knee (APPL-K), shown in Figure 6-3.
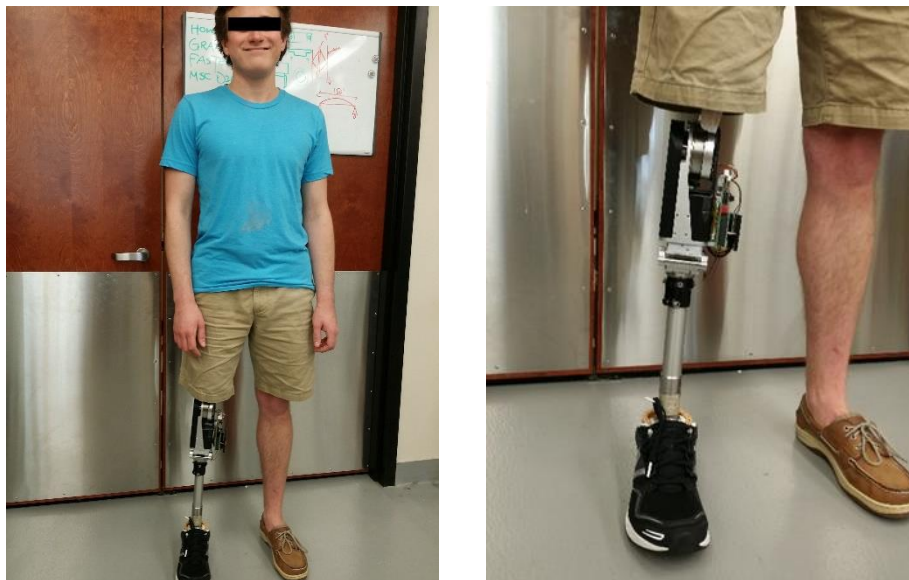
Figure 6-3 An amputee fitted with the powered knee prosthesis

The version of the powered knee prosthesis used in this study, APPL-K-E1, was powered by an 8-pole brushless DC motor with 70 W power rating (EC 45 flat, Maxon Motor, Sachseln, Switzerland). For short-term operation, this motor is able to generate a peak torque of 0.2 Nm, and a maximum rotation speed of 10,000 rpm. A two-stage transmission of 150:1 gear ratio is used, combined a timing belt drive as the first stage and a harmonic drive gearhead as the second

stage. Note that, in the design of the device, reducing the weight and simplifying the system structure was given higher priority than generating higher torque output, and the actuation torque is less than the peak value in the biomechanical data. This issue, however, did not affect the performance of the prosthesis in the STS, as indicated by the experimental results below.

For the implementation of the STS controller, the prosthesis is instrumented with various control components for computing, sensing and regulation of power delivery. The joint position is measured with a rotary magnetic encoder, and the position signal is digitally differentiated to obtain the joint angular velocity information. A custom load cell developed by the Center for Intelligent Mechatronics at Vanderbilt University [17] is mounted between the prosthesis and the standard pyramid connector to measure the axial force in the prosthesis. The power output of the DC motor is regulated with a PWM servo drive (AZBDC20A8, Advanced Motion Controls, Camarillo, CA, USA), which controls the motor current as a function of the PWM duty cycle. The controller is implemented on a microcontroller (Microstick II, Microchip Technology Inc., Chandler, AZ, USA), which communicates with a host desktop computer to record and display experimental results for controller tuning and data analysis.

Due to the limitation of available equipment, the data collected in the testing were all based on the sensors embedded in the prosthesis, primarily the joint angle and torque trajectories. After being fitted with the powered prosthesis, the subject repeated the STS motion to identify the best set of control parameters through his feedback and recorded experimented data. The stiffness of the artificial spring in the controller K was increased gradually, providing increasing extensional torque to assist the user to stand up. The final value, with which the user is most comfortable with, generates a peak torque of 25 N-m, much less than that in the biomechanical data. The primary reason, presumably, is that the subject is used to the lack of power supply in

107

his daily-use passive prosthesis, and thus the comfortable level of power supply in his prosthetic joint has been reduced significantly compared with that in a healthy biological joint. This observation, to some extent, validates the original decision of prioritizing low weight over high torque in the prosthesis design.

The damping of the artificial viscous damper was also tuned. With the function of controlling the speed of standing up, the damper reduces the extensional torque, or even generates a flexional torque if the extension of the knee becomes too fast. The damping value was also adjusted primarily according to the feedback of the test subject.

The typical trajectories of the experimentally measured prosthetic joint position and torque are shown in Figure 6-4, and a sequence of snapshots of the STS process is shown in Figure 6-5. The data window started when the triggering condition was met. As can been seen in Figure 6-4, the joint position stayed almost as a constant until the rising phase started, and the whole trajectory shows smooth and controlled motion throughout the process. Compared with the biomechanical data shown in Figure 6-1, the contour of the experimentally measured prosthetic position trajectory is highly similar. For the joint torque trajectory, the dynamics of the loading and rising phases can be clearly identified and distinguished, with a smooth transition in between. The overall contour is also similar to that of the biomechanical curve in Figure 6-1. Matching the observations from these figures, the subject also stated a natural control experience in which the prosthesis motion coordinates with the sound-side leg motion well, and the extensional torque in the prosthesis enabled him to stand up with less effort. Such quantitative and qualitative results fully demonstrated the effectiveness of the proposed controller, which provides the prosthesis user a significantly improved experience over the traditional passive prosthesis.

(a)

(b)
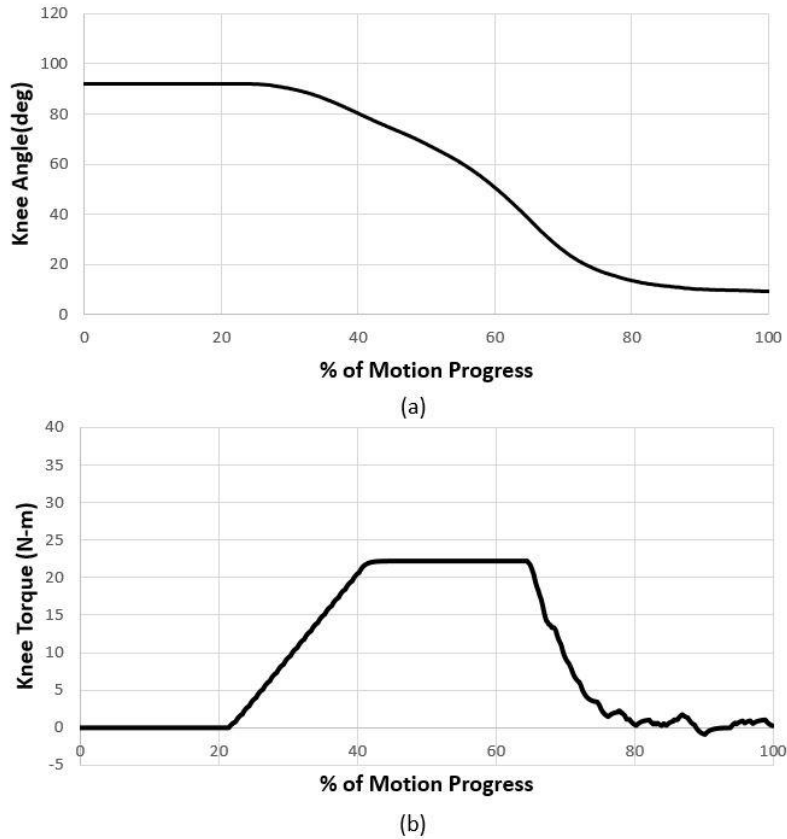
Figure 6-4 Typical trajectory of experimental result of joint position (a) and torque (b)

Figure 6-5 Sequence of snapshots of the STS process

6.4 Conclusions

This chapter presents a new control approach for powered knee prostheses in the STS motion. The objective was to develop an STS controller that regulates the extensional torque in powered knee prostheses to obtain smooth standing up motion. As the basis of the controller development, the biomechanical data from prior STS studies were analyzed. The dynamics in

the loading and rising phases are vastly different. However, a unique control structure was created, which combines the impedance function with a time-based ramp-up function. The impedance function was introduced to provide the gradual energy release in the rising phase, while the ramp-up function was included to mimic the gradual energy injection behavior in the loading phase. The use of such unified control structure simplifies the controller implementation while maintaining the unique biomechanical characteristics of each motion phase. This new STS controller was implemented on a powered knee prosthesis developed in the author's lab, and human testing results demonstrated the effectiveness of this approach in generating smooth standing-up motion according to the user's will.

References

[1]   Schenkman, M., Berger, R.A., Riley, P.O., Mann, R.W. and Hodge, W.A., 1990. Whole-body movements during rising to standing from sitting. Physical Therapy, 70(10), pp.638-648.

[2]   Winter, D.A., The Biomechanics and Motor Control of Human Gait: Normal, Elderly and Pathological. 2nd ed., Waterloo, ON, University of Waterloo Press, 1991.

[3]   Highsmith, M.J., Kahle, J.T., Carey, S.L., Lura, D.J., Dubey, R.V., Csavina, K.R. and Quillen, W.S., 2011. Kinetic asymmetry in transfemoral amputees while performing sit to stand and stand to sit movements. Gait & posture, 34(1), pp.86-91.

[4]   Flowers, W.C., and Mann, R.W., 1977. "Electrohydraulic knee-torque controller for a prosthesis simulator." ASME Journal of Biomechanical Engineering, vol. 99, no. 4, pp. 3-8.

[5]   Popovic, D. and Schwirtlich, L., 1988. "Belgrade active A/K prosthesis." in de Vries, J. (Ed.), Electrophysiological Kinesiology, Interm. Congress Ser. No. 804, Excerpta Medica, Amsterdam, The Netherlands, pp. 337–343.

[6]   Hata, N. and Hori, Y., 2002. "Basic research on power limb using gait information of able-side leg." 7th International Workshop on Advanced Motion Control, pp. 540-545.

[7]   Fite, K., Mitchell, J., Sup, F., and Goldfarb, M., 2007. "Design and control of an electrically powered knee prosthesis." Proceedings of the 2007 IEEE 10th International Conference on Rehabilitation Robotics, pp. 902-905.

[8]   Sup, F., Varol, H.A., Mitchell, J., Withrow, T.J., and Goldfarb, M., 2009. "Preliminary evaluations of a self-contained anthropomorphic transfemoral prosthesis." IEEE/ASME Transactions on Mechatronics, vol. 14, no. 6, pp. 667-676.

[9]   Martinez-Villalpando, E.C. and Herr, H., 2009. "Agonist-antagonist active knee prosthesis: A preliminary study in level-ground walking." Journal of Rehabilitation Research & Development, vol. 46, no. 3, pp. 361-374.

[10]   Hoover, C.D., Fulk, G.D., and Fite, K.B., 2012. "The design and initial experimental validation of an active myoelectric transfemoral prosthesis." ASME Journal of Medical Devices, vol. 6, p. 011005.

[11]   Sup, F., Bohara, A, and Goldfarb, M., 2008. "Design and control of a powered transfemoral prosthesis." The International Journal of Robotics Research, vol. 27, no. 2, pp. 263-273.

[12]   Waycaster, G., Wu, S.K. and Shen, X., 2011. "Design and control of a pneumatic artificial muscle actuated above-knee prosthesis." Journal of Medical Devices, vol. 5, no. 3, p.031003.

[13]   Grimes, D. L., Flowers, W. C., and Donath, M., 1977. "Feasibility of an Active Control Scheme for Above Knee Prostheses." ASME Journal of Biomechanical Engineering, vol. 99, no. 4, pp. 215-221.

[14]   Wu, S.K., Waycaster, G. and Shen, X., 2011. "Electromyography-based control of active above-knee prostheses." *Control Engineering Practice*, vol. 19, no. 8, pp.875-882.

[15]   Varol, H.A., Sup, F. and Goldfarb, M., 2010. Multiclass real-time intent recognition of a powered lower limb prosthesis. *IEEE Transactions on Biomedical Engineering*, *57*(3), pp.542-551.

[16]   Varol, H.A., Sup, F. and Goldfarb, M., 2009, June. Powered sit-to-stand and assistive stand-to-sit framework for a powered transfemoral prosthesis. In *2009 IEEE International Conference on Rehabilitation Robotics* (pp. 645-651). IEEE.

[17]   Lawson, B.E., Mitchell, J.E., Truex, D., Shultz, A., Ledoux, E., and Goldfarb, M., 2014. "A robotic leg prosthesis: Design, control, and implementation." *IEEE Robotics & Automation Magazine*, vol. 21, no. 4, pp. 70-81.

APPENDIX: IRB APPROVAL

Office for Research

Institutional Review Board for the
Protection of Human Subjects

THE UNIVERSITY OF
ALABAMA
R E S E A R C H

February 29, 2012

Xiangrong Shen, Ph.D.
Assistant Professor
Department of Mechanical Engineering
College of Engineering
The University of Alabama

Re: IRB Protocol # 12-002-ME
         "Exploration of Chemo-Muscle Actuation in Active Above-Knee
         Prostheses"

Dr. Shen:

The University of Alabama IRB has received the revisions requested by the
full board on 2/14/12. The board has reviewed the revisions and your
protocol is now approved for a one-year period. Please be advised that your
protocol will expire one year from the date of approval, 2/9/12.

If your research will continue beyond this date, complete the Renewal
Application Form. If you need to modify the study, please submit the
Modification of An Approved Protocol Form. <u>Changes in this study cannot
be initiated without IRB approval, except when necessary to eliminate
apparent immediate hazards to participants.</u> When the study closes, please
complete the Request for Study Closure Form.

Should you need to submit any further correspondence regarding this
proposal, please include the assigned IRB application number. Please use
reproductions of the IRB approved <u>stamped</u> consent/assent forms to obtain
consent from your participants.

Good luck with your research.

John C. Higginbotham, Ph.D., MPH
Medical IRB Chair
The University of Alabama

358 Rose Administration Building
Box 870127
Tuscaloosa, Alabama 35487-0127
(205) 348-8461
FAX (205) 348 7189
TOLL FREE (877) 820-3066

113

January 17, 2014

THE UNIVERSITY OF
ALABAMA
R E S E A R C H

Xiangrong Shen, Ph.D.
Assistant Professor
Department of Mechanical Engineering
College of Engineering
The University of Alabama

Re: IRB Protocol # 14-001-ME
        "Biologically-Inspired Actuation and Control of Robotic Above-Knee
        Prostheses"

Dr. Shen:

The University of Alabama IRB has received the revisions requested by the
full board on 1/17/14. The board has reviewed the revisions and your protocol
is now approved for a one-year period. Please be advised that your protocol
will expire one year from the date of approval, 1/9/14.

If your research will continue beyond this date, complete the Renewal
Application Form. If you need to modify the study, please submit the
Modification of An Approved Protocol Form. <u>Changes in this study cannot be
initiated without IRB approval, except when necessary to eliminate apparent
immediate hazards to participants</u>. When the study closes, please complete the
Request for Study Closure Form.

Should you need to submit any further correspondence regarding this
proposal, please include the assigned IRB application number. Please use
reproductions of the IRB approved <u>stamped</u> consent/assent forms to obtain
consent from your participants.

Good luck with your research.

Sincerely,

John C. Higginbotham, Ph.D., MPH
Medical IRB Chair
The University of Alabama

358 Rose Administration Building
Box 870127
Tuscaloosa, Alabama 35487-0127
(205) 348-8461
FAX (205) 348-7189
TOLL FREE (877) 820-3066

114

UNIVERSITY OF ALABAMA
INSTITUTIONAL REVIEW BOARD FOR THE PROTECTION OF HUMAN SUBJECTS
REQUEST FOR APPROVAL OF RESEARCH INVOLVING HUMAN SUBJECTS

I.   Identifying information

	Principal Investigator	Second Investigator	Third Investigator
Names:	Xiangrong Shen	Molei Wu	T. Mark Norris
Department:	Mechanical Engineering	Mechanical Engineering	
College:	Engineering	Engineering	
University:	The University of Alabama	The University of Alabama	Norris Limb and Brace
Address:	290 Hardaway Hall	290 Hardaway Hall	508 Paul Bryant Drive East, Tuscaloosa, AL 35401
Telephone:	205-348-6743		205-349-5388
FAX:	205-348-6419		205-752-4002
E-mail:	xshen@eng.ua.edu	mwu22@crimson.ua.edu	tmarknorriscp@aol.com

Title of Research Project: Biologically-Inspired Actuation and Control of Robotic Above-Knee Prostheses

Date Submitted: 12/10/2013
Funding Source: *NSF*

Type of Proposal	☒ New	☐ Revision	☐ Renewal Please attach a renewal application	☐ Completed	☐ Exempt
			Please attach a continuing review of studies form		
			Please enter the original IRB # at the top of the page		

UA faculty or staff member signature: ███████████

II. NOTIFICATION OF IRB ACTION (to be completed by IRB):
Type of Review: ____✓____ Full board _____ Expedited

IRB Action:
___ Rejected   Date: _____
___ Tabled Pending Revisions   Date: _____
___ Approved Pending Revisions   Date: _____
✓ Approved-this proposal complies with University and federal regulations for the protection of human subjects.
    Approval is effective until the following date: *1-9-15* ʔʔ
    Items approved: ___ Research protocol   (dated_____)
                    ___ Informed consent   (dated_____)
                    ___ Recruitment materials (dated_____)
                    ___ Other   (dated_____)

Approval signature ███████████████   Date __1/17/14__

115